The Interplay Between Collisionless Magnetic Reconnection and Turbulence

**J. E. Stawarz · P. A. Muñoz · N. Bessho ·
R. Bandyopadhyay · T. K. M. Nakamura ·
S. Eriksson · D. Graham · J. Büchner ·
A. Chasapis · J. Drake · M. A. Shay ·
R. E. Ergun · H. Hasegawa ·
Yu. V. Khotyaintsev · M. Swisdak ·
F. Wilder**

J. E. Stawarz
Department of Mathematics, Physics, and Electrical Engineering, Northumbria University,
Ellison Building, Newcastle upon Tyne NE1 8ST, United Kingdom.
E-mail: julia.stawarz@northumbria.ac.uk

P. A. Muñoz
Center for Astronomy and Astrophysics, Technical University of Berlin, 10623 Berlin, Germany.
Max Planck Institute for Solar System Research, 37077 Göttingen, Germany.

N. Bessho
Department of Astronomy, University of Maryland, College Park, MD 20742, USA.
NASA Goddard Space Flight Center, Greenbelt, MD 20771, USA.

R. Bandyopadhyay
Department of Astrophysical Sciences, Princeton University, Princeton, NJ 08544, USA.

T. K. M. Nakamura
Space Research Institute, Austrian Academy of Sciences, 8042 Graz, Austria.
Krimgen LLC, Hiroshima, 7320828, Japan.

S. Eriksson
Laboratory for Atmospheric and Space Physics, University of Colorado, Boulder, CO, USA.

D. Graham
Swedish Institute of Space Physics, Uppsala, Sweden.

J. Büchner
Max Planck Institute for Solar System Research, 37077 Göttingen, Germany.
Center for Astronomy and Astrophysics, Technical University Berlin, 10623 Berlin, Germany.

A. Chasapis
Laboratory for Atmospheric and Space Physics, Boulder, CO, USA.

J. Drake
Institute for Research in Electronics and Applied Physics, University of Maryland, College
Park, MD 20740, USA.
Department of Physics, the Institute for Physical Science and Technology and the Joint Space
Institute, University of Maryland, College Park, MD 20740, USA.

M. A. Shay
Department of Physics and Astronomy, University of Delaware, Newark, Delaware 19716, USA.

R. E. Ergun

Abstract Alongside magnetic reconnection, turbulence is another fundamental nonlinear plasma phenomenon that plays a key role in energy transport and conversion in space and astrophysical plasmas. From a numerical, theoretical, and observational point of view there is a long history of exploring the interplay between these two phenomena in space plasma environments; however, recent high-resolution, multi-spacecraft observations have ushered in a new era of understanding this complex topic. The interplay between reconnection and turbulence is both complex and multifaceted, and can be viewed through a number of different interrelated lenses - including turbulence acting to generate current sheets that undergo magnetic reconnection (*turbulence-driven reconnection*), magnetic reconnection driving turbulent dynamics in an environment (*reconnection-driven turbulence*) or acting as an intermediate step in the excitation of turbulence, and the random diffusive/dispersive nature of magnetic field lines embedded in turbulent fluctuations enabling so-called *stochastic reconnection*. In this paper, we review the current state of knowledge on these different facets of the interplay between turbulence and reconnection in the context of collisionless plasmas, such as those found in many near-Earth astrophysical environments, from a theoretical, numerical, and observational perspective. Particular focus is given to several key regions in Earth's magnetosphere - Earth's magnetosheath, magnetotail, and Kelvin-Helmholtz vortices on the magnetopause flanks - where NASA's *Magnetospheric Multiscale* mission has been providing new insights on the topic.

Keywords Magnetic Reconnection, Turbulence, Collisionless Plasmas

1 Introduction

Many natural plasmas where magnetic reconnection occurs have wide scale separations between the length scales where energy is injected into the system through dynamical processes and the smaller scales where energy is most effectively dissipated. Such systems are conducive to the excitation of complex and highly-nonlinear fluctuations, known as turbulence, that transfer energy across scales facilitating the dissipation of large-scale free energy.

While the basic physics underpinning individual reconnection sites can be considered using idealized models, magnetic reconnection is fundamentally a nonlinear and multi-scale process that both influences and is influenced by the turbulent

Laboratory for Atmospheric and Space Physics, University of Colorado at Boulder, Boulder, CO, USA.
Department of Astrophysical and Planetary Sciences, University of Colorado at Boulder, Boulder, CO, USA.

H. Hasegawa
Institute of Space and Astronautical Science, JAXA, Sagamihara, Japan.

Yu. V. Khotyaintsev
IRF Swedish Institute of Space Physics, Uppsala, Sweden.

M. Swisdak
Institute for Research in Electronics and Applied Physics, University of Maryland, College Park, MD, USA.

F. Wilder
University of Texas at Arlington, Arlington, TX, USA.

dynamics in the surrounding plasma. Therefore, a complete picture of the onset, development, and interaction of magnetic reconnection with the surrounding plasma requires coupling it into the turbulent dynamics. The study of this interaction between turbulence and reconnection has a long history; however, recent high-resolution space plasma observations, notably from NASA's *Magnetospheric Multiscale* (*MMS*) mission, have allowed us to observationally examine this interaction in greater detail than ever before.

In this review, we discuss our current understanding of the interaction between magnetic reconnection and turbulence – particularly within the nearly collisionless plasma regime applicable to many space and astrophysical systems – from an observational, numerical, and theoretical perspective. Sec. 1.1 provides an overview of the varied ways through which turbulence and reconnection can influence each other. Sec. 1.2 provides an introduction to elements of turbulence theory geared toward those that may be less familiar with the statistical theory of turbulence. Section 2 discusses *turbulence-driven reconnection* in which reconnection occurs at thin current sheets created by the turbulent dynamics, with Earth's magnetosheath highlighted as a key example where recent progress has been made. Sec. 3 discusses *reconnection-driven turbulence* in which reconnection at a pre-existing current sheet excites turbulence, with Earth's magnetotail highlighted as a key region of recent progress. Sec. 4 discusses magnetic reconnection as an element in the process of large-scale structures transitioning to a turbulent state, with a focus on the Kelvin-Helmholtz Instability (KHI) on Earth's magnetopause. Sec. 5 discusses how the stochastic nature of turbulent environments may impact magnetic reconnection. Sec. 6 summarizes our current state of knowledge and provides an outlook for future areas of research.

1.1 The Interaction Between Magnetic Reconnection and Turbulence

The interaction between magnetic reconnection and turbulence is a complex topic with multiple facets and, as such, it has been examined from a variety of distinct viewpoints in the literature. It is, therefore, important to consider what is meant by the interaction between turbulence and reconnection for a given environment, which may include:

1. *Turbulence-Driven Reconnection* – Turbulent plasmas are well-known to generate many thin current structures embedded within the fluctuations associated with the sheared, twisted, and tangled magnetic field topologies set up by the turbulent dynamics, which can be sites where reconnection occurs (as illustrated in Fig. 1 inset). The nature of these current structures is fundamentally linked to an aspect of turbulence referred to as intermittency, in which the turbulent dynamics have a tendency to generate coherent structures with extreme gradients. Turbulence-driven reconnection can play a role in facilitating both the nonlinear dynamics and dissipation of the turbulent fluctuations. Assessing the importance of these reconnection events in a turbulent medium requires both information about the prevalence of magnetic reconnection at turbulent current sheets and an understanding of the key question of how magnetic reconnection partitions energy as discussed in Liu et al. (this collection).
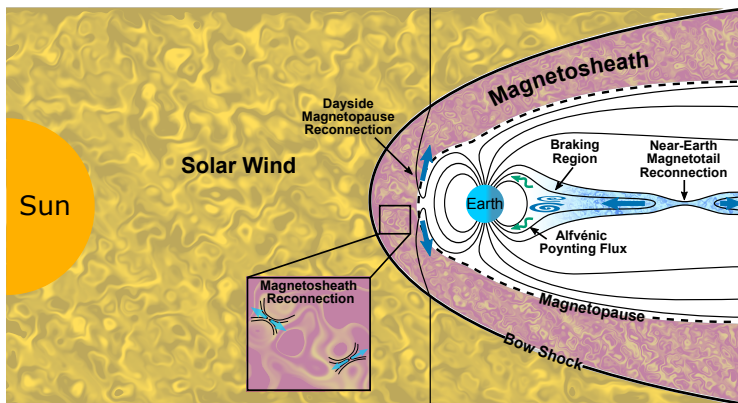
Fig. 1 Diagram illustrating the turbulent regions in near-Earth space along with the locations of the system-scale reconnection events associated with the Dungey cycle in Earth's magnetosphere. Turbulence can both interact with these system-scale reconnection events, as well as generate additional small-scale reconnection events within the turbulent regions.

2. *Reconnection-Driven Turbulence* – Space plasmas also contain regions where reconnection occurs at system-scale current sheets set up by the configuration of the system as a whole, such as the reconnecting current sheets associated with the Dungey cycle at Earth's magnetopause and in the magnetotail (as illustrated in Fig. 1), the heliospheric current sheet, or reconnection associated with the configuration of coronal loops on the Sun. Large-scale reconnection outflows associated with these current sheets can excite turbulent fluctuations in the system through the spontaneous destabilization of the outflows and the interaction of the outflow with the surrounding plasma. In this context, turbulence may impact the reconnection rate ($\mathcal{R}$) through anomalous resistivity/viscosity and can be thought of as a conduit through which energy released by reconnection is re-partitioned across different energy channels in the outflow (although it does not necessarily need to alter the net energy released).

3. *The Transition to Turbulence* – As well as system-scale reconnection driving turbulence, it can also be driven by other processes. Magnetic reconnection can play a key role as a secondary process in the transition of such systems into a fully-developed turbulent state. The degree to which this process can be clearly distinguished from *turbulence-driven reconnection* and *reconnection-driven turbulence* in observations may be more or less clear depending on the system in question; however, a good representative case where this transitory phase is readily accessible to spacecraft observations is the KHI on the flanks of Earth's magnetosphere. Numerical simulations of the development of turbulence from other initial configurations, including decaying Alfvénic turbulence (Franci et al., 2017) and systems of multiple current sheets (Gingell et al., 2017), have also highlighted the potential importance of reconnection in transitioning the initially large-scale fluctuations to a fully-developed turbulence.

4. *Stochastic Reconnection* – Whether reconnection self-generates turbulence or is embedded in a turbulent environment, the stochastic nature of magnetic field lines in a turbulent flow can potentially have a profound impact on the

global structure of the reconnection site. For example, the "rough" field line topology associated with the broadband distribution of fluctuations may lead to a broad, patchy region where the frozen-in flux theorem is violated and field line wandering in the turbulent flow may disperse field lines faster than otherwise expected. Since $\mathcal{R}$ is set by the aspect ratio of the diffusion region, these turbulent effects may significantly increase the reconnection rate if they play a dominant role in the dynamics. In this situation, $\mathcal{R}$ would no longer be controlled by microphysical effects, such as resistivity or collisionless processes, but instead by the properties of the turbulent fluctuations, such as the scale at which turbulent energy is injected into the system and fluctuation amplitudes.

While the above scenarios are not necessarily mutually exclusive, they provide a framework for conceptualizing different aspects of the complex multi-faceted interaction between reconnection and turbulence.

1.2 Concepts from Turbulence Theory

While many concepts in turbulence theory can be extended to more complete descriptions of collisionless plasmas, in this section we illustrate some of the basic concepts based on the simplest case of incompressible magnetohydrodynamics (MHD). When considering turbulent dynamics it can be useful to divide the particle and electromagnetic variables into spatially and temporally uniform average parts (denoted by subscript 0) and fluctuations about that mean (denoted by a leading δ), such that for an arbitrary quantity $\mathbf{g}(\mathbf{x}, t) = \mathbf{g}_0 + \delta\mathbf{g}(\mathbf{x}, t)$. Performing this decomposition, the incompressible MHD equations can be written as

$$\frac{\partial \delta\mathbf{u}}{\partial t} = -\overbrace{\frac{(\nabla \times \delta\mathbf{B}) \times \mathbf{B}_0}{\mu_0 \rho_0} - \frac{\nabla \delta p}{\rho_0}}^{Linear} \overbrace{- \delta\mathbf{u} \cdot \nabla \delta\mathbf{u} - \frac{(\nabla \times \delta\mathbf{B}) \times \delta\mathbf{B}}{\mu_0 \rho_0}}^{Nonlinear} + \overbrace{\nu \nabla^2 \delta\mathbf{u}}^{Dissipative} , \quad (1)$$

$$\frac{\partial \delta\mathbf{B}}{\partial t} = \nabla \times (\delta\mathbf{u} \times \mathbf{B}_0) + \nabla \times (\delta\mathbf{u} \times \delta\mathbf{B}) + \frac{\eta}{\mu_0} \nabla^2 \delta\mathbf{B}, \quad (2)$$

$$\nabla^2 \delta p = -\nabla \cdot \left(\frac{(\nabla \times \delta\mathbf{B}) \times \mathbf{B}_0}{\mu_0} \right) - \nabla \cdot \left(\rho_0 \delta\mathbf{u} \cdot \nabla \delta\mathbf{u} + \frac{(\nabla \times \delta\mathbf{B}) \times \delta\mathbf{B}}{\mu_0} \right), \quad (3)$$

where $\mathbf{u}$ is the single-fluid velocity with $\mathbf{u}_0$ taken to be zero since the equations are Galilean invariant, $\mathbf{B}$ is the (divergence free) magnetic field, p is the particle pressure, $\rho = \rho_0$ is the mass density that we have taken to be spatially and temporally uniform, and μ_0 is the vacuum permeability. We have included collisional viscous and resistive dissipation, which introduce the kinematic viscosity (ν) and the resistivity (η), for illustrative purposes; however, in collisionless plasmas dissipation occurs through kinetic process that are not present in the single-fluid MHD approximation. Eq. 3 follows from the incompressibility condition $\nabla \cdot \delta\mathbf{u} = 0$.

By dividing variables into mean and fluctuating parts, three classes of terms are apparent – 1) linear terms, which in isolation (e.g., for sufficiently small amplitude fluctuations, or if the dynamics preserve alignments that minimise the nonlinearities) give rise to linear wave modes, 2) nonlinear terms, which give rise to the turbulent dynamics, and 3) dissipative terms, which remove fluctuation energy from the system. In general, both linear and nonlinear terms contribute to the

dynamics in the fully nonlinear system and developing a theoretical description of the turbulence requires understanding the interplay between these dynamics. While under the right circumstances exact nonlinear solutions for, typically isolated, plasma structures may be possible, fully-developed turbulent systems are characterised by dynamics that are sufficiently nonlinear and made up of such a multitude of interacting structures and fluctuations that exact solutions to the equations become intractable.

The relative importance of the nonlinear to dissipative dynamics for a system can be estimated by comparing the typical amplitude of the nonlinear advection term $(-\mathbf{u} \cdot \nabla \mathbf{u})$ to the viscous dissipation term $(\nu \nabla^2 \mathbf{u})$ in Eq. 1 such that

$$\frac{|-\delta\mathbf{u} \cdot \nabla \delta\mathbf{u}|}{|\nu\nabla^2\delta\mathbf{u}|} \sim \frac{\mathcal{L}\mathcal{U}}{\nu} \equiv Re, \tag{4}$$

where $\mathcal{L}$ and $\mathcal{U}$ represent a characteristic length scale and velocity for the fluctuations. For MHD systems, two additional analogues to the Reynolds number can be defined based on the nonlinear Lorentz force term in Eq. 1 and the nonlinear magnetic advection term in Eq. 2. For sufficiently large Re, the nonlinear terms significantly dominate over the dissipative terms across a wide range of scales and the system becomes turbulent.

Nearly collisionless plasmas are by definition high-Re in the sense that $\nu \sim \eta \sim 0$; however, some care must be taken because, in the absence of collisions, kinetic phenomena associated with the breakdown of the fluid approximation can introduce dissipative effects at scales larger than those expected from collisions. An alternative way to interpret Re is as a measure of the scale separation between $\mathcal{L}$ and the so-called Kolmogorov microscale, defined as the scale ℓ_{kol} at which dissipative dynamics dimensionally become more important than the nonlinear dynamics, such that $Re = (\mathcal{L}/\ell_{kol})^{3/4}$. It has been suggested that an alternative way to characterize Re for collisionless plasmas is to consider the scale separation between $\mathcal{L}$ and the ion scales (Parashar et al., 2019).

The relative importance of the nonlinear to linear terms can be estimated by the dimensionless parameter

$$\chi = \frac{\tau_L}{\tau_{NL}} \tag{5}$$

where $\tau_L = \omega_L^{-1}$ is the linear timescale given by the inverse of the frequency of the associated wave and τ_{NL} is the timescale associated with the nonlinear dynamics of interest. If $\chi > 1$, nonlinear interactions are faster than linear dynamics (i.e., the propagation of linear waves) and the nonlinear dynamics dominate the behavior, while, if $\chi < 1$, the linear dynamics are faster than the nonlinear interactions. Eq. 5 is dimensionally equivalent to comparing the amplitudes of the nonlinear and linear terms in a given equation in analogy to the definition of Re; however, χ is more typically framed in terms of the ratio of timescales as this definition lends itself to comparing the importance of the nonlinear dynamics to the normal modes of the system. While in Eqs. 1 − 3, we have split the linear and nonlinear dynamics based on the global $\mathbf{B}_0$, it can also be illustrative to treat $\mathbf{B}_0$ as a scale dependant or locally defined quantity, with the conceptual picture that small-scale fluctuations see their locally averaged field as the background.

1.2.1 Cross-Scale Energy Transfer

Given the complex multiscale nature of turbulent systems, theoretical descriptions are typically formulated in terms of statistical properties of the ensemble of interacting fluctuations - either in physical or spectral space. In physical space, the autocorrelation tensor for an arbitrary variable $\mathbf{g}(\mathbf{x})$ is given by

$$R_{ij}^g(\mathbf{x}, \boldsymbol{\ell}) = \langle \delta g_i(\mathbf{x} + \boldsymbol{\ell}) \, \delta g_j(\mathbf{x}) \rangle, \tag{6}$$

where $\langle ... \rangle$ represents an ensemble average. The correlation function associated with the total fluctuation energy in $\mathbf{g}(\mathbf{x})$ is given by the trace of R_{ij}^g, such that $R^g(\mathbf{x}, \boldsymbol{\ell}) = \langle \delta \mathbf{g}(\mathbf{x} + \boldsymbol{\ell}) \cdot \delta \mathbf{g}(\mathbf{x}) \rangle$, while the off-diagonal part of the tensor encodes information about the helicity of the fluctuations (Matthaeus and Goldstein, 1982). One common measure of the characteristic scale associated with $\delta \mathbf{g}$ is the correlation length $(\lambda_{C,g})$ defined as

$$\lambda_{C,g} = \frac{1}{R^g(0)} \int_0^\infty R^g(\boldsymbol{\ell}) \, d\ell, \tag{7}$$

which represents the scale over which structures in $\delta \mathbf{g}$ decorrelate and can have different values along different directions if $R^g(\boldsymbol{\ell})$ is an anisotropic function.

The 2nd-order structure function is given by

$$S_2^{g_i}(\mathbf{x}, \boldsymbol{\ell}) = \langle [\Delta g_i(\mathbf{x}, \boldsymbol{\ell})]^2 \rangle = \langle g_i(\mathbf{x} + \boldsymbol{\ell}) - g_i(\mathbf{x}) \rangle. \tag{8}$$

with the total fluctuation energy in $\delta \mathbf{g}$ associated with $S_2^g(\mathbf{x}, \boldsymbol{\ell}) = \langle |\Delta \mathbf{g}(\mathbf{x}, \boldsymbol{\ell})|^2 \rangle$. A simplifying assumption often, but not always, made in turbulence theory, is that fluctuations are statistically homogeneous and average quantities do not depend on $\mathbf{x}$. In this case there is a relationship between $R_{ii}^g(\boldsymbol{\ell})$ and $S_2^{g_i}(\boldsymbol{\ell})$, such that

$$S_2^{g_i}(\boldsymbol{\ell}) = 2R_{ii}^g(0) - 2R_{ii}^g(\boldsymbol{\ell}). \tag{9}$$

The statistical evolution of the turbulence can be considered by re-expressing Eqs. 1-3 as equations for the evolution of the structure functions or correlation functions associated with the total (bulk kinetic + magnetic) fluctuation energy (i.e., $S_2(\boldsymbol{\ell}) = S_2^u(\boldsymbol{\ell}) + S_2^{B_A}(\boldsymbol{\ell})$ or $R(\boldsymbol{\ell}) = R^u(\boldsymbol{\ell}) + R^{B_A}(\boldsymbol{\ell})$ where $\mathbf{B}_A = \mathbf{B}/\sqrt{\mu_0 \rho}$). For $S_2(\boldsymbol{\ell})$, this gives (Politano and Pouquet, 1998a; Adhikari et al., 2023)

$$\frac{\partial S_2(\boldsymbol{\ell})}{\partial t} = \mathcal{P}(\boldsymbol{\ell}) - \frac{\partial}{\partial \boldsymbol{\ell}} \cdot \mathbf{Y}(\boldsymbol{\ell}) + 2D(\boldsymbol{\ell}) - 4\epsilon, \tag{10}$$

where $\mathcal{P}(\boldsymbol{\ell})$ describes the injection of fluctuation energy into the system through some external driving (such driving was not explicitly included in Eqs. 1-3 but is included here to aid in the interpretation of Eq. 10), $\mathbf{Y}(\boldsymbol{\ell}) = \langle \Delta \mathbf{u}(\boldsymbol{\ell}) |\Delta \mathbf{u}(\boldsymbol{\ell})|^2 + \Delta \mathbf{u}(\boldsymbol{\ell}) |\Delta \mathbf{B}_A(\boldsymbol{\ell})|^2 - 2\Delta \mathbf{B}_A(\boldsymbol{\ell}) [\Delta \mathbf{u}(\boldsymbol{\ell}) \cdot \Delta \mathbf{B}_A(\boldsymbol{\ell})] \rangle$ is a mixed 3rd-order structure function encoding the effect of the nonlinear terms, $D(\boldsymbol{\ell}) = \nu \frac{\partial^2}{\partial \boldsymbol{\ell}^2} S_2^u(\boldsymbol{\ell}) + \frac{\eta}{\mu_0} \frac{\partial^2}{\partial \boldsymbol{\ell}^2} S_2^u(\boldsymbol{\ell})$ describes the impact of dissipation, and ϵ is the average energy dissipation rate in the system. Eq. 10 highlights the closure problem that is one of the core challenges of developing a complete theory of turbulence – the evolution of $S_2(\boldsymbol{\ell})$ or any statistical quantity requires knowledge of higher-order structure functions such as $\mathbf{Y}(\boldsymbol{\ell})$, the evolution of which, in turn, require knowledge of progressively higher-order structure functions.

For turbulent systems in a statistically steady state, such that $\partial_t S_2\left(\boldsymbol{\ell}\right) = 0$, it is assumed that there will be a significant scale separation between the scales where $\mathcal{P}\left(\boldsymbol{\ell}\right)$ is significant and the scales where $D\left(\boldsymbol{\ell}\right)$ is significant. In order for Eq. 10 to be satisfied at intermediate scales, there must then be a range of scales - typically referred to as the *inertial range* - over which the $\mathbf{Y}\left(\boldsymbol{\ell}\right)$ term dominates and Eq. 10 reduces to

$$\frac{\partial}{\partial\boldsymbol{\ell}}\cdot\mathbf{Y}\left(\boldsymbol{\ell}\right) = -4\epsilon. \tag{11}$$

Eq. 11 gives an exact relationship between $\mathbf{Y}\left(\boldsymbol{\ell}\right)$ and ϵ, describing the role of the nonlinear dynamics in transporting energy across scales from the driving to the dissipation scales (Politano and Pouquet, 1998b,a) (see also, Kolmogorov (1941b) or Frisch (1995) for a discussion of Eq. 11 for hydrodynamics; and Marino and Sorriso-Valvo (2023) for a complete review of the derivation in plasmas).

Eq. 11 can also be extended to more general cases than homogeneous incompressible MHD, for example by including background velocity shears (Wan et al., 2009; Stawarz et al., 2011), compressibility (Banerjee and Galtier, 2013), or the Hall effect (Hellinger et al., 2018; Ferrand et al., 2019). The above expression, or variants of it, have been widely applied in both numerical simulations and observations to estimate the energy dissipation rate in turbulent plasmas (e.g. MacBride et al., 2005; Marino et al., 2008; Stawarz et al., 2009; Hadid et al., 2018; Bandyopadhyay et al., 2020). Applications of Eq. 11 to spacecraft data typically require assumptions about the average geometry of the fluctuations to simplify the divergence with respect to $\boldsymbol{\ell}$, with common examples being isotropy for which $\mathbf{Y}\left(\boldsymbol{\ell}\right)$ has no angular dependence (Politano and Pouquet, 1998a) or hybrid anisotropic geometries with separable variations parallel and perpendicular to the magnetic field (MacBride et al., 2008; Stawarz et al., 2009). However, multispacecraft measurements can be used to explicitly evaluate the divergence (Osman et al., 2011; Pecora et al., 2023) and alternative formulations may also provide ways to estimate ϵ without implicit assumptions about anisotropy (Banerjee and Galtier, 2017).

While the above formalism is typically derived and applied in the context of homogeneous turbulent systems, a series of recent studies (Adhikari et al., 2020, 2021, 2023, 2024), have explored the application of Eq. 10 to traditional periodic reconnection simulations (where reconnection is initiated in idealised current sheets at the scale of the periodic box) both with and without guide fields. In these works, it was found that the behavior of the terms in Eq. 10 are qualitatively similar to that found in fully developed turbulent systems, suggesting that the nonlinear dynamics associated with the reconnection process may, in some sense, embody an energy-cascade-like process.

Analogs of Eq. 10 can also be derived in spectral space (e.g., Alexakis et al., 2005; Grete et al., 2017) or using scale-filtering approaches, where a coarse-graining kernel is used instead of structure functions (Aluie, 2017; Yang et al., 2017; Manzini et al., 2022). In spectral space, the analogue of $R^g\left(\boldsymbol{\ell}\right)$ is the energy spectral density, $\mathcal{E}_g\left(\mathbf{k}\right)$. For statistically homogeneous fluctuations, $\mathcal{E}_g\left(\mathbf{k}\right)$ is the Fourier transform of $R^g\left(\boldsymbol{\ell}\right)$ and, given Eq. 9, is also the Fourier transform of $S_2^g\left(\boldsymbol{\ell}\right)$ for $\mathbf{k}\neq 0$. By manipulating the Fourier transforms of Eqs. 1-3 into an expression for the evolution of $\mathcal{E}\left(\mathbf{k}\right) = \mathcal{E}_u\left(\mathbf{k}\right) + \mathcal{E}_{B_A}\left(\mathbf{k}\right)$ or taking the Fourtier transform of Eq. 10 with respect to $\boldsymbol{\ell}$, a spectral representation of Eq. 10 can be obtained (e.g., Pope, 2000)

$$\frac{\partial\mathcal{E}\left(\mathbf{k}\right)}{\partial t} = \mathcal{P}\left(\mathbf{k}\right) + \mathcal{T}\left(\mathbf{k}\right) - 2D\left(\mathbf{k}\right) \tag{12}$$

where $\mathcal{T}(\mathbf{k})$ is the analogue of $-\frac{\partial}{\partial \boldsymbol{\ell}} \cdot \mathbf{Y}(\boldsymbol{\ell})$ – referred to as the transfer function in this context – and $\mathcal{P}(\mathbf{k})$ and $\mathcal{D}(\mathbf{k})$ are the Fourier transforms of $\mathcal{P}(\boldsymbol{\ell})$ and $\mathcal{D}(\boldsymbol{\ell})$, respectively. $\mathcal{T}(\mathbf{k})$ in general takes the form of a complex set of convolutions associated with the nonlinear terms, representing the net transfer of energy to/from wavevector $\mathbf{k}$ due to the sum of all possible interactions between other wavevectors and can be related to the cross-scale energy flux, $\boldsymbol{\Pi}(\mathbf{k})$, through a surface in $\mathbf{k}$-space, such that $\mathcal{T}(\mathbf{k}) = -\frac{\partial}{\partial \mathbf{k}} \cdot \boldsymbol{\Pi}(\mathbf{k})$. Often Eq. 12 is integrated over spherical shells and $\Pi(k)$ is interpreted as the isotropic energy flux; however, other surfaces may be relevant to different types of anisotropy (Yokoyama and Takaoka, 2021).

The spectral representation highlights two key assumptions often invoked in turbulence theory - 1) that the nonlinear interactions are local in k-space, such that the dominant contributions to the convolutions come from wave vectors with similar magnitudes and 2) that the magnitude of $\Pi(k) = \epsilon$ and is constant as a function of k. With these two assumptions, the conceptual picture of the *energy cascade* through the internal range emerges, where nonlinear interactions incrementally transport energy from scale-to-scale at a constant rate, which in a statistically steady-state, is equal to the average energy dissipation rate. Consequently, ϵ is often referred to as the energy cascade rate in turbulent systems. While the large-scale nonlinear dynamics set the flux of energy to the small scales, for collisionless plasmas understanding which processes are responsible for dissipating that energy remains a key challenge and in Sec. 2.3 we discuss the potential role reconnection may play in turbulent dissipation.

1.2.2 Energy Spectra

The shape of $\mathcal{E}(\mathbf{k})$ or $S_2(\boldsymbol{\ell})$ in the inertial range can be estimated by making assumptions about the nature of the dominant nonlinear interactions. The basic ingredients for estimating these scalings amount to 1) taking ϵ to be independent of scale within the inertial rage and 2) estimating the timescale τ_{tr} over which nonlinear interactions transfer energy between scales under a given set of assumptions. Relating $\mathcal{E}(\mathbf{k})$ to τ_{tr} dimensionally gives

$$\mathcal{E}(k) \sim \epsilon \frac{\tau_{tr}}{k}, \tag{13}$$

where, for simplicity, we have assumed the fluctuations are isotropic (although this assumption can be relaxed).[1] In principle, τ_{tr} can be a function of scale, the geometry of the fluctuations, and the physical properties of the medium, and its dependence on these parameters is intrinsically linked to the nature of the underlaying nonlinear interactions enabling the cascade, leading to different predictions for $\mathcal{E}(\mathbf{k})$. This link between predictions for the shape of $\mathcal{E}(\mathbf{k})$ and the nature of the nonlinear dynamics is one reason why $\mathcal{E}(\mathbf{k})$ is an important observable quantity for understanding turbulent dynamics, although it does not provide the full

---

[1] The units of $\mathcal{E}(\mathbf{k})$ are such that when integrated over all $\mathbf{k}$ it gives the average total fluctuation energy in the system, such that the quantity $\mathcal{E}(\mathbf{k}) d^3\mathbf{k}$ has units of energy. In some situations it is useful to consider the isotropic (omnidirectional) energy spectrum, defined such that $\mathcal{E}(k) dk$ has units of energy, and in plasmas it is often useful to consider the gyrotropically integrated spectrum, defined such that $\mathcal{E}(k_{||}, k_\perp) dk_{||} dk_\perp$ has units of energy. Furthermore, in the gyrotropic case, it is sometimes useful to consider the spectra marginalized over $k_{||}$ or $k_\perp$, such that $\mathcal{E}(k_\perp) dk_\perp$ and $\mathcal{E}(k_{||}) dk_{||}$ have units of energy, respectively.

Table 1 Summary of example models for the turbulent energy spectrum.

Model	τ_{tr}	Spectral Prediction	Anisotropy
Kolmogorov[a]	$\tau_{NL} \sim \frac{1}{k\delta u(k)}$	$\mathcal{E}(k) \sim \epsilon^{2/3} k^{-5/3}$	Isotropic
Iroshnikov[b]-Kraichnan[c]	$\frac{\tau_{NL}}{\chi} \sim \frac{V_A}{k[\delta u(k)]^2}$	$\mathcal{E}(k) \sim (\epsilon V_A)^{1/2} k^{-3/2}$	Isotropic
Weak Alfvénic[d]	Derived exactly assuming $\chi \ll 1$	$\mathcal{E}(k_{\|\|}, k_\perp) \sim f(k_{\|\|})(\epsilon V_A)^{1/2} k_\perp^{-2}$	Purely $\perp$
Goldreich-Sridhar[e]	$\chi \sim 1 \to \frac{1}{k_\perp \delta u_\perp(k_\perp)} \sim \frac{1}{k_{\|\|} V_A}$	$\mathcal{E}(k_\perp) \sim \epsilon^{2/3} k_\perp^{-5/3}$	$k_{\|\|} \sim \epsilon^{1/3} V_A^{-1} k_\perp^{2/3}$
Dynamic Alignment[f]	$\chi \sim 1 \to \frac{V_A}{k_\perp[\delta u_\perp(k_\perp)]^2} \sim \frac{1}{k_{\|\|} V_A}$	$\mathcal{E}(k_\perp) \sim (\epsilon V_A)^{1/2} k_\perp^{-3/2}$	$k_{\|\|} \sim \epsilon^{1/2} V_A^{-3/2} k_\perp^{1/2}$
Strong Hall MHD[g]	$\tau_{NL} \sim \frac{1}{d_i k^2 \delta B(k)}$	$\mathcal{E}(k) \sim \mathcal{E}_B(k) \sim \epsilon^{2/3} d_i^{-2/3} k^{-7/3}$	Isotropic

[a]Kolmogorov (1941a); [b]Iroshnikov (1964); [c]Kraichnan (1965); [d]Galtier et al. (2000);
[e]Goldreich and Sridhar (1995); [f]Boldyrev (2006); [g]Biskamp et al. (1999)

picture as discussed in Sec. 1.2.3. Single spacecraft measurements are capable of providing spacecraft-frame frequency spectra; however, assuming the background flow ($\mathbf{U}_0$) is sufficiently fast, comparisons can be made between observed spectra and theoretical predictions for $\mathcal{E}(\mathbf{k})$ by employing the so-called Taylor hypothesis discussed in Appendix A. Table 1 illustrates some example models for $\mathcal{E}(\mathbf{k})$. The first five models are based on MHD, while the final model gives an example for sub-proton-scale dynamics.

Strongly nonlinear models where $Re \gg 1$ and $\chi \gg 1$, as in the *Kolmogorov* model, assume τ_{tr} is governed by the nonlinear timescale (τ_{NL}) associated with the advection terms. Kolmogorov (1941a) originally applied this model to incompressible hydrodynamic turbulence, predicting the well-known $k^{-5/3}$-spectrum. However, since the additional nonlinear advective and Lorentz force terms in the MHD equations are dimensionally equivalent to the advective term in hydrodynamics, an analogous approach can be taken with incompressible MHD, producing an equivalent spectral prediction (Biskamp and Müller, 2000).

On the other hand, the introduction of a magnetic field, as well as other effects such as compressibility, collisionless dynamics, etc., also introduces linear terms describing the effect of waves. For $Re \gg 1$ and $\chi \ll 1$, often referred to as "weak" or "wave" turbulence, nonlinear interactions are strongly mediated by wave-like dynamics. The *Iroshnikov-Kraichnan* model is a simple isotropic model for incompressible MHD in this regime, whereby τ_{tr} is lengthened by a factor of χ^{-1}, since multiple "collisions" between propagating Alfvén wave packets are required for the nonlinearities to fully distort the wave packets and transfer fluctuation energy across scales if the wave propagation is much faster than the nonlinear timescale, resulting in a $k^{-3/2}$-spectrum. However, in the weak turbulence regime, exact analytical progress can also be made (Nazarenko, 2011; Galtier, 2023). Galtier et al. (2000) applied weak turbulence formalism to derive a *weak Alfvénic* model for incompressible MHD, illustrating that, in the limit of weak turbulence, the cascade is fundamentally anisotropic with the cascade of energy proceeding purely in the direction perpendicular to $\mathbf{B}_0$ and resulting in a spectrum scaling as $k_\perp^{-2}$ and following an arbitrary function of $k_{\|\|}$ set by the driving.

Anisotropic strong turbulence models, such as the *Goldreich-Sridhar* and *Dynamic Alignment* models, often incorporate a constraint known as critical balance, whereby $\chi \sim 1$ such that the linear and nonlinear terms balance scale-by-scale. In these models, τ_{tr} is again related to τ_{NL} associated with nonlinear advection,

except now the nonlinear interaction is assumed to be inherently anisotropic with only $k_\perp$ contributing to the nonlinear interaction. Since the dispersion relation for Alfvén waves is also anisotropic, the critical balance constraint then provides a prediction for the anisotropy of the spectrum. While the *Goldreich-Sridhar* model essentially applies analogous phenomenology as the *Kolmogorov* model to predict a $k_\perp^{-5/3}$-spectrum, the *Dynamic Alignment* model argues that geometrical constraints associated with the strength of $\mathbf{B}_0$ reduce the the efficiency of nonlinear interactions, producing a $k_\perp^{-3/2}$-spectrum reminiscent of the *Iroshnikov-Kraichnan* model but based on different phenomenological arguments.

The same general framework can be used in systems where other nonlinearities play a dominant role, such as at sub-proton-scales where the single-fluid MHD approximation breaks down. The *Strong Hall MHD* model provides an example of analysing the nonlinear Hall term in the induction equation under the assumption that the Hall term significantly dominates the dynamics (often referred to as electron-MHD) in a manner similar to the *Kolmogorov* model. In this situation, $\mathbf{B}$ carries the majority of the fluctuation energy and, because of the presence of an additional derivative in the Hall term, a steeper $k^{-7/3}$-spectrum is obtained. However, other analyses of the sub-proton scale dynamics, such as critical balance models invoking kinetic-scale wave modes like whistler waves (Narita and Gary, 2010; Boldyrev et al., 2013; Narita, 2016), kinetic Alfvén waves (Boldyrev and Perez, 2012), and inertial kinetic Alfvén waves (Chen and Boldyrev, 2017), are also commonly employed to explain spacecraft observations.

The models discussed above implicitly assume turbulent fluctuations are space-filling and self-similar. Violations of this assumption, discussed further in Sec. 1.2.3, may also have an impact on $\mathcal{E}(\mathbf{k})$. Such corrections to predicted power laws have been proposed and are often invoked, particularly at sub-proton-scales, to explain steeper power laws of $\sim k^{-2.8}$ or $\sim k^{-3}$ in space plasmas (Boldyrev and Perez, 2012). Other complexities may also be present that are not illustrated in the examples provided in Table 1, such as constraints on the alignments between fluctuations in different vector fields that may be imposed by other conserved quantities (e.g., magnetic helicity, cross helicity, or generalized helicity) (Pouquet et al., 2019; Meyrand et al., 2021; Squire et al., 2022). In Sec. 2.3, we discuss further how reconnection, in particular, may alter $\mathcal{E}(\mathbf{k})$.

1.2.3 Intermittency & Current Sheets

The energy spectrum on its own does not provide the full picture of turbulence. Notably, turbulent systems are not simply comprised of uncorrelated randomly superposed normal modes and, in fact, phase correlations between modes at different scales are spontaneously generated by the nonlinear dynamics. These phase correlations manifest as localized *coherent structures* in physical space. Coherent structures can take the form of vorticity sheets and filaments in hydrodynamics (Okamoto et al., 2007) and, with the inclusion of $\mathbf{B}$, current sheets and magnetic discontinuities, among other complex structures (Mininni et al., 2006; Greco et al., 2009; Uritsky et al., 2010; Matthaeus et al., 2015). This feature of turbulence is referred to as *intermittency*, so-called because it results in a statistically non-uniform "intermittent" distribution of dissipative structures in the domain. A key aspect of intermittency is that it violates the assumed self-similar and space-filling nature

of the nonlinearly interacting fluctuations that are an inherent feature of many
of the theoretical models discussed in Sec. 1.2.2. Magnetic shears associated with
coherent structures (e.g. current sheets or more generalized current structures)
are potential sites where reconnection can occur in turbulent plasmas. The in-
trinsic link between the intermittent nature of the turbulence and the statistical
properties (e.g., structure, prevalence, distribution throughout the domain, etc.) of
coherent structures means intermittency is likely an important feature to consider
in the case of turbulence-driven reconnection.

Intermittency is typically analyzed by examining higher-order statistics, such
as the pth-order structure functions given by

$$S_p^g\left(\boldsymbol{\ell}\right) = \langle[\Delta g\left(\boldsymbol{\ell}\right)]^p\rangle. \tag{14}$$

While $S_2\left(\boldsymbol{\ell}\right)$ has a direct relationship to $\mathcal{E}\left(\mathbf{k}\right)$, higher-order statistics encode ad-
ditional information about cross-scale correlations. The Kolmogorov (1941a) the-
ory of turbulence, which does not include the effect of intermittency, predicts
$S_p^{u_\ell}\left(\boldsymbol{\ell}\right) \sim \ell^{\zeta_p}$ with $\zeta_p = p/3$ and u_ℓ the component of $\mathbf{u}$ along $\boldsymbol{\ell}$. Turbulent sys-
tems typically exhibit strong deviations from this scaling, with increasingly sub-$p/3$
scalings as p increases, in both hydrodynamic (Anselmet et al., 1984) and plasma
systems (Marsch and Tu, 1997; Biskamp and Müller, 2000). Toy models, such as
so-called β, multi-fractal, and random cascade models (see Frisch (1995) for a de-
tailed discussion), which relax assumptions about self-similarity and the statistical
homogeneity of dissipation in various ways, demonstrate that intermittency offers
an explanation for this behavior.

While some numerical studies indicate intermittency is more intense in MHD
than hydrodynamics (Biskamp and Müller, 2000), observations from the solar
wind suggest, at sub-proton-scales ζ_p is linear with p, as in the non-intermittent
case (Kiyani et al., 2009). The behavior at sub-proton-scales may not be univer-
sal, however, with observations in Earth's magnetosheath (Chhiber et al., 2018)
and numerical simulations (Franci et al., 2015), continuing to show signatures of
intermittency well into the sub-proton-scales. A complete understanding of this
variation behaviour, remains an open question and may suggest a dynamically
significant variation in the nature or distribution of nonlinear fluctuations at sub-
proton-scales across different turbulent environments.

Since $S_p^g\left(\boldsymbol{\ell}\right)$ are the statistical moments of the distribution of increments $\Delta g\left(\boldsymbol{\ell}\right)$,
characterizing intermittency can be framed as considering how the probability dis-
tribution function of increments varies with scale. Typically distributions of $\Delta\mathbf{u}\left(\boldsymbol{\ell}\right)$
or $\Delta\mathbf{B}\left(\boldsymbol{\ell}\right)$ exhibit nearly Gaussian shapes for large ℓ and become progressively
more heavy-tailed (larger than Gaussian probability of extreme values) for small ℓ
(Frisch, 1995; Sorriso-Valvo et al., 1999). Given the heavy-tailed nature of the dis-
tributions, one common measure of intermittency is the scale-dependant kurtosis
given by $\kappa\left(\ell\right) = S_4^g\left(\boldsymbol{\ell}\right)/\left[S_2^g\left(\boldsymbol{\ell}\right)\right]^2$, which is expected to have a value of 3 at large
ℓ where the distribution is Gaussian and then become increasingly larger through
the inertial range (Wu et al., 2013). Heuristically, this behavior can be understood
from the fact that at large separations ($\gg \lambda_{C,g}$), quantities at two different points
will be uncorrelated and $\Delta g\left(\boldsymbol{\ell}\right)$ will be an uncorrelated random variable, while at
small separations $\Delta g\left(\boldsymbol{\ell}\right)$ will be sensitive to the gradients in these quantities, which
are spatially inhomogeneous and intermittent. In fact, detailed examinations of the
distributions of the vorticity and current density in turbulent plasmas present a

picture where particularly intense vorticity and current structures form at the interfaces between large regions of reduced nonlinear activity, consistent with the heavy-tailed distributions (Servidio et al., 2008; Greco et al., 2009; Pecora et al., 2021, 2023). Furthermore, locating extreme values in $\Delta g\left(\boldsymbol{\ell}\right)$ has been proposed as a means of identifying coherent (potentially dissipative) structures, e.g., by examining the so-called partial variance of increments ($PVI = \Delta g\left(\boldsymbol{\ell}\right)/\sqrt{S_2^g\left(\boldsymbol{\ell}\right)}$; Greco et al. (2009)) or the integrands of $\mathbf{Y}\left(\boldsymbol{\ell}\right)$ (i.e., $\Delta\mathbf{u}\left(\boldsymbol{\ell}\right)\left|\Delta\mathbf{u}\left(\boldsymbol{\ell}\right)\right|^2$, $\Delta\mathbf{u}\left(\boldsymbol{\ell}\right)\left|\Delta\mathbf{B}_A\left(\boldsymbol{\ell}\right)\right|^2$, and $\Delta\mathbf{B}_A\left(\boldsymbol{\ell}\right)\left[\Delta\mathbf{u}\left(\boldsymbol{\ell}\right)\cdot\Delta\mathbf{B}_A\left(\boldsymbol{\ell}\right)\right]$; Sorriso-Valvo et al. (2018)).

2 Turbulence-Driven Reconnection

In situ spacecraft observations of turbulent plasmas in near-Earth space, such as the solar wind (Greco et al., 2009), magnetosheath (Gingell et al., 2021; Schwartz et al., 2021), and plasma sheet (Ergun et al., 2018), are filled with current structures and associated magnetic shears that can be sites of reconnection. The extent to which reconnection is self-consistently initiated at these current sheets and the impact that this has on the turbulent dynamics has long been a topic of interest and there is a rich body of literature attempting to explore this issue both observationally and in numerical simulations.

The solar wind is one region of turbulence that has been extensively studied with *in situ* spacecraft observations. Numerous studies have provided evidence for reconnection exhausts at solar wind current sheets (Gosling et al., 2005; Gosling, 2007; Phan et al., 2020; Eriksson et al., 2022; Fargette et al., 2023). However, solar wind reconnection exhausts are often encountered hundreds or even thousands of ion inertial lengths (d_i) away from the x-line (Mistry et al., 2015b), suggesting that reconnecting current sheets in the solar wind extend over large length-scales. It is, therefore, challenging to distinguish reconnecting current sheets in the solar wind that may be self-consistently generated by the turbulent dynamics from those associated with the evolution of large-scale solar wind structure (e.g., heliospheric current sheet, stream interaction regions, coronal mass ejections) and it remains an open question as to the extent to which these two populations contribute to the identified reconnection exhausts in the solar wind (Eriksson et al., 2022). Recently, however, there has been new progress in observationally examining turbulence-driven magnetic reconnection in Earth's magnetosheath, where high-resolution measurements from *MMS* have provided evidence for small-scale reconnection events embedded within the recently excited turbulent fluctuations downstream of Earth's bow shock.

2.1 Bow Shock & Magnetosheath Reconnection

Earth's bow shock forms at the interface between the solar wind and Earth's magnetosphere, where the super-Alfvénic solar wind suddenly slows down to a sub-Alfvénic speed due to Earth's strong magnetic field and the kinetic energy in the solar wind is converted to magnetic, thermal, and fluctuation energy. In the shock, the electron motion is frozen-in to $\mathbf{B}$, while the ion motion is decoupled from the electron motion and $\mathbf{B}$. Ions can penetrate deep inside the shock transition layer without gyration and, as a result, a shock potential is generated, which

reflects some ions to produce ion beams propagating upstream of the shock. The ion-ion beam instability caused by the reflected and solar wind ion populations generates large amplitude electromagnetic waves and the plasma in the shock becomes turbulent. Particles crossing the shock are rapidly heated, forming a region downstream of the shock where $|\mathbf{B}|$, number density (n), and temperature (T) are enhanced compared to the upstream solar wind - referred to as the magnetosheath.

Fluctuations in the magnetosheath have features consistent with turbulent dynamics, including broadband power law spectra as discussed in Sec. 1.2.2 (Sahraoui et al., 2006; Alexandrova et al., 2008; Huang et al., 2014, 2017), higher-order statistics consistent with intermittency as discussed in Sec. 1.2.3 (Yordanova et al., 2008; Chhiber et al., 2018), and evidence of an active cross-scale energy cascade as discussed in Sec. 1.2.1 (Hadid et al., 2018; Bandyopadhyay et al., 2018, 2020). In contrast to the solar wind, magnetosheath fluctuations typically have a much shorter λ_C that varies from tens to hundreds of d_i (Stawarz et al., 2022). Furthermore, other fluctuation properties - such as the MHD-scale spectral index and turbulent Mach number (ratio of velocity fluctuation amplitude to sound speed) - also vary across the magnetosheath (Huang et al., 2017; Li et al., 2020). These features suggest that the processing of the solar wind plasma by the shock, potentially through processes such as large-amplitude wave-generation associated with the quasi-parallel shock, temperature anisotropy instabilities downstream of the shock, or the interaction of turbulent fluctuations in the solar wind with the shock (Omidi et al., 1994; Bessho et al., 2020; Trotta et al., 2023), drives new fluctuations into the system that interact nonlinearly and evolve into a turbulent state.

Spacecraft observations demonstrate these fluctuations are associated with many current sheets. Using *Cluster* observations, Retinò et al. (2007) found that, among the turbulent current sheets in Earth's magnetosheath, there are current sheets with signatures of reconnection. Retinò et al. (2007) showed that the thickness of one such reconnecting current sheet was $\sim d_i$ and observed the out-of-plane reconnection $\mathbf{E}$, the quadrupolar Hall $\mathbf{B}$, the bipolar Hall $\mathbf{E}$ pointing toward the center of the current sheet, and a positive value of $\boldsymbol{j} \cdot \boldsymbol{E}$, indicating energy exchange from the electromagnetic fields to the particles in accordance with Poynting's theorem. The reconnection outflow inferred from the $\mathbf{E} \times \mathbf{B}$ drift was 0.1 times the Alfvén speed, indicating $\mathcal{R} \sim 0.1$. Notably, due to the small length scale, and associated short time scale over which the event was advected over the spacecraft, all of the signatures of turbulence-driven magnetosheath reconnection identified with *Cluster* were obtained from the electromagnetic field measurements.

Subsequent *MMS* observations also revealed many reconnecting current sheets in the magnetosheath. Yordanova et al. (2016) and Vörös et al. (2016) identified several reconnecting current sheets in Earth's magnetosheath, where reconnection outflows and enhancements of $\boldsymbol{j} \cdot \boldsymbol{E}$ were observed. Vörös et al. (2016) detected electron diffusion region (EDR) signatures by investigating the decoupling of the electron velocity from the $\mathbf{E} \times \mathbf{B}$ drift, the agyrotropy parameter Q (Swisdak, 2016), and electron distribution functions. Inside the EDR, $\boldsymbol{j} \cdot \boldsymbol{E'}$, where $\boldsymbol{E'} = \boldsymbol{E} + \boldsymbol{u_e} \times \boldsymbol{B}$, was positive, indicating conversion of magnetic energy to particle kinetic and thermal energy via the non-ideal $\mathbf{E}$.

Phan, et al. (2018) examined two nearby segments of high-resolution burst data from *MMS* in detail, totalling ~ 21 minutes of magnetosheath observations, revealing that while many current sheets had evidence of reconnection in the form of electron outflows, none had clear evidence of ion outflows. The relative lack of

clear ion outflows was despite the fact that fully accelerated ion outflows should occupy a larger volume of space – and thus should be statistically more likely to be encountered – than the ion diffusion region (IDR), where fully accelerated ion outflows would not be expected. Since electrons appeared to be the only species participating in the reconnection process, this type of reconnection has come to be known as "electron-only" reconnection. An example of one electron-only reconnection event identified by Phan, et al. (2018) is shown in Fig. 2a–j. For the event in Fig. 2a–j the thickness of the current sheet was significantly thinner than the ion scales at ~ 4 electron inertial lengths (d_e). During the current sheet crossing, *MMS3* observed super-Alfvénic electron outflows of ~ 250 km/s in the outflow direction (L direction) relative to an Alfvén speed associated with the reconnecting component of the field of $V_{A,L} \sim 25$ km/s. The other three *MMS* spacecraft also observed super-Alfvénic electron outflows, but in the opposite direction, providing direct evidence for the two oppositely directed jets. The electrons in the current sheet were not frozen-in to $\mathbf{B}$, and a large $E_{||}$ was observed, producing a large $\mathbf{j} \cdot \mathbf{E}'$. It was proposed that the reason ions did not appear to be participating in the reconnection process was because the length of the current sheets along the outflow direction was short enough that there was not enough time/space for the reconnected $\mathbf{B}$ to accelerate ion jets before the field fully relaxed. This picture was supported by idealized numerical experiments, where the lengths of reconnecting current sheets were artificially constrained – resulting in reconnection with unique properties compared to ion-coupled reconnection when the length of the current sheet along the outflow direction was $\lesssim 10d_i$ (Sharma Pyakurel et al., 2019). These features included the reconnection event being embedded within a thin electron-scale current sheet (in contrast to ion-coupled reconnection, where the electron-scale gradients associated with the EDR are embedded in a broader ion scale current sheet), only featuring fast electron outflows, and having higher reconnection rates. Similar results were also found in the fluctuations self-consistently generated in shock simulations (Bessho et al., 2019, 2020, 2022, 2023).

Since the Phan, et al. (2018) work, examples of both standard ion-coupled reconnection and electron-only reconnection have been observed in Earth's magnetosheath (Wilder et al., 2018, 2022; Vörös et al., 2019; Stawarz et al., 2019, 2022). Vörös et al. (2019) revealed whistler and lower hybrid waves in the reconnecting current sheets. Wilder et al. (2018, 2022) investigated the energy conversion, demonstrating that reconnection with a small guide field (less than 30% of the reconnecting magnetic field) exhibits $\mathbf{j} \cdot \mathbf{E}'$ primarily associated with $\mathbf{E}_\perp$ and agyrotropic electron distributions. In contrast, large guide fields are associated with $\mathbf{j} \cdot \mathbf{E}'$ generated by $E_{||}$. Bandyopadhyay et al. (2021) examined the so-called pressure-strain interaction terms, quantifying local energy exchange between the bulk flow and internal energy (defined as the second moment of the distribution function), demonstrating magnetosheath reconnection events are sites of enhanced pressure-strain interaction alongside $\mathbf{j} \cdot \mathbf{E}$. In the small selection of events considered, Bandyopadhyay et al. (2021) found both positive and negative pressure-strain signatures, suggesting both local "heating" and "cooling" (although with a slight preference for positive "heating" signatures), with typically more intense signatures in the electrons compared to the ions.

Stawarz et al. (2022) statistically examined the reconnecting current sheets in the turbulent magnetosheath with *MMS* data. A total of 256 reconnection events (including 18 ion-coupled reconnection events) were investigated to understand
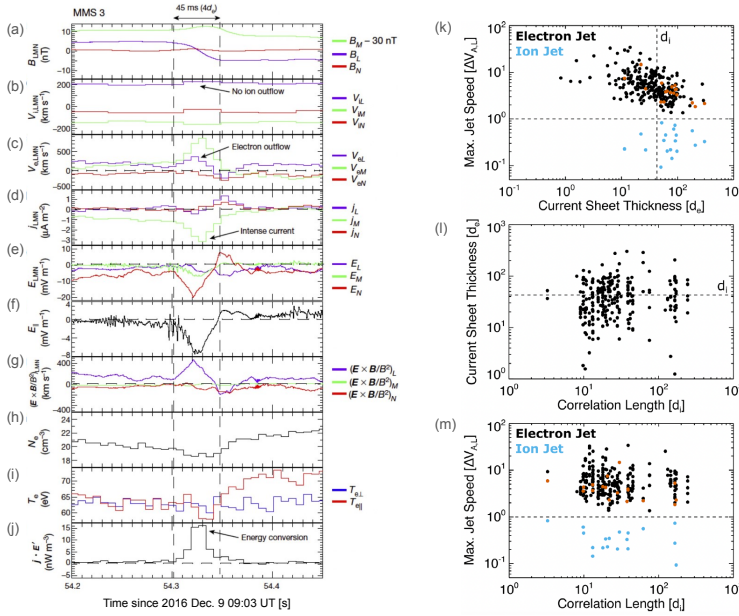
Fig. 2 Example of electron-only reconnection in the magnetosheath showing (a) **B**, (b) ion velocity, (c) electron velocity, (d) **j**, (e) **E**, (f) the component of **E** along **B**, (g) **E** × **B**-drift velocity, (h) electron number density, (i) electron parallel and perpendicular temperatures, and (j) **j** · **E**′. All vector quantities are in a local current sheet coordinate system based on a hybrid minimum variance analysis (reproduced from Phan, et al., 2018). (k)-(m) Statistical study of 256 reconnection events in the turbulent magnetosheath, comparing electron (and ion if present) reconnection jet speeds, current sheet thickness, and $\lambda_{C,\mathbf{B}}$ (reproduced from Stawarz et al., 2022).

the relationship between $\lambda_{C,\mathbf{B}}$ and the type of reconnection present. Stawarz et al. (2022) found thinner current sheets tended to have higher outflow speeds (Fig. 2k), such that when the thickness is $\lesssim d_i$, the electron jet speed becomes super-Alfvénic. These super-Alfvénic flows can reach the order of the electron Alfvén speed, indicating reconnection in the electron-only regime. Stawarz et al. (2022) further showed that intervals with $\lambda_{C,\mathbf{B}} \lesssim 20d_i$ are associated with thinner reconnecting current sheets and faster super-Alfvénic electron jets on average (Figs. 2l,m). The relationship with $\lambda_{C,\mathbf{B}}$ suggests a scenario where current sheets form at the interface of $\lambda_{C,\mathbf{B}}$-scale magnetic structures – implying $\lambda_{C,\mathbf{B}}$ controls the average length of current sheets along the outflow direction. When $\lambda_{C,\mathbf{B}}$ approaches tens of d_i, it becomes more likely there will be insufficient space for the reconnected field lines to accelerate ion outflows, increasing the prevalence of electron-only reconnection.

In addition to Earth's magnetosheath, the shock transition region and foreshock regions are often turbulent, and many reconnection events have been detected by *MMS* in these regions. Wang et al. (2019) and Gingell et al. (2019) found evidence of electron-only reconnection in the shock transition region. Gingell et al. (2019) observed that T_e rose from 20eV to 33eV across the shock ramp and an additional 7eV increase occurred in the shock transition region, suggesting 35% of the total electron heating across the shock occurs in the transition layer in association with electron-only reconnection. Wang et al. (2019) additionally
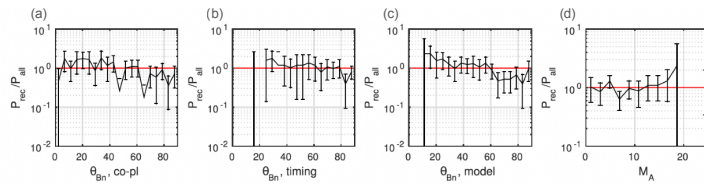
Fig. 3 Probability to detect reconnecting current sheets in the shock-transition-region/magnetosheath as a function of (a)-(c) shock normal angle θ_{Bn} using three different methods and (d) Alfvén Mach number of the upstream shock (reproduced from Gingell et al., 2020).

observed ion-coupled reconnection with both ion and electron jets in the shock transition region. Liu et al. (2020) and Wang et al. (2020) investigated reconnection in the foreshock. Wang et al. (2020) found electron-only reconnection in Short Large-Amplitude Magnetic Structures (SLAMS), suggesting that reconnection occurs due to the compression of the SLAMS. Liu et al. (2020) found electron-only reconnection in shock transients in the ion foreshock. Within the transients, $|\mathbf{B}|$ and n were low and the plasma was turbulent. *MMS* detected high-speed electron jets, enhancements of $\boldsymbol{j} \cdot \boldsymbol{E'}$, and enhancements in T_e during the crossings of current sheets in the transient.

Gingell et al. (2020) further statistically studied 223 shock crossings by *MMS* - investigating reconnection in the shock transition region of both quasi-parallel and quasi-perpendicular shocks. Gingell et al. (2020) demonstrated reconnection occurs ubiquitously regardless of shock angle, although quasi-parallel shocks and high Alfvén Mach number shocks show slightly higher probability than quasi-perpendicular shocks and low Alfvén Mach number shocks as shown in Fig. 3.

2.2 Simulations of Turbulence-Driven Reconnection

Over the past several decades, numerous numerical simulations of turbulence have demonstrated the process of turbulence-driven reconnection. While such simulations are able to reveal vital information about the configuration of turbulence-driven reconnection events that are inaccessible with *in situ* observations, the initial identification of reconnection in the simulations presents a challenge, particularly in 3D, which has been a major focus of much of the research. Furthermore, the computational challenge of simultaneously resolving all of the collisionless dynamics alongside the large scale separation characteristic of turbulent plasmas, has prompted the exploration of how different plasma models impact turbulence-driven reconnection (see Shay et al. (this collection) for a detailed discussion of different numerical plasma models).

As early as the 1980s, resistive MHD turbulence simulations demonstrated the presence of coherent structures resembling current sheets, where magnetic reconnection can take place (e.g. Matthaeus and Lamkin, 1986; Biskamp and Welter, 1989; Politano et al., 1989; Carbone et al., 1990). The characterization and statistical analysis of the distribution and geometry of current sheets formed in those numerical simulations of MHD turbulence, as well as their reconnection rates, have been investigated using diverse methodologies (Dmitruk et al., 2004; Ser-

vidio et al., 2009, 2010; Zhdankin et al., 2013, 2014, 2016). Servidio et al. (2009, 2010) statistically analyzed reconnection events in 2D MHD turbulence, quantifying, for example, the distribution of reconnection rates and the aspect ratio at each x-point. In order to find those x-points, they used a topological approach based on classifying the eigenvalues of the Hessian matrix of the vector potential and finding the saddle critical points. A generalization of this method to a 3D geometry for x-points with a guide field, which makes the topological classification more complex, was recently proposed by Wang et al. (2024). Zhdankin et al. (2013) developed an algorithm to identify and characterize the geometrical properties of current sheets in 3D MHD turbulence, and examined how those properties related to the presence of x-points. Zhdankin et al. (2013) quantified the energy dissipation in 3D MHD turbulence simulations, finding relatively uniformly distributed energy dissipation in the current sheets and also that the number of current sheets increases while their thickness decreases as the magnetic Reynolds number increases. The relationship between current sheets and other coherent structures was further numerically explored in the 3D MHD simulations of Zhdankin et al. (2016).

Similar coherent structures have been identified in simulations using other plasma models, such as two fluid and Hall MHD (Donato et al., 2012; Camporeale et al., 2018; Papini et al., 2019) that can resolve d_i and capture the physics of whistler and kinetic Alfvén waves that are thought to play a fundemental role in the sub-proton-scale turbulence in the solar wind and other environments. Donato et al. (2012) compared statistics of reconnection events between Hall-MHD and resistive MHD turbulence simulations. Hall-MHD effects led to faster and broader distributions of reconnection rates compared to resistive MHD. Camporeale et al. (2018) developed a space-filter method to analyze the features of the turbulent cascade due to current sheets in 2D simulations carried out with a two-fluid simulation, which also includes electron inertia. Using this approach, Camporeale et al. (2018) was able to quantify how the cascade was modified due to the presence of coherent structures by means of the cross-scale spectral energy-transfer at specific locations in real space.

In contrast to Hall MHD, hybrid-kinetic models also contain ion kinetic physics, which among other effects can describe temperature-anisotropy instabilities and, in general, any process driven by deviations from an equilibrium Maxwell distribution function. Hybrid-kinetic simulations of turbulence have often been used to investigate and reproduce the ion-scale spectral break and other observed properties of space plasma turbulence (Franci et al., 2015; Franci et al., 2020). Hybrid-kinetic simulations have revealed the process of current sheet formation and how reconnection can play an important role in regulating the turbulent cascade near d_i (Cerri and Califano, 2017; Franci et al., 2017; Papini et al., 2019; Hu et al., 2020; Sisti et al., 2021; Manzini et al., 2023). Papini et al. (2019) compared turbulence simulations using Hall-MHD and hybrid-kinetic models, finding good agreement in many turbulent properties between both models. Papini et al. (2019) found similar reconnection rates between both plasma models, and by means of quantifying the energy transfer, that there might exist a reconnection-mediated regime at sub-ion scales. By means of 3D hybrid-kinetic turbulence simulations, Fadanelli et al. (2021) analyzed the energy exchanges near a reconnection site in this scenario. They did not determine the energy budget as usually done, but instead a point-to-point analysis that revealed that the conversion to thermal and kinetic energies is statistically related to the local scale of the system, with the largest

conversion rate occuring at scales comparable to a few d_i. Manzini et al. (2023) developed a coarse-graining method to measure the nonlinear cross-scale energy transfer at specific locations. Applying this method to both *MMS* observations in the magnetosheath and hybrid-kinetic turbulence simulations, both cases showed clear indications of a preferential energy transfer to sub-proton scales associated with reconnection. Consolini et al. (2023) quantified the fractal dimension of current sheets in 2D hybrid-kinetic turbulence, finding a relationship between this quantity with the spectral features of **B** fluctuations at ion-scales

Other works have developed algorithms to characterize current sheet properties both in 2D and 3D turbulence. In 2D, Hu et al. (2020) developed such an algorithm based on a convolutional neural network, in which first humans detected reconnection events in turbulence based on several physical signatures including a sufficiently strong **j**, $\mathbf{u}_e$, and $\mathbf{E}'$ in the out-of-plane direction. With this training data, the algorithm automatically identified up to 70% of the reconnection events in turbulence successfully. In 3D, Sisti et al. (2021) developed and compared different methods to extract the three characteristic lengths of the formed current sheets. By comparing with earlier electron-MHD simulations of turbulence by Meyrand and Galtier (2013), Sisti et al. (2021) concluded that the additional physics included in the hybrid-kinetic plasma model changed the shape of the most predominant current sheets from "cigar-like" to "knife-like".

Most hybrid-kinetic simulations have been carried out with a model neglecting electron mass. As a result, reconnection is driven by physical or numerical resistivity, not by collisionless processes as expected. In addition, it has been shown that the current sheet width is mainly limited by the grid size (Azizabadi et al., 2021), so the current sheet thinning process is mainly limited by numerics and not by physical processes. The affect of electron inertia on current sheets formed by turbulence was further investigated in 2D hybrid-kinetic simulations by Jain et al. (2022), which quantified the errors introduced by approximations used in previous hybrid-kinetic codes with electron inertia, concluding that an accurate consideration of electron inertia is important to properly characterize the evolution of electron-scale current sheets in turbulent plasmas. Muñoz et al. (2023) extended this work to 3D, showing how the electron inertia modifies **j**, unexpectedly, even at scales $> d_e$ along the direction parallel to $\mathbf{B}_0$. In addition, Muñoz et al. (2023) emphasized the importance of the electron inertia term in the generalized Ohm's law to balance the reconnection electric field in low-β turbulence simulations. Califano et al. (2020) used another hybrid-kinetic plasma model with electron inertia to investigate the presence of electron-only reconnection in turbulence. The presence of electron-only reconnection was dependent on the wavenumber of the injected fluctuations with more electron-only reconnection events when the fluctuations were injected at wavenumbers comparable to the ion scale, while ion-coupled reconnection appeared when the fluctuations were injected at much larger scales, consistent with the observational work of Stawarz et al. (2022). Arró et al. (2020) used a similar code and numerical setup to Califano et al. (2020) in order to determine the influence of electron-only reconnection on the turbulence. However, they did not find significant differences between the turbulent fluctuations and intermittency between the cases with electron-only reconnection or ion-coupled reconnection.

Another approach used to investigate turbulence is gyrokinetics. This is a reduced kinetic model for both electrons and ions that is based on averaging the

particle gyromotion and following instead the guiding center of the particles. The model itself is based on an asymptotic expansion of a small parameter associated with small fluctuations of the distribution function or a small value of the wavenumber anisotropy $k_\parallel/k_\perp$, among other quantities. As a consequence, gyroresonances and whistler waves are ruled out of the model, while effects such as electron/ion Landau damping and kinetic Alfvén waves are retained. Turbulence simulations using the gyrokinetic approach have, not only revealed the presence of electron-scale current sheets, but also allowed the quantification of their relative contributions to dissipation (TenBarge and Howes, 2013; TenBarge et al., 2013; Howes, 2016). For example, it was found that Landau damping plays a fundamental role in dissipating the energy contained in the current sheets. Li et al. (2023) applied a method to identify current sheets based on a measure of the magnetic flux transport from the separatrices to the reconnection x-line in 3D simulations of gyrokinetic turbulence, revealing that the current sheets formed unexpectedly extended x-lines in the turbulent system.

Fully kinetic turbulence simulations have also shown the presence of both ion and electron-scale current sheets and magnetic reconnection (Karimabadi et al., 2013, 2014; Wan et al., 2012, 2015, 2016; Haynes et al., 2014; Haggerty et al., 2017; Vega et al., 2020; Agudelo-Rueda et al., 2021; Franci et al., 2022; Vega et al., 2023). Karimabadi et al. (2013) investigated reconnection in 2D fully kinetic simulations of Kelvin-Helmholtz/shear flow generated turbulence, showing how the current sheets are regions with strong localized electron heating due to the parallel reconnection $\mathbf{E}$. This heating was found to be much stronger than the heating due to the damping of waves formed in the same system. Haynes et al. (2014) investigated the relation between reconnection and electron temperature anisotropy via 2D fully kinetic simulations with an implicit PIC code, which allowed them to use a realistic ion-to-electron mass ratio, finding that reconnection sites are associated with strong parallel electron temperature anisotropy, contributing to dissipation. Wan et al. (2016) compared several 2D and 3D fully kinetic and MHD simulations of turbulence in order to determine the relation between intermittency and dissipation in coherent structures, finding the dissipation measure, $\mathbf{j} \cdot \mathbf{E}' - \rho_c \mathbf{u}_e \cdot \mathbf{E}$ where ρ_c is the charge density, scales as $\sim |\mathbf{j}|^2$ in all cases. Haggerty et al. (2017) analyzed the statistics of reconnection X-points in 2D fully-kinetic turbulence simulations by applying similar methods to those of Servidio et al. (2009) for a MHD model. In contrast to previous MHD simulations, Haggerty et al. (2017) found that the distribution of reconnection electric fields is broader and can reach up to 0.5 of the local Alfvén speed, while keeping an average of 0.1. Vega et al. (2020) focused on electron-only reconnection in 2D fully kinetic simulation, finding that electron-only reconnection occurs at both high and low electron-β with similar reconnection rates. Vega et al. (2023) further analyzed 3D fully kinetic simulations of turbulence using an algorithm based on a medial axis transform from image processing , which was capable of identifying and characterizing arbitrary shaped current structures. The current structures tended to have half-widths of at most one d_e with a length between d_e and d_i. Most energy dissipation took place in current structures occupying $\sim 20\%$ of the total simulation volume and, by identifying large variations in electron flow and characteristic features in the pressure-strain interaction terms, it was estimated that 1% of current sheets were reconnecting - in contrast to the observational work of Stawarz et al. (2022) which found $\sim 10\%$ of intense current sheets underwent reconnection, although this discrepancy may

owe to different methodologies for identifying distinct current structures. Using 3D fully-kinetic anisotropic Alfvénic turbulence simulations, Agudelo-Rueda et al. (2021) found that the current sheets generated by the turbulence tended to be less anisotropic than that of the large-scale driving and used several proxies (e.g., $|\mathbf{j}|$, $\mathbf{u}_e$, $\mathbf{u}_i$, and $\mathbf{E}'$) to identify reconnection sites. In a follow-up study, Agudelo-Rueda et al. (2022) further examined the energy transport and dissipation associated with both collionless and effective collision-like terms at the reconnection sites in the simulation. Franci et al. (2022) analyzed reconnection events in 2D fully kinetic simulations of turbulence, identifying several reconnection events with a thickness on the order of d_e. Reminiscent of the work of Califano et al. (2020) and Stawarz et al. (2022), which looked at the statistical prevalence of electron-only reconnection relative to the dynamics of the driving scale, Franci et al. (2022) found that even within a given simulation turbulent current sheets with shorter lengths tended to appear more electron-only-like, while current sheets with longer lengths appeared ion coupled.

While many numerical studies of turbulence-driven reconnection have been performed in idealised periodic boxes of turbulence, a number of works, particularly in recent years, spurred on by the *MMS* results from Earth's turbulent magnetosheath discussed in Sec. 2.1, have begun to examine reconnection events generated by turbulence self-consistently excited in shock simulations. Reconnection driven by shock turbulence has been studied using kinetic simulations of quasi-perpendicular shocks (Matsumoto et al., 2015; Bohdan et al., 2020; Lu et al., 2021; Guo et al., 2023), quasi-parallel shocks (Gingell et al., 2017; Bessho et al., 2019, 2020, 2022, 2023; Lu et al., 2020; Ng et al., 2022, 2024), and across both regimes (Karimabadi et al., 2014; Gingell et al., 2023; Steinvall and Gingell, 2024).

2.3 The Role of Reconnection in Turbulent Plasmas

Beyond the existence and identification of turbulence-driven reconnection, it is important to consider how and to what extent reconnection contributes to the turbulent dynamics. There are several avenues through which turbulence-driven reconnection might impact turbulence, with reconnection potentially i) acting as the dominant nonlinear interaction over some range of scales and ii) contributing to the dissipation of the turbulence.

2.3.1 Impact on the Energy Spectrum.

As discussed in Sec. 1.2.2, theoretical descriptions of turbulence are built on assumptions about the physical interactions controlling the nonlinear dynamics. Several works have explored how to incorporate reconnection into this framework, with early work basing the analysis on the isotropic weak turbulence formalism of Iroshnikov-Kraichnan (Carbone et al., 1990), while recent works have examined the topic using anisotropic MHD (Loureiro and Boldyrev, 2017b; Mallet et al., 2017) and collisionless (Loureiro and Boldyrev, 2020; Mallet, 2020) turbulence.

In the theoretical scenarios proposed in these works, turbulent dynamics form current-sheet-like structures with aspect ratios (length relative to thickness) that become progressively more anisotropic at smaller scales in a manner consistent with the spectral anisotropy predicted by an anisotropic turbulence model. The

tearing instability is assumed to initiate reconnection at these current sheets once the aspect ratio becomes sufficiently large and alters the turbulence by "disrupting"/"destroying" the elongated current sheets over the timescale of the tearing instability growth, thereby altering the distribution of energy in spectral space. While the tearing instability growth is treated as a linear instability, it is both initiated via the formation of a nonlinear structure and leads to the development of a fully nonlinear perturbation to the current sheet and, in this sense, the linear growth rate is taken to characterise the rate at which the nonlinear reconnection dynamics develop. If a range of scales exists over which this tearing timescale is faster than the dynamical timescales of other nonlinear effects, such as those generating the current sheets, then it is supposed that the tearing timescale will be the relevant timescale to associate with τ_{tr}. This picture relies on reconnection being sufficiently prevalent so as to make a significant impact, the scale-dependant anisotropy of current structures reflecting the spectral anisotropy of the turbulence model, and the linear tearing instability being the correct way to characterize the initiation of reconnection in a turbulent environment.

Based on this scenario, predictions for two key parameters can be derived - the critical scale (a_c) at which reconnection becomes the dominant nonlinear interaction and the power law scaling $\mathcal{E}(\mathbf{k})$. Constraining these parameters requires both a model for the large-scale turbulent dynamics setting up the current sheets and a description of the tearing instability, which depends on whether the system is resistive or collisionless and on the exact profile of the current sheets.

For resistive MHD, several 3D anisotropic turbulence models have been proposed, including the dynamic alignment model of Boldyrev (2006) and intermittency models of Chandran et al. (2015) and Mallet and Schekochihin (2017). Loureiro and Boldyrev (2017b) and Mallet et al. (2017) demonstrated that for these models, at sufficiently large Re, a range of scales exists where the resistive tearing instability is faster than the nonlinear dynamics generating the current sheets, suggesting the presence of a reconnection mediated inertial range. For the case of a hyperbolic tangent current sheet profile, a_c was found to be

$$a_c/\lambda_C \sim \left(V_{A,\lambda_C}\lambda_C/\eta\right)^{-4/7}, \tag{15}$$

where we have identified λ_C with the outer scale of the turbulence and V_{A,λ_C} is the Alfvén speed for fluctuations at the outer scale; and $\mathcal{E}(k_\perp) \sim k_\perp^{-11/5}$ in the reconnection-mediated range. Recent simulations of high-Re MHD turbulence in 2D (Dong et al., 2018) and 3D (Dong et al., 2022) have provided evidence for the presence of reconnection and the expected steepening of the inertial range spectrum at a_c.

Collisionless effects both alter the tearing instability, as well as the nonlinear dynamics of the turbulence. Two scenarios, one where a_c is larger than the ion scales and one where a_c is smaller than the ion scales, can potentially occur. In the former scenario, the analysis proceeds in a similar manner to the resistive case, but with a modified expression for the tearing instability leading to

$$a_c/\lambda_C \sim \left(d_e/\lambda_C\right)^{4/9}\left(\rho_s/\lambda_C\right)^{4/9} \tag{16}$$

where ρ_s is the ion acoustic scale, and $\mathcal{E}(k_\perp) \sim k_\perp^{-3}$ is obtained for a hyperbolic tangent current sheet profile (Loureiro and Boldyrev, 2017a, 2020). The range of spectral indices found for different current sheet profiles is reminiscent of those

reported in the so-called transition range of solar wind turbulence, although reconnection is not the only explanation that can produce such slopes (Bowen et al., 2020). The later scenario, where a_c occurs in the kinetic scales, is more challenging due to less well understood anisotropic turbulence models; however, some work has been done on this scenario (Loureiro and Boldyrev, 2017a; Boldyrev and Loureiro, 2019; Mallet, 2020; Loureiro and Boldyrev, 2020; Boldyrev and Loureiro, 2020), which may be relevant for understanding the impact of electron-only reconnection.

2.3.2 Contribution to Energy Dissipation.

Magnetic reconnection can also facilitate the dissipation of turbulence. Simulations (Servidio et al., 2011) and observations (Osman et al., 2012; Chasapis et al., 2017, 2018) suggest intermittent structures are locations of enhanced temperature and energy conversion. As discussed in Sec. 2.1, missions such as *Cluster* and *MMS* have enabled the identification of thin reconnection events and the direct examination of the local energy conversion associated with them, which may account for nontrivial amounts of energy conversion when compared with estimates of the overall energy budget (Sundkvist et al., 2007; Schwartz et al., 2021). However, other studies, such as that by Hou et al. (2021), which examined integrated $\mathbf{j} \cdot \mathbf{E}'$ at intense PVI structures, while simultaneously identifying PVI structures associated with reconnection, concluded that, while reconnection events may have large energy conversion signatures, their integrated contribution to energy dissipation may be small ($\sim 15\%$ of the dissipation associated with large PVI structures and $\sim 1\%$ of the total integrated $\mathbf{j} \cdot \mathbf{E}'$ in the analysed interval) due to the small size of the diffusion region and limited occurrence rate.

One limitation of local analyses of energy conversion, is that, while the diffusion regions, which contain some of the strongest gradients, occupy a small volume; the entire volume of the reconnection outflows and separatrices, occupy a much larger volume and can also be energetically important for the particle acceleration and heating. Furthermore, since reconnection involves the inflow of particles from the surrounding environment, in can lead to the acceleration and heating of a larger effective volume of particles than expected from the size of the current sheet alone.

An alternative way to assess the importance of reconnection for turbulent dissipation is to consider the energy budget of the reconnection events generated by the turbulent dynamics. The amount of magnetic energy released by reconnection that is available to each electron-proton pair is given by

$$\mathcal{E}_{rec} = m_i V_{A,inflow}^2, \tag{17}$$

where m_i is the ion mass and $V_{A,inflow}$ is the Alfvén speed associated with the inflowing reconnecting component, B_L, of the magnetic field. Taking into account the potential effect of asymmetry on either side of a reconnecting current sheet, $V_{A,inflow}$ is given by

$$V_{A,inflow} = \sqrt{\frac{|B_{L,1}| |B_{L,2}| (|B_{L,1}| + |B_{L,2}|)}{\mu_0 m_i (n_1 |B_{L,2}| + n_2 |B_{L,1}|)}}, \tag{18}$$

with subscripts 1 and 2 denoting values on either side of the current sheet. The total rate of energy dissipation associated with reconnection can be quantified by

taking into account the fraction of $\mathcal{E}_{rec}$ converted into particle heating (or energetic particle acceleration) and the rate that magnetic flux is reconnected. Denoting the net rate of energy dissipation per unit mass associated with reconnection within a turbulent volume as ϵ_{rec}, which will be equivalent to ϵ if reconnection accounts for all of the dissipation in the volume, gives (Shay et al., 2018; Stawarz et al., 2022)

$$\epsilon_{rec} = \sum_j f_{rec,j} \alpha_j V_{A,inflow,j}^2 \left(\frac{V_{A,inflow,j}}{\lambda_j} \mathcal{R}_j \right). \tag{19}$$

In Eq. 19, f_{rec} is the fraction of particles in the turbulent volume processed by a given reconnection event, α is the fraction of $\mathcal{E}_{rec}$ converted into particle heating, λ is the length of the inflow region, and $\mathcal{R}$ is the dimensionless reconnection rate, such that $\mathcal{R} V_{A,inflow}/\lambda$ represents the inverse timescale over which magnetic flux is reconnected. The summation over j represents a sum over each reconnection event in the turbulent region at any given time, such that subscript j denotes a quantity for a given reconnection event.

While Eq. 19 can be straightforwardly computed if all reconnection events within a volume can be characterized, in many cases this is not possible and it can be beneficial to estimate Eq. 19 based on characteristic values for the reconnection events, such that

$$\epsilon_{rec} \sim N_{rec} f_{rec} \alpha V_{A,inflow}^2 \left(\frac{V_{A,inflow}}{\lambda} \mathcal{R} \right), \tag{20}$$

where N_{rec} is the number of reconnection events in a turbulent volume. Rough estimates of the above parameters constrained by the reconnection events observed in the systematic survey of reconnection in the turbulent magnetosheath by Stawarz et al. (2022) obtained dissipation rates of 1×10^4 to 3×10^6 J/kg-s, assuming $\lambda \sim \lambda_{C,\mathbf{B}}$ consistent with reconnection occuring at the interface of correlation length magnetic structures. While there was a large spread, these estimates were in rough agreement with previous independent estimates of ϵ in the magnetosheath obtained from expressions similar to Eq. 11 (Hadid et al., 2018; Bandyopadhyay et al., 2018), suggesting reconnection is a non-trivial contributor to dissipation - potentially alongside other processes.

Shay et al. (2018) derived a related expression for the energy dissipation associated with reconnection, which can be thought of as an extension to Eq. 20 that parameterize α based on expectations from guide field reconnection. Based on a series of 2D laminar symmetric guide field reconnection simulations Shay et al. (2018) find that ion and electron heating is well parameterized by

$$\Delta T_i = c_i \left(\frac{|B_L|}{|\mathbf{B}|} \right)^2 m_i V_{A,inflow}^2 \tag{21}$$

$$\Delta T_e = c_e \left(\frac{|B_L|}{|\mathbf{B}|} \right) m_i V_{A,inflow}^2 \tag{22}$$

where $\Delta T_{i,e}$ are increases in ion and electron temperatures and $c_{i,e}$ are constants of proportionality associated with ion and electron heating, respectively. While these expressions were empirically derived, Eq. 21 is consistent with theoretical expectations for ion acceleration in contracting magnetic islands (Drake et al., 2009). Based on Eqs. 21 and 22, $\alpha_j = c_i \left(|B_{L,j}|/|\mathbf{B}_j| \right)^2 + c_e \left(|B_{L,j}|/|\mathbf{B}_j| \right)$ in Eq. 19. Using

this value of α_j, Eq. 19 is then consistent with Eq. 3 of Shay et al. (2018) divided by the total mass in the turbulent volume, noting that f_{rec} is equivalent to the volume of magnetic island that have reconnected in the Shay et al. (2018) formalism divided by the total volume of the region. Due to the different scaling of the ion and electron heating, the relative ion to electron heating varies depending on the distribution of local guide field strength at turbulence-driven reconnection sites. Relating the expressions for the ion and electron heating rates to the properties of the turbulent fluctuations in a heuristic manner and comparing with the heating rates obtained from 2.5D PIC simulations of turbulence, Shay et al. (2018) found that, while the individual scalings for ion and electron heating did not agree with the prediction, the ratio did agree well.

3 Reconnection-Driven Turbulence

The converse of the scenario discussed in Sec. 2, referred to here as reconnection-driven turbulence, in which large-scale reconnection sites set up by system-scale dynamics act to generate turbulent dynamics, has also been an active area of investigation. As discussed in Graham et al. (this collection), reconnection is known to generate a variety of waves in the diffusion regions, along the separatrix, and in the exhausts that are excited by the free energy available in non-Maxwellian distributions or strong gradients. As these waves grow to large amplitudes and nonlinearly interact, they can lead to turbulence. The plasmoid/tearing instability can also destabilize the reconnecting current sheet and spontaneously generate multiple x-lines with plasmoids (or flux ropes in 3D) between them. These plasmoids/flux ropes can interact and merge in the outflows, producing a complex turbulent character to the current layer (Daughton et al., 2011; Oishi et al., 2015; Huang and Bhattacharjee, 2016). Turbulent dynamics also can be generated by the interaction of the exhaust with its surroundings, such as through shear instabilities or the exhaust encountering an obstacle.

Given the relatively large amount of data, spanning many correlation lengths, needed to perform typical turbulence analyses, relatively limited observational analyses of the fluctuations within reconnection exhausts have been performed in the solar wind (Miranda et al., 2021; Eastwood et al., 2021; Wang et al., 2023) and at Earth's magnetopause (Ergun et al., 2017), which suggest enhanced turbulent fluctuations within the exhausts. However, Earth's magnetotail has provided an ideal environment for the observational examination of reconnection-driven turbulence. This status is partially associated with the central role that system-scale Dungey-Cycle-like reconnection plays in energy transport in the magnetotail and the need to understand the role of turbulence in mediating this transport. Additionally, due to the nature of the system, the effective spacecraft trajectory through a reconnection event in the magnetotail is often such that significant dwell times in the reconnection exhaust are obtained, which is conducive to turbulence analyses (in contrast to solar wind or magnetopause reconnection encounters where significant and sustained components of the background motion normal to the current sheet, combined with relatively narrow outflow thicknesses, mean that rapid transits of the outflow are the norm). Although it may be possible to identify additional regions in near-Earth space, such as the heliospheric current sheet in the inner heliosphere, where extended dwell times are also possible.

3.1 Magnetotail Turbulence

As illustrated in Fig. 1, the stretched magnetic field in Earth's magnetotail can be broadly divided into two regions - the northern and southern lobes featuring low n and strong $|\mathbf{B}|$; and the relatively high density plasma sheet surrounding the $\mathbf{B}$ reversal at the center of the magnetotail. The plasma sheet is a dynamic region and early studies examined the fluctuations in the plasma sheet as a whole, demonstrating the region exhibits nonlinear behavior consistent with turbulence albeit with differences relative to classical homogeneous turbulence potentially associated with boundary effects, coupling to Earth's ionosphere, and nonuniform driving (Borovsky et al., 1997; Borovsky and Funsten, 2003; Weygand et al., 2005).

In the plasma sheet, system-scale reconnection occurs at x-lines near Earth at $\sim 25 R_E$ and in the distant tail at $> 60 R_E$ from Earth (see Fuselier et al., 2024; this collection), driving tailward and Earthward exhausts. These outflows can drive turbulent fluctuations in the plasma sheet and subsequent analyses demonstrated such flows contain some of the clearest and most intense signatures of turbulence in the plasma sheet (Bauer et al., 1995; Vörös et al., 2004, 2006; Stawarz et al., 2015). Reconnection outflows in the magnetotail are typically transient and likely linked with Bursty Bulk Flows (BBFs) in observations. As the flows plow through the surrounding plasma, they relax the stretched $B_{x,GSM}$ component of the field in Geocentric Solar Magnetic (GSM) coordinates and enhance the dipolar $B_{z,GMS}$ component producing so-called Dipolarization Fronts. On the Earthward side, as the flows impinge on the strong nearly dipolar near-Earth field, the flows are slowed and deflected generating large-scale vorticies (Panov et al., 2010).

Cluster and *MMS* have provided clear examples of extended encounters with reconnection x-lines and adjacent outflows featuring exceptionally intense turbulent fluctuations (Ergun et al., 2018), as well as tailward and Earthward exhausts likely further from the x-line with clear evidence of turbulent dynamics (Vörös et al., 2004; Eastwood et al., 2009). Fig. 4 illustrates a notable example from 26 July 2017 where *MMS* continually observed a near-Earth x-line featuring exceptionally intense fluctuations for 20 minutes. While the event has intense fluctuations in all quantities, an overall variation from $B_{z,GSE} > 0$ to $B_{z,GSE} < 0$ in conjunction with a variation from $u_{x,GSE} < 0$ to $u_{x,GSE} > 0$ during the encounter, consistent with *MMS* traversing through the x-line from the tailward to Earthward outflows. An overall variation from $B_{x,GSE} > 0$ to $B_{x,GSE} < 0$ also occurs, consistent with *MMS* concurrently traveling from southward to northward of the current sheet. In this and other similar events, n is exceptionally low, suggesting field lines carrying dense plasma from the plasma sheet have already reconnected and been evacuated from the region, and now lobe field lines are reconnecting. Ergun et al. (2020a) suggested the large amount of energy imparted to each particle in the reconnection region ($\sim 3\text{keV/s}$ per proton/electron pair in this event), owing to the low n and large incoming Poynting flux from the lobes, may be a key reason why such strongly turbulent fluctuations are generated in this type of event.

$\mathbf{B}$ and $\mathbf{E}$ spectra in these turbulent x-lines and outflows show broadband power law scalings across MHD, sub-proton, and electron scales consistent with theory and observations of other turbulent environments (Vörös et al., 2004; Eastwood et al., 2009; Ergun et al., 2018, 2020a). At sub-proton scales, the fluctuations appear consistent with kinetic Alfvén waves, the dissipation of which may lead to significant proton heating (Chaston et al., 2012, 2014). Due to the variable flows
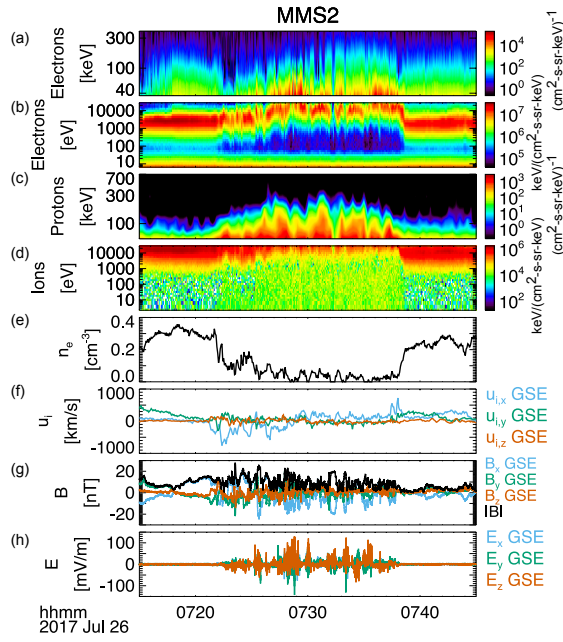
Fig. 4 Example turbulent x-line crossing observed by *MMS*, showing (a) high-energy omni-directional electron energy fluxes, (b) low-energy omnidirectional electron differential energy fluxes, (c) high-energy omnidirectional proton energy fluxes, (d) low-energy omnidirectional ion differential energy fluxes, (e) electron number density, (f) ion flow velocity, (g) **B**, and (h) **E**. All vector quantities are in Geocentric-Solar-Ecliptic (GSE) coordinates.

in the magnetotail, even within fast reconnection outflows, some care needs to be taken in the analysis of spectra and other scaling properties, since the Taylor hypothesis is likely not strictly valid. Based on a careful analysis of multipoint timing velocities of **E** and **B** structures in the turbulent x-line shown in Fig. 4g–h, Ergun et al. (2020a) found that, while the direction of propagation was random, the speed of structures were typically between the Alfvén and ion acoustic speeds and within a factor of two of each other. Using the average speed as a conversion between frequency and wavenumber, Ergun et al. (2020a) found good agreement between the location of spectral break points and characteristic plasma length scales, as well as good correspondence between spatial and temporal correlation functions. Bandyopadhyay et al. (2021) examined Eq. 11 using *MMS* measurements of a reconnection outflow on 16 June 2017, providing evidence of an active cascade of energy to small scales within the reconnection exhaust. Jin et al. (2022) examined higher-order turbulence statistics in another turbulent x-line encountered by *MMS* on 28 May 2017, finding evidence of turbulent intermittency. By dividing the extended reconnection outflow into subintervals, Jin et al. (2022) found evidence of increasingly intermittent behaviour with distance from the x-line, suggesting an evolution of the turbulent dynamics through the outflow region. Recently, Richard et al. (2024) performed a statistical survey of turbulence in BBFs observed from $15–25 R_E$ downtail of Earth by *MMS*, which confirmed many of the results inferred from case studies of magnetotail reconnection jets. Importantly, it was determined that turbulence quickly develops within a few ion gyroperiods with a driving scale

comparable to the size of the jet. An intense energy cascade rate (relative to the solar wind or magnetosheath) was also identified, which extend over an order of magnitude in scale.

While somewhat rare, in several turbulent x-line events, EDRs have been encountered and identified using *MMS* data. Despite the strong fluctuations, the basic properties and structure of the EDR appears broadly consistent with quasi-2D laminar reconnection and the reconnection process continues amidst the turbulent fluctuations for an extended duration (Ergun et al., 2022a; Qi et al., 2024). Ergun et al. (2022a) found by analysing one event observed on 27 August 2018 that the typical features of reconnection (e.g., a persistent ion jet, $\mathbf{B}$ profile including a B_L reversal and Hall fields) were all present as expected, but with additional fluctuations on top of them. Off-diagonal terms of the electron stress tensor, which encode off-diagonal contributions to generalised Ohm's law from both the electron pressure and electron inertial effects, were found to both account for the observed reconnection electric field and could be understood from a laminar reconnection perspective. Qi et al. (2024) examined another event, noting that, while large reconnection electric fields may be present, the overall aspect ratio of the event, which provides another estimate of the reconnection rate, gives a value of ~ 0.2 consistent with typical estimates of "fast" reconnection rates.

While turbulence may not significantly alter the electron dynamics at the x-line itself, at least for the few examples that have lent themselves to detailed examination, they may contribute to repartitioning energy in the exhausts. As seen in Fig. 4a and c, intermittent bursts of energetic ions and electrons are interspersed with the fluctuations. Ergun et al. (2018) found that both structures with $\mathbf{j} \cdot \mathbf{E}'$ dominated by the components parallel and perpendicular to $\mathbf{B}$ contribute to the turbulent dissipation. $\mathbf{j}_\perp \cdot \mathbf{E}'_\perp$ contributed to 80% of the net dissipation and primarily acted at frequencies near the ion cyclotron frequency, while $\mathbf{j}_{||} \cdot \mathbf{E}'_{||}$ primarily acted at higher frequencies and led to the acceleration of some of the most energetic electrons. Further analyses using observations and test particle models demonstrated that magnetic deletions associated with the intense fluctuations enabled particle trapping in regions of energy conversion (Ergun et al., 2020b,a). Notably, perpendicular energization tended to occur making it more difficult for particles to escape, thus leading to further energization and the generation of the non-thermal energetic particles seen in the observations. Bergstedt et al. (2020) performed a statistical analysis of magnetic structures in the same event finding $\mathbf{j}_{||} \cdot \mathbf{E}'_{||}$ dissipation occured at current sheets at the interface of plasmoid-like structures, which may be consistent with the dynamic production and merger of plasmoids by the reconnecting current sheet. Oka et al. (2022) examined particle energization, both in reconnection events like the example in Fig.4 where lobe field lines reconnect and in events where plasma sheet field lines carrying denser plasma reconnect, demonstrating larger $\mathbf{E}$ fluctuations are present in lobe reconnection. Interestingly, the stronger $\mathbf{E}$ fluctuations were linked to a smaller nonthermal energy fraction. This discrepancy with Ergun et al. (2020b) may be linked to differences in the definition of nonthermal particles, with Oka et al. (2022) focusing on the high-energy power law tail to the particle distributions, while Ergun et al. (2020b) focused on a high-energy non-thermal shoulder to the distribution.

Turbulent fluctuations can also be excited through the interaction of the exhaust with the surroundings. Volwerk et al. (2007) found evidence of the Kelvin-Helmholtz instability associated with the velocity shear along the edges of a BBF

using a conjunction between *Cluster* and *DoubleStar* and Divin et al. (2015) found evidence of turbulence caused by the LHDI at the dipolarization front. Closer to Earth in the BBF braking region, studies have identified broadband turbulent spectra of kinetic-Alfvén-wave-like fluctuations, the excitation of which is likely partially associated with the flow braking process and may play a role in the conversion of bulk flow kinetic energy into other forms (Chaston et al., 2012; Ergun et al., 2015; Stawarz et al., 2015). Ergun et al. (2015) and Stawarz et al. (2015) found using *THEMIS* data that the BBF braking region was filled with large-amplitude high-frequency $E_{||}$ structures such as double layers and electron phase space holes, potentially excited by field-aligned current instabilities associated with the turbulence. Stawarz et al. (2015) estimated these $E_{||}$ structures could play a significant role in the dissipation of the turbulent fluctuations and heating of the plasma; and subsequent large-scale statistical surveys have supported the picture of the braking region as a region of enhanced solitary wave activity, as well as proton and electron heating (Hansel et al., 2021; Usanova and Ergun, 2022; Usanova et al., 2023). Based on a statistical examination of BBF events, Chaston et al. (2014) found an enhanced divergence of field-aligned Poynting flux associated with kinetic Alfvén waves away from the center of the plasma sheet for distances $< 15 R_E$ downtail of Earth, suggesting a fraction of the small-scale fluctuations excited in the region propagate along the field-lines depositing energy in the auroral region. In this scenario, the turbulent dynamics, while not responsible for dissipating the energy radiated from the region, convert bulk flow energy into small-scale fluctuations capable of propagating to the ionosphere. Stawarz et al. (2015) estimated the energy budget in the braking region, finding turbulent energy dissipation, adiabatic heating due to the compression of the magnetic field in the braking region, and radiated Poynting flux were similar in magnitude and the sum of these energy losses were comparable to the energy input into the region due to the bulk flows. At the inner edge of the flow braking region around $\sim 7 R_E$ downtail of Earth, BBFs have been associated with enhanced turbulence and the dissipation of these fluctuations has been implicated in seeding the outer radiation belt (Ergun et al., 2022b).

3.2 Simulations of Reconnection-Driven Turbulence

Numerical simulations have also long been used to examine the turbulence that is self-generated by magnetic reconnection under certain circumstances. Arguably, most of the numerical work on reconnection-driven turbulence has been performed using MHD plasma models, for example in the context of the plasmoid instability or other secondary fluid instabilities; however, the impact of kinetic effects and instabilities more appropriate to the collisionless space plasmas of the near Earth environment have been historically less well understood. In particular, turbulence near and in the diffusion regions has been a critical area of research due to its potential role in balancing the reconnection electric field, and thereby enabling reconnection, through anomalous resistive and viscous effects that can potentially enhance the reconnection rate. Such anomalous effects arise from the nonlinear contributions to generalized Ohm's law due fluctuating quantities that are not typically treated in the traditional quasi-laminar reconnection picture. Note that this way in which turbulence affects reconnection is somewhat different from the

stochastic reconnection picture, often analysed in the MHD context and discussed further in Sec. 5. In this section, we discuss a selection of the most important findings from the past several years, with a focus on instabilities causing turbulence in kinetic reconnection simulations applied to space plasmas.

In 2D, several works have shown streaming instabilities between different electron and/or ion populations can generate turbulence, particularly at the separatrices that are known to host a variety of waves due to instabilities and other nonlinear mechanisms (Fujimoto, 2014; Goldman et al., 2014). Cattell et al. (2005) and Pritchett (2005) performed 2D fully kinetic PIC simulations of magnetic reconnection with a guide field and parameters appropriate to Earth's magnetotail. This configuration produced electron holes and associated turbulence via streaming (Buneman) instabilities at the separatrices, consistent with in-situ observations. Later simulations with more realistic parameters, such as a realistic ion-to-electron mass ratio and larger domain, demonstrated this process occurs for all guide fields and is, therefore, expected under a variety of conditions in Earth's magnetosphere (Lapenta et al., 2011). Muñoz and Büchner (2016) showed using 2D fully kinetic PIC simulations that there is a strong guide field regime in which broadband electrostatic turbulence develops in the separatrices and outflows, with the key finding that the separatrix/outflow turbulence is associated with double-peaked and anisotropic electron distribution functions and wave activity near the lower-hybrid frequency whose strength is correlated with the instantaneous reconnection rate. This turbulence was shown to be associated with anomalous resistivity, which was smaller than the electron inertia or non-gyrotropic electron pressure tensor in generalised Ohm's law (Muñoz et al., 2017). However, since the process was not occurring at the x-line, it was not associated with enabling the reconnection process itself. Using 2D fully-kinetic simulations with a sufficient scale separation between d_e and the Debye length (a parameter that is typically small in PIC simulations of reconnection), Jara-Almonte et al. (2014) showed that Debye-scale turbulence was excited near the x-line as well, through the action of streaming instabilities in the reconnection plane.

3D fully kinetic reconnection simulations tend to be more turbulent than their 2D counterparts due to the presence of the additional degree of freedom enabling more instabilities with wavenumbers along the additional dimension. Drake et al. (2003), Che et al. (2011), and Che (2017) found that in 3D the current layer develops filamentary magnetic structures due to electron-shear flow and Buneman instabilities along the direction parallel to the current sheet using PIC simulations with a relatively strong guide field, small spatial domain, and initially force-free equilibrium. During the non-linear phase of these instabilities, electron holes and turbulence were generated, which produced anomalous resistivity and viscosity. Daughton et al. (2011) carried out 3D PIC simulations but with a smaller guide field, much larger spatial domain, and initialized with a Harris current sheet equilibrium. In these simulations, the current sheet developed flux ropes at electron scales due to the tearing instability, which were not seen in previous simulations because of their smaller spatial domain. These flux ropes underwent complex 3D interactions that lead to continuously self-generated and inhomogeneous turbulence within the electron current layer. Later simulations by Liu et al. (2013) revealed that the turbulence generated under similar conditions to Daughton et al. (2011) does not modify the reconnection rate via anomalous resistivity or viscosity, in contrast to the earlier results by Drake et al. (2003) and Che et al. (2011). The

discrepancy was explained as being due to the lack of streaming or electron shear flow instabilities in the higher plasma-β regime appropriate to magnetospheric conditions and enhanced parallel heating that can be developed in simulations with larger spatial domains. Fujimoto and Sydora (2021, 2023) demonstrated that in 3D simulations without a guide field a different scenario occurs, in which electromagnetic turbulence is generated by an electron Kelvin-Helmholtz instability that produce. These fluctuations are capable of producing anomalous viscosity due to electron transport that is capable of breaking the electron frozen-in condition, but not anomalous resistivity since the turbulence mainly effects the electrons, while the ions remain decoupled.

Another source of free energy to drive turbulence is the lower-hybrid drift instability (LHDI) generated by gradients in the density or magnetic field associated with diamagnetic currents. This instability can be particularly important in the case of asymmetric reconnection, such as at Earth's dayside magnetopause, where the strong density gradients across the reconnecting current sheet are conducive to exciting the instability. The LHDI typically generates waves initially at the edge of the current sheet that can spread toward its center. Turbulence associated with the LHDI has been historically considered as a source of anomalous resistivity. However, only in the last decade have 3D fully-kinetic PIC simulations with a large-enough scale separation between electron and ion scales been able to reveal under which conditions this instability can modify the reconnection properties. Roytershteyn et al. (2012) and Pritchett et al. (2012) found that the LHDI can cause enough turbulence near the current sheet center to sustain the reconnection electric field if the plasma-beta is low enough under asymmetric conditions, although most of the LHDI-driven turbulence is confined to the separatrices. Such conditions are unlikely to be met for magnetopause reconnection. Later similar simulations obtained different conclusions under different conditions. Price et al. (2016, 2017) carried out 3D fully kinetic simulations of an asymmetric magnetopause reconnection event based on observations made by *MMS*. Unlike Roytershteyn et al. (2012), these simulations found LHDI-driven turbulence at both the x-line and sparatricies that was strong enough to balance the reconnection electric field. The discrepancy was attributed to different boundary conditions and a stronger than previously expected density jump across the current sheet in the observed *MMS* event. Although, Le et al. (2017, 2018) modelled the same reconnection event as Price et al. (2016, 2017), concluding that anomalous resistivity was small, but that the turbulence acted to enhance plasma mixing and heating in the event. The simulations by Price et al. (2016) also revealed that crescent-shaped electron distribution functions, an important hallmark of magnetopause reconnection often observed by *MMS*, were not affected by the turbulence developed in the current sheet. Later, Price et al. (2020) explored a similar system but under the presence of a significant guide field, showing that in this case turbulence develops in the diffusion region due to a variant of the LHDI. While the anomalous resistivity produced by the electromagnetic fluctuations at the x-line were small, other anomalous terms were significant, but did not significantly impact the reconnection rate. *MMS* observations of lower hybrid fluctuations associated with reconnection at the magnetopause are often consistent with the properties found in 3D simulations (for a detailed overview of the LHDI associated with reconnection from spacecraft observations and simulations see Graham et al., this collection) and feature broadband power-law spectra suggestive of turbulent dynamics. How-

ever, such fluctuations (both in observations and simulations) are often observed in narrow boundary regions, making it challenging to apply typical turbulence analyses and it remains unclear whether nonlinear processes play a significant or dominant role in the evolution of the waves or if there is significant energy transfer across spatial scales.

As discussed in Sec. 3.1, turbulence is also generated in the reconnection outflows. Pritchett and Coroniti (2010) and Vapirev et al. (2013) showed that in 3D fully kinetic simulations a Rayleigh-Taylor-like interchange instability occurs in association with the density gradients at the dipolarization front, generating a turbulent outflow. Lapenta et al. (2015) investigated the outflows using similar simulations, finding signatures of secondary reconnection events embedded within the complex turbulent fluctuations in the outflows. Subsequent works were able to automatically identify such secondary reconnection events using machine learning methods (Lapenta et al., 2022). Numerical simulations have also demonstrated the ability of turbulence in the outflows to efficiently accelerate electrons into nonthermal power-law tails similar to those observed in the magnetotail observations (Lapenta et al., 2020a).

For extended (long) current sheets, the plasmoid instability is also well-known to occur in numerical simulations. In the context of MHD, theory predicts a long current sheet can generate a chain of secondary magnetic islands with secondary current sheets between them if the Lundqvist number ($S = \mathcal{L}V_A/\eta$; i.e., similar to the magnetic Reynolds number but based on the Alfvén velocity) is large enough relative to the aspect ratio of the current sheet (Shibata and Tanuma, 2001; Loureiro et al., 2007). In this regime, the reconnection rate is expected to be independent on resistivity. Each secondary current sheet can also be plasmoid-unstable with possibly leading to a downward cascade of plasmoids in a fractal way until they eventually reach kinetic scales, triggering kinetic reconnection. Turbulence arises due to the interaction between those plasmoids (or flux ropes in 3D). This plasmoid instability has received significant attention and has been mainly analyzed using MHD simulations (see, e.g., Bárta et al., 2011; Huang and Bhattacharjee, 2016, and references therein). The transition from a collision-dominated plasmoid instability to kinetic reconnection was studied in 3D PIC simulations including a collision operator (Stanier et al., 2019). But, in general, there has been relatively little work of collisionless kinetic reconnection simulations of plasmoids with a focus on the self-generated turbulence. One relevant example of such a work is Fujimoto and Sydora (2012), who simulated 3D reconnection with a long current sheet, finding the plasmoid formation precedes the enhancement of electromagnetic turbulence due to shear flows, associated with anomalous momentum transport. The turbulence is first enhanced around the plasmoid and later, after the plasmoid ejection from the x-line, expands toward the X-line. Fermo et al. (2012) found using 2D simulations that the electron Kelvin-Helmholtz instability can generate plasmoids at small-scales in the kinetic regime. Markidis et al. (2013) simulated a long 3D current sheet, finding evidence for the complex interaction of the resulting plasmoids formed by the tearing instability and bump-on-tail instability together, which generated electron holes and complex electrostatic fluctuations near the plasmoids. Nakamura et al. (2021) used 2D PIC simulations of a current sheet initially seeded with an ensemble of magnetic field perturbations in order to generate multiple X-points. The evolution of the system led to a broadband power-law magnetic energy spectrum with a spectral index of -4 below ion

scales. The merging of islands led to a decrease in the reconnection rate and a reduction of the aspect ratio of the electron diffusion region. As a result, magnetic islands/plasmoids can grow within the electron diffusion region, allowing an (inverse) energy transfer to larger scales.

While the above simulation works identified instabilities and the development of seemingly turbulent dynamics during the nonlinear evolution of those instabilities, they generally did not perform the detailed statistical analyses of the fluctuations typical of turbulence theory. Leonardis et al. (2013) analyzed the simulations of Daughton et al. (2011), finding evidence of intermittency both in the increments of $\mathbf{B}$ and in $\mathbf{j} \cdot \mathbf{E}$, indicative of the turbulent nature of the dynamics. Pucci et al. (2017) analyzed the outflows of 3D reconnection simulations with a similar setup and parameters as those of Vapirev et al. (2013) and Lapenta et al. (2015), demonstrating the development of a turbulent cascade and intense dissipation at the boundary between the reconnection outflow and the ambient plasma with turbulence statistics similar to those reported in magnetotail observations. Further work explored the dynamics associated with the collision of two reconnection jets in an O-point/magnetic island geometry, showing the development of broadband non-stationary fluctuations between the ion and electron cyclotron frequencies confined to the interaction region between the jets. Muñoz and Büchner (2018) characterized the magnetic spectra in simulations similar to those of Che et al. (2011), demonstrating the development of broadband kinetic-scale turbulence with typical frequencies between the lower-hybrid and up to the electron-cyclotron frequencies. The magnetic spectra steepened as the instabilities evolved, eventually reaching a power-law of $\sim k^{-2.8}$ (typical of observations of kinetic-scale turbulence) once the reconnection rate reached a normalized value of 0.1. Interestingly, the reconnection rate is enhanced beyond the typical value of 0.1 as the system evolved further, in conjunction with the spectral slope steepening. Zharkova and Xia (2021) performed a similar analysis to Muñoz and Büchner (2018) but for a simulation with a more extended current sheet that led to the formation of more plasmoids, emphasising the role of accelerated particles in generating the unstable beam distributions that excite the turbulence. In contrast to the previous works, Adhikari et al. (2020) analyzed not a turbulent but initially laminar 2D PIC reconnection simulation, analyzing the spectral properties of the resulting fluctuations. In steady state, where the reconnection rate was near 0.1 (in normalized units), the fluctuations featured a double power law spectra following $\sim k^{-5/3}$ for scales larger than d_i (fluid scales) and $\sim k^{-8/3}$ for scales between d_i and d_e (kinetic scales). Similar to the 3D simulations by Muñoz and Büchner (2018), Adhikari et al. (2020) found a correlation between the reconnection rate and the energy spectrum, but mainly for wavenumbers near d_i^{-1}. In addition, Adhikari et al. (2020) determined that, while initial energy spectrum associated with the current sheet is highly anisotropic, the anisotropy diminishes as reconnection develops. Lapenta et al. (2020b) explored the spectra of the turbulent fluctuations in diverse regions around the main reconnection site using 3D fully kinetic PIC simulations, finding a relationship between the local values of the plasma-β and the coupling between plasma and electromagnetic field fluctuations In the high-β regions corresponding to the reconnection outflows, plasma and electromagnetic fluctuations are coupled and turbulent, while, in the low-β region corresponding to the reconnection inflow, diffusion region and around the separatrices, the plasma flows appear laminar while the electromagnetic fluctuations appear turbulent. Such

results potentially suggest that anomalous resistivity and viscosity primarily play a role in the outflow regions.

4 The Kelvin-Helmholtz Instability & the Role of Reconnection in the Transition to Turbulence

Alongside reconnection, other large-scale structures/instabilities can drive turbulence in a plasma and reconnection can play role as a secondary instability in the initial development of the system into a turbulent state. While this scenario has connections with those discussed in Secs. 2 and 3, it is worth considering some of its unique features. Several numerical studies have looked at the role of reconnection in the destabilization of large-scale initial configurations and the onset of turbulence, noting the apparent non-local energy exchange as reconnection rapidly excites small sub-proton-scale fluctuations (Gingell et al., 2017; Franci et al., 2017; Manzini et al., 2023). One region where the excitation of such a large-scale instability and the subsequent transition to turbulence has been clearly observed in space plasmas is along the strong velocity shear boundary on the flanks of Earth's magnetopause in which the Kelvin-Helmholtz instability (KHI) is well-known to occur. Magnetic and velocity shears, such as those found at the magnetopause, coexist in many boundaries in dynamic plasma environments, such as planetary magnetopauses, the heliopause, solar and stellar flares, and astrophysical jets. While, for sufficiently large magnetic shears, reconnection is expected to be a dominant process, strong velocity shears approaching the Alfvén speed based on the sheared component of $\mathbf{B}$ are expected to suppress instabilities, such as the tearing instability, that are thought to initiate reconnection (Chen and Morrison, 1990; Faganello et al., 2010) and can excite the KHI. Theory and numerical simulations suggest the vortical flow produced by the nonlinear evolution of the KHI can strongly distort and twist $\mathbf{B}$, inducing secondary reconnection that may contribute to the evolution of the KHI into a turbulent boundary layer. Recent large-scale simulations further predict that this so-called vortex-induced reconnection (VIR) process can cause mass and energy transfer as efficiently as that caused by regular reconnection induced under large magnetic shears and in-situ observations by various spacecraft have confirmed the evolution of VIR at the magnetopause.

4.1 Vortex-Induced Reconnection

Based on linear MHD theories and 2-D two-fluid simulations, Nakamura et al. (2008) summarized two-types of VIR that can be excited in the 2D vortex plane. Type-I VIR occurs when pre-existing magnetic shear is locally compressed by the non-linear vortex flow (Pu et al., 1990; Knoll and Chacón, 2002) as shown in Fig. 5a. Since Type-I VIR reconnects field lines originally located on different sides of the shear layer, this process can cause rapid plasma mixing across the layer (Nakamura et al., 2011; Nakamura and Daughton, 2014). In addition, linear theory predicts Type-I VIR is commonly triggered in boundaries where moderate amplitude magnetic and velocity shears co-exist, as often seen at Earth's magnetopause (Nakamura et al., 2006).
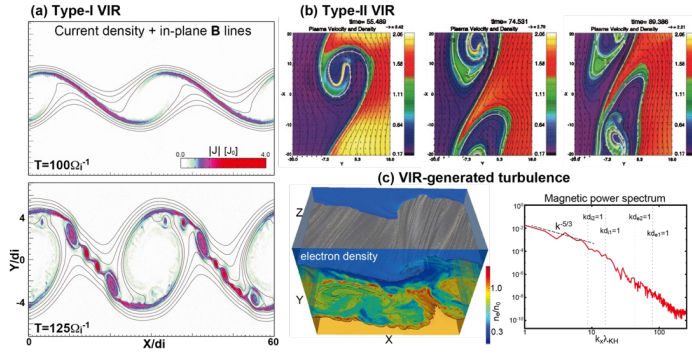
Fig. 5 (a) Current density and in-plane magnetic field lines of a 2D fully kinetic simulation of Type-I VIR, showing formation of multiple magnetic islands in the compressed current layer (reproduced from Nakamura et al., 2013). (b) Plasma density and field lines of a 2-D MHD simulation of Type-II VIR, showing island formation in vortex arms (reproduced from Nykyri and Otto, 2001). (c) 3D view of electron density and magnetic power spectrum of a 3D fully kinetic simulation of Type-I VIR, showing generation of turbulence (reproduced from Nakamura et al., 2017b).

Type-II VIR is driven in highly rolled-up vortices where the wrapped field lines secondarily form thin current sheets (Nykyri and Otto, 2001; Nakamura and Fujimoto, 2005; Faganello et al., 2008) as shown in Fig. 5b. Nakamura and Fujimoto (2005) performed a parameter study suggesting Type-II VIR is triggered when the velocity shear is significantly larger ($\gtrsim 5\times$) than the Alfvén speed based on the component of **B** along the shear. Since Type-II VIR divides the vortex and forms magnetic islands penetrating through the vortex layer, this process can also cause efficient plasma transport across the boundary (Nykyri and Otto, 2001). However, since the magnetic topology change in Type-II VIR occurs within a single wrapped field line, the process of Type-II VIR on its own cannot cause plasma mixing in 2D and additional 3D effects, collisionless cross-field diffusion, and/or the coupling with other types of VIR are necessary to enable cross-field mixing and transport. Based on numerical simulations, both types of VIR are expected to coexist in the KHI vortex layer (Nakamura et al., 2008, 2013; Karimabadi et al., 2013).

In these VIR processes, vortical flows strongly compress the current layers down to electron-scales (Nakamura et al., 2011). When the length of the compressed current layers, which depends on the size of the parent KH vortex, is sufficiently long compared to electron-scales, multiple plasmoids, with initial sizes comparable to election scales, are observed to form in the compressed current layers for both Type-I and Type-II VIR based on numerical simulations (Nakamura et al., 2011, 2013; Karimabadi et al., 2013), as shown in Fig. 5a. Reminiscent of the plasmoid instability discussed in Sec. 3, this tertiary instability contributes to the generation of complex turbulent dynamics within the shear layer through the interaction of magnetic islands from electron to MHD scales. In addition, recent 3D kinetic simulations demonstrated that, Type-I VIR can be triggered and evolve over a broad range of oblique angles, which significantly enhances the rate of plasma mixing, as well as the amplitude of the turbulence (Nakamura et al., 2013, 2017b) as shown in Fig. 5c.

While the above studies considered relatively small magnetic shears appropriate to northward interplanetary magnetic field (IMF) conditions at the magnetopause, 3D MHD and kinetic simulations have suggested that, when the magnetic shear is large enough, the turbulent evolution of Type-I VIR quickly disturbs and destroys the vortex structure (Ma et al., 2014; Nakamura et al., 2020a). On the other hand, more recent 3D kinetic simulations modeling realistic magnetopause conditions under southward IMF showed that when the density jump across the magnetopause is sufficiently large, which would happen more often under southward IMF, the rapid evolution of the LHDI at the compressed current layers quickly diffuses the layers and suppresses Type-I VIR (Nakamura et al., 2022a), although the substructure produced by the vortex-induced LHDI can itself induce small-scale reconnection (Nakamura et al., 2022b).

Although most of the above assumed the initial equilibrium varied only in the boundary normal direction, the conditions can also vary in different directions in many realistic situations. At Earth's magnetopause, the KHI is unstable at lower latitudes on the magnetopause and stable above and below at higher latitudes (Takagi et al., 2006). Numerical simulations modeling these conditions have demonstrated the KHI vortex motion twists **B** generating additional magnetic shears in the transition region between the low-latitude unstable and high-latitude stable layers, inducing reconnection at mid-latitudes as illustrated in Fig. 6a,b. Contrary to Type I VIR, in this mid-latitude reconnection (ML VIR) magnetic shear is created even if the pre-existing magnetic fields are aligned across the boundary. Furthermore, since the evolution of the KH vortices and thus ML VIR is symmetric with respect to the equatorial plane, reconnection occurs simultaneously in both hemispheres, creating "double-reconnected" field lines topologically connected to the Earth but embedded in the magnetosheath at low-latitudes (Faganello et al., 2012a,b; Borgogno et al., 2015). The creation of such field lines enhances particle transport across the boundary (Faganello et al., 2012b; Borgogno et al., 2015), and can explain the specific entropy increase on the magnetospheric side of the boundary (Johnson and Wing, 2009).

In the presence of pre-existing magnetic shear, both Type-I VIR and ML VIR occur, with Type-I VIR dominating at low latitudes. The pre-existing magnetic shear breaks the symmetry in the ML VIR process - gradually enhancing the magnetic shear by differential advection in one hemisphere, while reducing it in the other. The evolution of magnetic topology is quite complex, with a dominant Type-I VIR acting close to the equatorial plane, and ML VIR going on in only one hemisphere, as shown in Fig. 6c, leading to a less efficient, but still important, production of double-reconnected lines (Sisti et al., 2019; Faganello et al., 2022).

4.2 Observations of Vortex-Induced Reconnection

Hasegawa et al. (2004) presented evidence of the coexistence of solar wind and magnetospheric ions on the same field lines, suggesting particle transport across the magnetopause, in association with KH waves using *Cluster* observations. However, magnetic reconnection was initially ruled out as the cause of the plasma transport given the absence of ion reconnection exhaust observations and reconnection-associated D-shaped ion velocity distributions (e.g., Cowley, 1982; Fuselier et al., 2014) throughout the KH-active interval. A further analysis of the same event
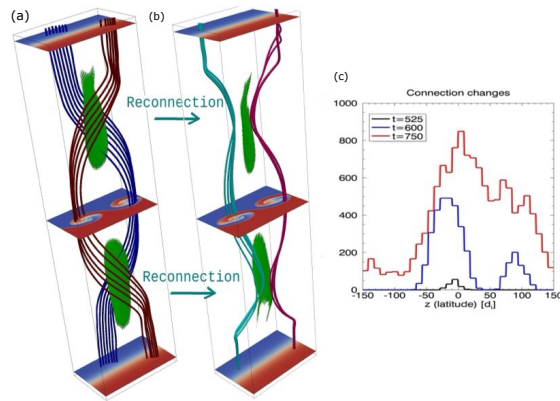
Fig. 6 (a) 3D view of field line deformation due to differential advection in the symmetric case. Blue (magnetospheric) and red (magnetosheath) field lines are initially parallel and twisted by differential advection, creating magnetic shears (green regions). (b) Double-reconnected field lines created by ML VIR, with pale blue lines connecting to magnetospheric (blue) plasma at high-latitudes and magnetosheath (red) plasma at the equator (adapted from Faganello et al., 2012a). (c) Latitude distribution of connection changes (created by reconnection), for different times, in the asymmetric case. At t=600, the main peak is due to Type-I VIR, while the secondary peak is due to ML VIR (reproduced from Sisti et al., 2019).

by Hasegawa et al. (2009) provided the first direct indication that magnetic reconnection was involved with the plasma trasport associated with the KHI on the flanks of Earth's magnetopause. High-cadence **B** measurements across the so-called spine-regions between neighboring KH vortices captured several localized current sheets with thicknesses of only a few d_i. One such current sheet showed evidence of bifrucation (Gosling and Szabo, 2008) and Alfvénic outflow signatures, inferred from the $\mathbf{E} \times \mathbf{B}$ drift, in agreement with predictions of Type-I VIR (e.g., Pu et al., 1990; Nakamura et al., 2006, 2008), although direct measurement of the outflow jet with the particle measurements was not possible.

MMS provided the high cadence ion measurement capabilities necessary to resolve the ion jets embedded with in the KH vortices. Eriksson et al. (2016a) surveyed an extended KH wave-train observed for over an hour at the magnetopause on 8 September 2015, providing the first direct confirmation of ion reconnection exhausts at the quasi-periodic compressed current sheets in the spine region of the KHI associated with Type-I VIR. In total, reconnection exhausts were found at 22 of the 42 currents sheets with equal probability of encountering reconnection outflows in either direction relative to the x-lines Thicknesses normal to the reconnecting current sheets were $4.4 \pm 1.9 d_i$. In addition to outflow signatures, Hall magnetic field perturbations (Eriksson et al., 2016a) and particle fluxes across the locally open magnetopause (Li et al., 2016; Vernisse et al., 2016) were also identified in these events. Furthermore, in one case, evidence of the EDR was also identified with two of the *MMS* spacecraft (*MMS*1 and *MMS*2) encountering the ion exhaust, while the other two spacecraft did not but instead encountered signatures indicative of the EDR (Eriksson et al., 2016b). In particular, strong parallel electric fields ($E_{||} \sim -15$ mV/m) and enhanced $\mathbf{j} \cdot \mathbf{E}' \sim 8 - 9$ nW/m^3 were identified. Since the KHI events under generally northward IMF conditions are expected to produce reconnection at current sheets with relatively low magnetic shear, this

event provided one of the first direct measurements of the EDR under strong guide field conditions, with an observed guide field $\sim 4\times$ the reconnecting field.

Evidence of ML VIR has also been identified in observations. Faganello et al. (2014) reported a short-duration interval of 100–500 eV counter-streaming electrons in *THEMIS* observations and interpreted them as magnetosheath electrons accelerated along recently closed field lines at two ML VIR regions, and Vernisse et al. (2016) confirmed a similar signature in *MMS* electron measurements in the 8 September 2015 KHI event. Eriksson et al. (2021) also reported several short-duration "burst" of counter-streaming field-aligned ion beams in the 8 September 2015 KHI event. The ion velocity distributions were typically "D-shaped" in phase-space, as commonly associated with magnetopause reconnection (Cowley, 1982). It was concluded that the counter-streaming ion beams, which were encountered in the leading edge of the vortices in contrast with the Type-I VIR events that were encountered at the trailing edge current sheets, were associated with two nearby ML VIR events above and below the spacecraft, in agreement with predictions of double-reconnected field lines in numerical simulations (Sisti et al., 2019).

Many other aspects of plasma dynamics have been explored using *MMS* observations from the 8 September 2015 KHI event, including several detailed reports on the generation of plasma turbulence and plasma wave activity within the vortices (e.g., Stawarz et al., 2016; Wilder et al., 2016; Nakamura et al., 2017b; Sturner et al., 2018; Sorriso-Valvo et al., 2019; Hasegawa et al., 2020; Quijia et al., 2021). Stawarz et al. (2016) showed that electromagnetic fluctuations observed in the KH vortices were characterized by a Kolmogorov-like power spectrum at large MHD scales (Fig. 7b) with signatures of intermittency potentially associated with secondary current sheets formed through the nonlinear KHI development. Hasegawa et al. (2020) further investigated the turbulence suggesting the **B** fluctuations in the KH vortices were convective structures associated with interlinked flux tubes generated through 3D turbulent VIR (Nakamura et al., 2013, 2017a), rather than propagating waves. Further analyses have attempted to probe the evolution of KHI turbulence by examining KHI events encountered at different distances along the magnetopause by *THEMIS* and *Geotail*, although challenges arise from convolving event-to-event variation with the temporal evolution (Di Mare et al., 2019).

While the above studies primarily focused on turbulence generation within KH vortices through the lens of KHI and VIR processes, seed perturbations induced by pre-existing magnetosheath turbulence can also act to enhance the KHI growth, and were suggested as an explanation for the apparently rapid onset of turbulent dynamics in the 8 September 2015 KHI event compared to simulations (Nykyri et al., 2017; Nakamura et al., 2020b). Furthermore, for southward IMF, the KHI growth can not only induce reconnection but also form thin density gradient layers at the edge of the KH waves or vortices, which may become unstable to the LHDI (Blasl et al., 2022). The resulting LHDI waves or turbulence can in turn cause diffusive plasma mixing across the magnetopause (Nakamura et al., 2022b). Thus, there may be an intriguing interplay among turbulence, magnetic reconnection, and MHD and kinetic instabilities, which needs to be further explored.
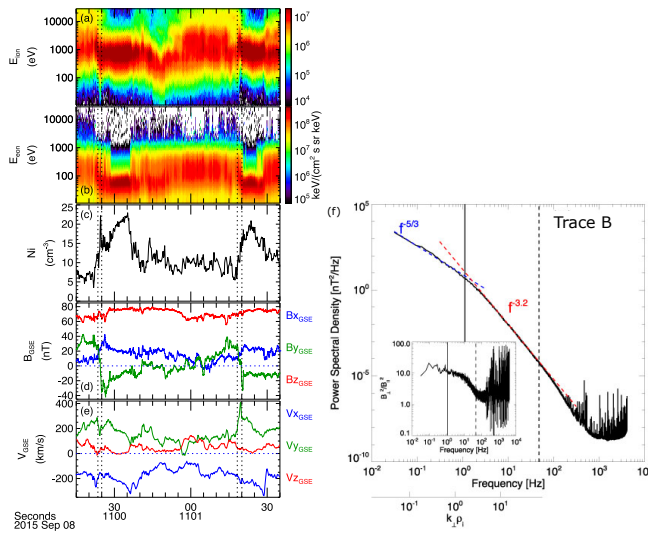
Fig. 7 Example *MMS* observations of two consecutive KH vortices associated with Type-I VIR ion exhausts as highlighted between pairs of vertical dotted lines, showing the (a) omnidirectional ion differential energy flux, (b) omnidirectional electron differential energy flux, (c) ion number density, (d) **B**, and (e) ion bulk flow velocity. Vector quantities are shown in GSE coordinates. (f) Magnetic power spectrum within the KH vortices observed by *MMS* on 8 September 2015, which is characterized by a Kolmogorov-like ($k^{-5/3}$) power law at MHD scales (reproduced from Stawarz et al., 2016).

5 Stochastic Reconnection

A final facet of turbulent reconnection is so-called stochastic reconnection, whereby the wandering of magnetic field lines associated with the turbulent fluctuations plays a dominant role in setting the reconnection rate. The ways in which turbulence may impact magnetic reconnection in this manner were discussed by Matthaeus and Lamkin (1986); however, more complete theoretical treatments were developed by Lazarian and Vishniac (1999) and Eyink et al. (2011). Several reviews discussing the details of this topic have been written over the years (e.g., Lazarian et al., 2012, 2015, 2020) and we will refrain from reiterating a detailed discussion of the process here. However, in this review we provide a brief overview of the conceptual picture and how it interfaces with the other facets of turbulent reconnection discussed in the previous sections.

Stochastic reconnection envisions a "large-scale" magnetic shear, potentially associated with a pre-existing current sheet embedded within a turbulent environment or a variation in the field orientation associated with larger-scale turbulent fluctuations, that is superposed with small-scale turbulent fluctuations introducing a stochastic wandering of the field lines. This field line wandering is akin to Richardson diffusion in hydrodynamic turbulence and, importantly, introduces a rate of diffusion (or perhaps more intuitively dispersion) of the field lines set by the properties of the turbulence, which is independent of the particular non-ideal mechanisms (be that collisional resistivity or collisionless effects) operating in the plasma. In this sense, the stochastic reconnection picture may have applications

to both the turbulence-driven reconnection and reconnection-driven turbulence scenarios discussed in the previous sections.

As discussed in Liu et al. (this collection), $\mathcal{R}$ is dictated by the aspect ratio (thickness over length) of the diffusion region. Stochastic reconnection allows the thickness of the diffusion region (often referred to as a reconnection layer in this context) to be set by the stochastic field line wandering, resulting in a much wider reconnection layer than otherwise expected. In this way, stochastic reconnection is capable of producing a reconnection rate that is both fast and independent of microphysical nonideal effects. In terms of generalized Ohm's law (see Liu et al., this collection), one can view stochastic reconnection as exploring the effect of the nonlinear contribution of the ideal MHD term ($-\delta\mathbf{u}\times\delta\mathbf{B}$) associated with the turbulent fluctuations on the reconnection process (see the discussion of generalized Ohm's law in Eyink, 2015; Stawarz et al., 2021; Lewis et al., 2023). Stochastic reconnection is subtly different than facilitating reconnection by invoking anomalous resistivity/viscosity (as discussed in Sec. 3.2) with regard to the order of averaging that one considers. In contrast to anomalous resistivity, where one considers reconnection of an averaged $\mathbf{B}$, stochastic reconnection considers the cumulative stochastic effect of reconnection of the full field lines.

Lazarian and Vishniac (1999) presented a physical picture in which the resulting wider reconnection outflow was supported by a multitude of small-scale local reconnection events enabled by the "rough" perturbed magnetic field line topology of the turbulent fluctuations in the reconnection layer that cumulatively fill the outflow region. For a Goldreich-Sridhar-type spectrum, this picture results in an outflow velocity given by

$$V_{outflow} \approx V_{A,inflow}\min\left[\left(\frac{L_x}{\lambda_{inject}}\right)^{1/2}, \left(\frac{\lambda_{inject}}{L_x}\right)^{1/2}\right]\mathcal{M}^2_{A,\lambda_i}, \qquad (23)$$

where L_x is the length of the reconnection layer along the outflow direction, λ_i is the injection scale of the turbulent fluctuations (which might be considered as $\lambda_{C,\mathbf{B}}$), and $\mathcal{M}_{A,\lambda_i} = \delta u_{\lambda_i}/\delta V_{A,\lambda_i}$ is the turbulent Alfvén Mach number for fluctuations at the injection scale. Eyink et al. (2011) and Eyink (2015) supported this picture in an alternative more mathematically rigorous way by showing that for turbulent velocity fields $\mathbf{B}$ is only frozen-in to the flow in a stochastic sense even in the limit of vanishing nonideal effects, obtaining equivalent results to those of Lazarian and Vishniac (1999).

The clearest evidence for stochastic reconnection comes from numerical simulations. Kowal et al. (2009) examined MHD simulations of a reconnecting current layer with different levels of turbulence manually injected into the system, finding $\mathcal{R}$ scaled in a manner similar to the predictions of Lazarian and Vishniac (1999). Further, while in the absence of turbulence $\mathcal{R}$ scaled with resistivity in a manner consistent with Sweet-Parker reconnection, in the presence of turbulence $\mathcal{R}$ was independent of resistivity. The structure of the reconnection layer was broadened in the presence of turbulence and made up of many thinner intense current regions, the cumulative effect of which resulted in the overall $\mathcal{R}$ (Kowal et al., 2009, 2012; Vishniac et al., 2012). Using large MHD turbulence simulations, Eyink et al. (2013) further demonstrated the Richardson-like dispersion behavior of field lines, enabling stochastic breaking of the frozen-in condition.

Clear observational evidence demonstrating stochastic reconnection has not been extensively demonstrated and, in fact, is likely difficult to obtain from the local *in situ* measurements. Lalescu et al. (2015) reported similarities between solar wind reconnection events and turbulent MHD simulations in which the stochastic field line wandering effect was demonstrated to occur - although it remains to be seen whether such qualitative similarities are unique to the proposed scenario. Tangential evidence has also been suggested for the stochastic violation of the frozen-in theorem based on statistical analyses of the Parker spiral (Eyink, 2015).

A key aspect of stochastic reconnection is that it requires the existence of an extended MHD-scale inertial range into which the reconnection dynamics of interest are well coupled - that is, the lengths, widths, and thicknesses of the reconnection layers are within the MHD-scale inertial range. In the solar wind, reconnection outflows can be hundreds or even thousands of d_i (Mistry et al., 2017) and the length of the x-line (in the direction orthogonal to the quasi-2D reconnection plane) can be $10^4 d_i$ (Phan et al., 2006, 2009) - both of which are well within the MHD-scale inertial range of solar wind turbulence. The quasi-laminar collisionless reconnection viewpoint would typically treat these large length scales, particularly the width of the observed outflows, as being indicative of traversing the outflow far from the x-line (e.g., Mistry et al., 2015b). Stochastic reconnection, on the other hand, would suggest that these large length scales are driven by the stochastic wandering effect. In the solar wind, there is some evidence for complex distorted structure of reconnection outflow boundaries from multipoint observations (Mistry et al., 2015a), which may be suggestive of the stochastic reconnection picture (although not necessarily conclusive). However, it is generally challenging to tease out direct evidence distinguishing these view points from *in situ* measurements.

This requirement of an extended MHD-scale inertial range may make stochastic reconnection, most relevant to the solar wind, solar corona, and some astrophysical environments with larger dynamical ranges of fluctuations in contrast to the magnetospheric environments such as the magnetosheath, magnetotail, and magnetopause shear layer, which, while present, have more modest MHD-scale inertial ranges. Furthermore, it also does not necessarily preclude the existence of localised kinetic-scale reconnecting structures well described by collisionless reconnection dynamics embedded within the turbulent environment. As discussed in Secs. 2 – 4, clear evidence of such kinetic reconnection dynamics is found within turbulent environments, including electron-only reconnection embedded within the magnetosheath and electron diffusion regions that appear consistent with quasi-2D collisionless reconnection in turbulent magnetotail events. In this light, the further exploration of stochastic reconnection principles in the context of nonlinear collisionless effects, for example the Hall effect or relatedly advection in electron MHD, may be an interesting avenue of research for environments with less extended MHD-scale inertial ranges.

6 Conclusions

As illustrated in this review, the interaction between magnetic reconnection and turbulence is a rich field of study that can be approached from multiple viewpoints, each of which has unique nuances and applications to a variety of plasma

environments. In a broad sense, the study of turbulence aims to understand the general nonlinear dynamics arising in a fluid or plasma due to the coupled interaction of a vast array of fluctuations that might consist, for example, of a mixture of waves, current sheets, plasmoids/flux ropes, vortices, and other localized structures. As a fundamental plasma process that can occur in a diverse range of settings, magnetic reconnection events have the potential to be one of these nonlinear structures, which can act to mediate the nonlinear interaction of magnetic structures and facilitate energy dissipation both in systems that are in a fully-developed turbulent state or that are developing into one. In other configurations, where magnetic reconnection is the primary process acting at a system scale current sheet, secondary processes associated with magnetic reconnection can act to excite turbulent fluctuations in the plasma, which mediate the partition of energy released by the reconnection event. Furthermore, the presence of complex turbulent fluctuations can also potentially impact how magnetic reconnection proceeds, for example, by enhancing the reconnection rate through the action of anomalous resistivity/viscosity near the x-line or through stochastic field line wandering.

While these various aspect of turbulent reconnection have been examined in a wide array of theoretical, numerical, and observational studies over the past several decades, recent high-resolution spacecraft measurements, in particular from the *Magnetospheric Multiscale* mission, have ushered in a new era of investigating this complex topic. Analyses enabled by these measurements have provided new insights ad observational constraints that have spurred on a range of new theoretical and numerical investigations. Several areas of recent progress that are of particular note and that have been highlighted in this review are:

1. Recent observations of turbulence-driven magnetic reconnection in the transition region and downstream magnetosheath of Earth's bow shock. Systematic surveys of small-scale reconnection events in this environment have allowed statistical examinations of how the turbulent dynamics influence the nature of the magnetic reconnection events and the potential role that magnetic reconnection plays in the turbulent dynamics. Observations in this environment have revealed that so-called electron-only magnetic reconnection can occur when the correlation length of the turbulent magnetic field fluctuations sufficiently limits the extent of the reconnecting current sheets. This was a novel discovery that had not been extensively explored prior to the *MMS* observations, which highlights how the properties of the large-scale turbulent fluctuations can shape the dissipative processes operating in the plasma and may have implications for how the energy dissipated by turbulence is partitioned.

2. Detailed observations of turbulent x-lines and bursty bulk flow braking regions in Earth's magnetotail. These regions have revealed how turbulence facilitates the energization of high-energy non-thermal particles, how turbulence mediates the re-partitioning of energy released by magnetic reconnection both through spontaneously generated turbulence and the interaction with the surrounding environment, and demonstrated that identifiable electron diffusion region signatures, reminiscent of the quasi-laminar picture, can be identified even amidst the complex turbulent fluctuations.

3. New observations of the Kelvin-Helmholtz instability on Earth's magnetopause that have both revealed clear evidence of the various forms of vortex-induced magnetic reconnection and the coupled evolution of the instability into a tur-

bulent boundary layer, which can play a key role in the transport of mass, momentum, and energy across the magnetopause and, potentially, other velocity shear boundaries throughout the Universe.

Despite this recent progress a variety of open questions remain. The systematic identification of turbulence-driven reconnection events allows the estimation of the extent to which magnetic reconnection contributes to turbulent dissipation. However, more refined analyses require further constraints on the reconnection rate and particle heating/energisation associated with magnetic reconnection – in particular, in terms of the contrast between electron-only and ion-coupled reconnection. Both these factors could, in principle, be further examined using numerical simulations either of fully turbulent domains or well designed numerical experiments using idealised configurations.

Another key area of advancement will be in adapting our understanding of turbulence-driven reconnection to other astrophysical environments. Addressing this point requires further understanding of the configuration of reconnecting current sheets (e.g., whether they are fragmented, "rolled-up", or otherwise deformed) and how this may depend on the Reynolds number/scale separation in the system, as well as how the prevalence of turbulence-driven magnetic reconnection is impacted by the driving, fluctuation characteristics, and ambient plasma conditions. Such factors may have an influence on the number of reconnection events per unit volume in the turbulent domain and the extent to which electron-only reconnection and ion-coupled reconnection are important in different systems. A useful path to pursue in this regard may be in contrasting turbulence-driven reconnection across the different turbulent environments that we have access to in near-Earth space, such as Earth's magnetosheath and the solar wind – particularly given the extreme contrast in effective scale separation between the driving and kinetic scales between these two environments. However, a key component of such studies would need to involve clearly assessing the extent to which reconnection events in the solar wind are related to locally generated turbulent structure rather than large-scale solar wind structure. Upcoming missions, such as NASA's *HelioSwarm* (Klein et al., 2023) which aims to specifically target the multi-scale nature of solar wind turbulence with a large swarm of spacecraft, may aid in assessing the role of turbulence-driven reconnection in the solar wind, but it may also require new technology and mission concepts capable of probing the electron scales in the solar wind to determine the extent to which electron-only reconnection may be relevant at fragmented current sheets in the solar wind (Verscharen et al., 2022). Numerical studies will also likely be a key component of probing how such dynamics may change in more exotic environments that are not directly accessible with spacecraft observations. Given the challenge in identifying 3D magnetic reconnection events in the complex magnetic environments of turbulent plasmas, machine learning or partially machine learning based approaches to systematically identifying turbulence-driven magnetic reconnection events may prove to be a useful tool.

The recent theoretical and numerical work on reconnection-mediated turbulence, which explore the potential role of reconnection in mediating the nonlinear interactions in turbulent plasmas, have also presented intriguing results that still stand to be observationally confirmed. However, further observational tests that go beyond strictly spectral slope based analyses may be necessary to unambiguously confirm the presence of this regime given the similarity of the spectral predictions

to commonly observed kinetic-scale turbulent spectra that can be predicted by other means.

In the context of turbulence-driven reconnection, key areas of future research will likely come from developing a further understanding of how the turbulent processes associated with magnetic reconnection couple into and govern the energy transport of the global system. For Earth's magnetotail, such work could involve clear and systematic surveys of the extent to which the turbulent fluctuations accelerate energetic particles particularly in the braking region where they may act to seed the energetic particles in the radiation belts, exploring the wave radiation associated with confined regions of turbulence that may be generated in reconnection outflows, and systematically quantifying how the partition of energy evolves with both time and distance from the x-line in turbulent reconnection outflows. As well as having relevance to the magnetotail, such studies may also be relevant to reconnection in solar coronal loops, astrophysical jets, and possibly magnetopause reconnection. The impact of anomalous resistivity/viscosity and stochastic field line wandering on the magnetic reconnection rate, which is particularly useful for its application in parameterising the effects of turbulence in astrophysical environments, still require clear and unambiguous observational confirmation. The potential impacts of turbulent inflow conditions on system-scale reconnection events, such as the impact of turbulent magnetosheath flow on magnetopause reconnection, may also be an interesting and related avenue of research.

Given the recent advances in our understanding of the interplay between turbulence and magnetic reconnection and further upcoming and potential missions such as NASA's *HelioSwarm* (Klein et al., 2023) and *Plasma Observatory* recently proposed to ESA (Retinò et al., 2022) that specifically target turbulence and cross-scale coupling in the solar wind and Earth's magnetosphere, there is a bright future for the further development of our understanding of this complex problem which stands to unlock new insights into the role of magnetic reconnection throughout the Universe.

Conflict of interest

The authors have no conflicts of interest to declare.

A Taylor's Hypothesis

Taylor's "frozen-in flow" hypothesis has been widely used to study the properties of space plasma fluctuations (Taylor, 1938). The hypothesis states that the advection of the small-scale fluctuations over a measurement point by the large-scale background flow occurs faster than any significant dynamical evolution of those fluctuations. Therefore, a time series measured at a single point in space can be interpreted as a spatial sample through the system. Using Taylor's hypothesis, ℓ is given by $\ell = \mathbf{U}_0 \tau$, where τ is a temporal lag. Similarly, the spacecraft-frame

frequency (f) spectrum can be interpreted as a k spectrum with the relation $k = 2\pi f/U_0$, although the spectrum computed this way should be interpreted as a reduced spectrum averaged onto the direction of $\mathbf{U}_0$ (Horbury et al., 2012). Taylor's hypothesis is satisfied for MHD scales when $U_0 \gg V_A$ and $U_0 \gg \delta u$. This assumption is typically well satisfied in the solar wind, where background flows are super-Alfvénic; however, in other environments, such as those found in the magnetosphere, the validity is less clear. Furthermore, at sub-proton-scales, the validity may be called into question due to the faster phase speeds at those scales.
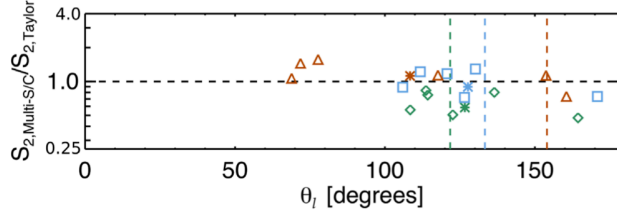
Fig. 8 Ratio of multi-spacecraft to single-spacecraft estimates of $S_2^{\mathbf{B}}(\ell)$ as a function of θ_ℓ for several intervals of magnetosheath turbulence measured by *MMS* (blue squares, red triangles, green diamonds). The six points for each interval correspond to the six spacecraft pairs in the formation. Averages of the six points are marked with asterisks, and vertical dashed lines mark the $\mathbf{U}_0$ direction (reproduced from Stawarz et al., 2019).

Using multi-spacecraft missions, such as *MMS* or *Cluster*, the Taylor hypothesis can be tested at the scale of the multi-spacecraft formation by comparing single-spacecraft statistics (e.g., structure functions or correlation functions) with their multi-point counterparts computed from pairs of spacecraft. For anisotropic turbulence, as expected in the presence of a strong $\mathbf{B}_0$, the correspondence between single- and multi-spacecraft statistics at a given scale may only occur along the direction of $\mathbf{U}_0$; however, the dependence on the angle between the lag and $\mathbf{B}_0$ (θ_ℓ) may provide insight into the validity of the Taylor hypothesis. Stawarz et al. (2019) compared single- and multi-spacecraft estimates of $S_2^{\mathbf{B}}(\ell)$ for *MMS* observations of turbulence in the magnetosheath, as shown in Fig. 8. For the super-Alfvénic flows (orange triangle and blue sqaures), good agreement is found for both intervals, with no particular dependence on θ, demonstrating the Taylor hypothesis can be valid even down to the small (~ 6km) separations of the *MMS* formation, which are much smaller than the proton scales, during these intervals In contrast, the green diamonds display a systematic overestimate of the single-spacecraft estimates relative to the multi-spacecraft estimates for all six spacecraft pairs, indicating that the Taylor hypothesis may not work well during this interval. Stawarz et al. (2022) performed a similar analysis across a range of turbulent intervals in the magnetosheath, demonstrating a clear signature of anisotropy in the turbulent fluctuations as a function of θ_ℓ with increasing strength for $\delta b_{rms}/B_0 < 1$. Good agreement was found between single- and multi-point statistics when θ_ℓ was equivalent to the angle between $\mathbf{B}_0$ and $\mathbf{U}_0$ for intervals where the Taylor hypothesis was valid. Other similar analyses have been performed by across the magnetosheath and other regions of the magnetosphere (e.g., Chasapis et al., 2017; Parashar et al., 2018; Bandyopadhyay et al., 2020).

References

Adhikari S, Shay MA, Parashar TN, et al (2020) Reconnection from a turbulence perspective. Phys Plasmas 27:042305, DOI 10.1063/1.5128376

Adhikari S, Parashar TN, Shay MA, et al (2021) Energy transfer in reconnection and turbulence. Phys Rev E 104:065206, DOI 10.1103/PhysRevE.104.065206

Adhikari S, Shay MA, Parashar TN, et al (2023) Effect of a guide field on the turbulence like properties of magnetic reconnection. Phys Plasmas 30:082904, DOI 10.1063/5.0150929

Adhikari S, Yang Y, Matthaeus WH, et al (2024) Scale filtering analysis of kinetic reconnection and its associated turbulence. Phys Plasmas 31:020701, DOI 10.1063/5.0185132

Agudelo-Rueda JA, Verscharen D, Wicks RT, et al (2021) Three-dimensional magnetic reconnection in particle-in-cell simulations of anisotropic plasma turbulence. J Plasma Phys 87:905870228, DOI 10.1017/S0022377821000404

Agudelo-Rueda JA, Verscharen D, Wicks RT, et al (2022) Energy transport during 3d small-scale reconnection driven by anisotropic plasma turbulence. Astrophys J 938:4, DOI 10.3847/1538-4357/ac8667

Alexakis A, Mininni PD, Pouquet A (2005) Shell-to-shell energy transfer in magnetohydrodynamics. I. Steady state turbulence. Phys Rev E 72:046301, DOI 10.1103/PhysRevE.72.046301

Alexandrova O, Lacombe C, Mangeney A (2008) Spectra and anisotropy of magnetic fluctuations in the Earth's magnetosheath: Cluster observations. Ann Geophys 26:3585–3596, DOI 10.5194/angeo-26-3585-2008

Aluie H (2017) Coarse-grained incompressible magnetohydrodynamics: analyzing the turbulent cascades. New J Phys 19:025008, DOI 10.1088/1367-2630/aa5d2f

Anselmet F, Gagne Y, Hopfinger EJ, Antonia RA (1984) High-order velocity structure functions in turbulent shear flows. J Fluid Mech 140:63–89, DOI 10.1017/S0022112084000513

Arró G, Califano F, Lapenta G (2020) Statistical properties of turbulent fluctuations associated with electron-only magnetic reconnection. Astron Astrophysics 642:A45, DOI 10.1051/0004-6361/202038696

Azizabadi AC, Jain N, Büchner J (2021) Identification and characterization of current sheets in collisionless plasma turbulence. Phys Plasmas 28(5):052904, DOI 10.1063/5.0040692

Bandyopadhyay R, Chasapis A, Chhiber R, et al (2018) Incompressive Energy Transfer in the Earth's Magnetosheath: Magnetospheric Multiscale Observations. Astrophys J 866:106, DOI 10.3847/1538-4357/aade04

Bandyopadhyay R, Chasapis A, Gershman DJ, et al (2020) Observation of an inertial-range energy cascade within a reconnection jet in the earth's magnetotail. M Not R Astron Soc Lett 500:L6–L10, DOI 10.1093/mnrasl/slaa171

Bandyopadhyay R, Sorriso-Valvo L, Chasapis Aaea (2020) In Situ Observation of Hall Magnetohydrodynamic Cascade in Space Plasma. Phys Rev Lett 124:225101

Bandyopadhyay R, Chasapis A, Gershman DJ, et al (2021) Observation of an inertial-range energy cascade within a reconnection jet in the Earth's magnetotail. Mon Not R Astro Soc 500:L6–L10, DOI 10.1093/mnrasl/slaa171

Banerjee S, Galtier S (2013) Exact relation with two-point correlation functions and phenomenological approach for compressible magnetohydrodynamic turbulence. Phys Rev E 87:013019, DOI 10.1103/PhysRevE.87.013019

Banerjee S, Galtier S (2017) An alternative formulation for exact scaling relations in hydrodynamic and magnetohydrodynamic turbulence. J Phys A 50:015501, DOI 10.1088/1751-8113/50/1/015501

Bárta M, Büchner J, Karlický M, Skála J (2011) Spontaneous Current-Layer Fragmentation And Cascading Reconnection In Solar Flares. I. Model And Analysis. Astrophys J 737:24, DOI 10.1088/0004-637X/737/1/24

Bauer TM, Baumjohann W, Treumann RA, et al (1995) Low-frequency waves in the near-Earth plasma sheet. J Geophys Res 100:9605–9618, DOI 10.1029/95JA00136

Bergstedt K, Ji H, Jara-Almonte J, et al (2020) Statistical Properties of Magnetic Structures and Energy Dissipation during Turbulent Reconnection in the Earth's Magnetotail. Geophys Res Lett 47:e88540, DOI 10.1029/2020GL088540

Bessho N, Chen LJ, Wang S, et al (2019) Magnetic Reconnection in a Quasi-Parallel Shock: Two-Dimensional Local Particle-in-Cell Simulation. Geophys Res Lett 46:9352–9361, DOI 10.1029/2019GL083397

Bessho N, Chen LJ, Wang S, et al (2020) Magnetic reconnection and kinetic waves generated in the Earth's quasi-parallel bow shock. Phys Plasmas 27:092901, DOI 10.1063/5.0012443

Bessho N, Chen LJ, Stawarz JE, et al (2022) Strong reconnection electric fields in shock-driven turbulence. Phys Plasmas 29:042304, DOI 10.1063/5.0077529

Bessho N, Chen LJ, Hesse M, Ng J, Wilson LB, Stawarz JE (2023) Electron Acceleration and Heating during Magnetic Reconnection in the Earth's Quasi-parallel Bow Shock. Astrophys J 954:25, DOI 10.3847/1538-4357/ace321

Biskamp D, Müller WC (2000) Scaling properties of three-dimensional isotropic magnetohydrodynamic turbulence. Phys Plasmas 7:4889–4900, DOI 10.1063/1.1322562

Biskamp D, Welter H (1989) Dynamics of decaying two-dimensional magnetohydrodynamic turbulence. Phys Fluids 1:1964–1979, DOI 10.1063/1.859060

Biskamp D, Schwarz E, Zeiler A, et al (1999) Electron magnetohydrodynamic turbulence. Phys Plasmas 6:751–758, DOI 10.1063/1.873312

Blasl KA, Nakamura TKM, Plaschke F, et al (2022) Multi-scale observations of the magnetopause Kelvin-Helmholtz waves during southward IMF. Phys Plasmas 29:012105, DOI 10.1063/5.0067370

Bohdan A, Pohl M, Niemiec J, et al (2020) Kinetic Simulations of Nonrelativistic Perpendicular Shocks of Young Supernova Remnants. III. Magnetic Reconnection. Astrophys J 893:6, DOI 10.3847/1538-4357/ab7cd6

Boldyrev S (2006) Spectrum of Magnetohydrodynamic Turbulence. Phys Rev Lett 96(11):115002, DOI 10.1103/PhysRevLett.96.115002

Boldyrev S, Loureiro NF (2019) Role of reconnection in inertial kinetic-Alfvén turbulence. Phys Rev Res 1:012006, DOI 10.1103/PhysRevResearch.1.012006

Boldyrev S, Loureiro NF (2020) Tearing Instability in Alfvén and Kinetic-Alfvén Turbulence. J Geophys Res 125:e28185, DOI 10.1029/2020JA028185

Boldyrev S, Perez JC (2012) Spectrum of Kinetic-Alfvén Turbulence. Astrophys J Lett 758:L44, DOI 10.1088/2041-8205/758/2/L44

Boldyrev S, Horaites K, Xia Q, Perez JC (2013) Toward a Theory of Astrophysical Plasma Turbulence at Subproton Scales. Astrophys J 777:41, DOI 10.1088/0004-637X/777/1/41

Borgogno D, Califano F, Faganello M, Pegoraro F (2015) Double-reconnected magnetic structures driven by Kelvin-Helmholtz vortices at the Earth's magnetosphere. Phys Plasmas 22:032301, DOI 10.1063/1.4913578

Borovsky JE, Funsten HO (2003) MHD turbulence in the Earth's plasma sheet: Dynamics, dissipation, and driving. J Geophys Res 108:1284, DOI 10.1029/2002JA009625

Borovsky JE, Elphic RC, Funsten HO, Thomsen MF (1997) The Earth's plasma sheet as a laboratory for flow turbulence in high-β MHD. J Plasma Phys 57:1–34, DOI 10.1017/S0022377896005259

Bowen TA, Mallet A, Bale SD, et al (2020) Constraining Ion-Scale Heating and Spectral Energy Transfer in Observations of Plasma Turbulence. Phys Rev Lett 125:025102, DOI 10.1103/PhysRevLett.125.025102

Califano F, Cerri SS, Faganello M, et al (2020) Electron-only reconnection in plasma turbulence. Fron Physics 8, DOI 10.3389/fphy.2020.00317

Camporeale E, Sorriso-Valvo L, Califano F, Retinò A (2018) Coherent Structures and Spectral Energy Transfer in Turbulent Plasma: A Space-Filter Approach. Phys Rev Lett 120:125101, DOI 10.1103/PhysRevLett.120.125101

Carbone V, Veltri P, Mangeney A (1990) Coherent structure formation and magnetic field line reconnection in magnetohydrodynamic turbulence. Phys Fluids 2:1487–1496, DOI 10.1063/1.857598

Cattell C, Dombeck J, Wygant J, et al (2005) Cluster observations of electron holes in association with magnetotail reconnection and comparison to simulations. J Geophys Res 110:A01211, DOI 10.1029/2004JA010519

Cerri SS, Califano F (2017) Reconnection and small-scale fields in 2D-3V hybrid-kinetic driven turbulence simulations. New J Phys 19:025007, DOI 10.1088/1367-2630/aa5c4a

Chandran BDG, Schekochihin AA, Mallet A (2015) Intermittency and Alignment in Strong RMHD Turbulence. Astrophys J 807:39, DOI 10.1088/0004-637X/807/1/39

Chasapis A, Matthaeus WH, Parashar TN, et al (2017) Electron Heating at Kinetic Scales in Magnetosheath Turbulence. Astrophys J 836:247, DOI 10.3847/1538-4357/836/2/247

Chasapis A, Matthaeus WH, Parashar TN, et al (2017) High-resolution statistics of solar wind turbulence at kinetic scales using the magnetospheric multiscale mission. Astrophys J Lett 844:L9, DOI 10.3847/2041-8213/aa7ddd

Chasapis A, Matthaeus WH, Parashar TN, et al (2018) In Situ Observation of Intermittent Dissipation at Kinetic Scales in the Earth's Magnetosheath. Astrophys J Lett 856:L19, DOI 10.3847/2041-8213/aaadf8

Chaston CC, Bonnell JW, Clausen L, Angelopoulos V (2012) Energy transport by kinetic-scale electromagnetic waves in fast plasma sheet flows. J Geophys Res 117:A09202, DOI 10.1029/2012JA017863

Chaston CC, Bonnell JW, Salem C (2014) Heating of the plasma sheet by broadband electromagnetic waves. Geophys Res Lett 41:8185–8192, DOI 10.1002/2014GL062116

Che H (2017) How Anomalous Resistivity Accelerates Magnetic Reconnection. Phys Plasmas 24:082115, DOI 10.1063/1.5000071

Che H, Drake JF, Swisdak M (2011) A current filamentation mechanism for breaking magnetic field lines during reconnection. Nature 474:184–187, DOI 10.1038/nature10091

Chen CHK, Boldyrev S (2017) Nature of Kinetic Scale Turbulence in the Earth's Magnetosheath. Astrophys J 842:122, DOI 10.3847/1538-4357/aa74e0

Chen XL, Morrison PJ (1990) Resistive tearing instability with equilibrium shear flow. Phys Fluids B 2:495–507, DOI 10.1063/1.859339

Chhiber R, Chasapis A, Bandyopadhyay R, et al (2018) Higher-Order Turbulence Statistics in the Earth's Magnetosheath and the Solar Wind Using Magnetospheric Multiscale Observations. J Geophys Res 123:9941–9954, DOI 10.1029/2018JA025768

Consolini G, Alberti T, Benella S, et al (2023) On the fractal pattern of the current structure at ion scales in turbulent space plasmas. Chaos, Solitons & Fractals 177:114253

Cowley SWH (1982) The Causes of Convection in the Earth's Magnetosphere: A Review of Developments During the IMS (Paper 2R0568). Rev Geophys Space Phys 20:531, DOI 10.1029/RG020i003p00531

Daughton W, Roytershteyn V, Karimabadi H, et al (2011) Role of electron physics in the development of turbulent magnetic reconnection in collisionless plasmas. Nat Phys 7:539–542, DOI 10.1038/nphys1965

Di Mare F, Sorriso-Valvo L, Retinò A, et al (2019) Evolution of Turbulence in the Kelvin–Helmholtz Instability in the Terrestrial Magnetopause. Atmosphere 10:561, DOI 10.3390/atmos10090561

Divin A, Khotyaintsev YV, Vaivads A, et al (2015) Evolution of the Lower Hybrid drift instability at reconnection jet front. J Geophys Res 120:2675, DOI 10.1002/2014JA020503

Dmitruk P, Matthaeus WH, Seenu N (2004) Test Particle Energization by Current Sheets and Nonuniform Fields in Magnetohydrodynamic Turbulence. Astrophys J 617:667–679, DOI 10.1086/425301

Donato S, Servidio S, Dmitruk P, et al (2012) Reconnection events in two-dimensional Hall magnetohydrodynamic turbulence. Phys Plasmas 19:092307, DOI 10.1063/1.4754151

Dong C, Wang L, Huang YM, et al (2018) Role of the Plasmoid Instability in Magnetohydrodynamic Turbulence. Phys Rev Lett 121:165101, DOI 10.1103/PhysRevLett.121.165101

Dong C, Wang L, Huang YM, et al (2022) Reconnection-driven energy cascade in magnetohydrodynamic turbulence. Science Advances 8:eabn7627, DOI 10.1126/sciadv.abn7627

Drake JF, Swisdak M, Cattell C, et al (2003) Formation of Electron Holes and Particle Energization During Magnetic Reconnection. Science 299:873–877, DOI 10.1126/science.1080333

Drake JF, Swisdak M, Phan TD, et al (2009) Ion heating resulting from pickup in magnetic reconnection exhausts. J Geophys Res 114:A05111, DOI 10.1029/2008JA013701

Eastwood JP, Phan TD, Bale SD, Tjulin A (2009) Observations of Turbulence Generated by Magnetic Reconnection. Phys Rev Lett 102:035001, DOI 10.1103/PhysRevLett.102.035001

Eastwood JP, Stawarz JE, Phan TD, et al (2021) Solar Orbiter observations of an ion-scale flux rope confined to a bifurcated solar wind current sheet. Astron Astrophys 656:A27, DOI 10.1051/0004-6361/202140949

Ergun RE, Goodrich KA, Stawarz JE, et al (2015) Large-amplitude electric fields associated with bursty bulk flow braking in the Earth's plasma sheet. J Geophys Res 120:1832–1844, DOI 10.1002/2014JA020165

Ergun RE, Chen LJ, Wilder FD, et al (2017) Drift waves, intense parallel electric fields, and turbulence associated with asymmetric magnetic reconnection at the magnetopause. Geophys Res Lett 44:2978–2986, DOI 10.1002/2016GL072493

Ergun RE, Goodrich KA, Wilder FD, et al (2018) Magnetic Reconnection, Turbulence, and Particle Acceleration: Observations in the Earth's Magnetotail. Geophys Res Lett 45:3338–3347, DOI 10.1002/2018GL076993

Ergun RE, Ahmadi N, Kromyda L, et al (2020a) Observations of Particle Acceleration in Magnetic Reconnection-driven Turbulence. Astrophys J 898:154, DOI 10.3847/1538-4357/ab9ab6

Ergun RE, Ahmadi N, Kromyda L, et al (2020b) Particle Acceleration in Strong Turbulence in the Earth's Magnetotail. Astrophys J 898:153, DOI 10.3847/1538-4357/ab9ab5

Ergun RE, Pathak N, Usanova ME, et al (2022a) Observation of Magnetic Reconnection in a Region of Strong Turbulence. Astrophys J Lett 935:L8, DOI 10.3847/2041-8213/ac81d4

Ergun RE, Usanova ME, Turner DL, Stawarz JE (2022b) Bursty Bulk Flow Turbulence as a Source of Energetic Particles to the Outer Radiation Belt. Geophys Res Lett 49:e98113, DOI 10.1029/2022GL098113

Eriksson S, Lavraud B, Wilder FD, et al (2016a) Magnetospheric Multiscale observations of magnetic reconnection associated with Kelvin-Helmholtz waves. Geophys Res Lett 43:5606–5615, DOI 10.1002/2016GL068783

Eriksson S, Wilder FD, Ergun RE, et al (2016b) Magnetospheric Multiscale Observations of the Electron Diffusion Region of Large Guide Field Magnetic Reconnection. Phys Rev Lett 117:015001, DOI 10.1103/PhysRevLett.117.015001

Eriksson S, Ma X, Burch JL, et al (2021) MMS Observations of Double Mid-Latitude Reconnection Ion Beams in the Early Non-Linear Phase of the Kelvin-Helmholtz Instability. Fron Astron Space Sci 8:188, DOI 10.3389/fspas.2021.760885

Eriksson S, Swisdak M, Weygand JM, et al (2022) Characteristics of Multi-scale Current Sheets in the Solar Wind at 1 au Associated with Magnetic Reconnection and the Case for a Heliospheric Current Sheet Avalanche. Astrophys J 933:181, DOI 10.3847/1538-4357/ac73f6

Eyink G, Vishniac E, Lalescu C, et al (2013) Flux-freezing breakdown in high-conductivity magnetohydrodynamic turbulence. Nature 497:466–469, DOI 10.1038/nature12128

Eyink GL (2015) Turbulent General Magnetic Reconnection. Astrophys J 807:137, DOI 10.1088/0004-637X/807/2/137

Eyink GL, Lazarian A, Vishniac ET (2011) Fast Magnetic Reconnection and Spontaneous Stochasticity. Astrophys J 743:51, DOI 10.1088/0004-637X/743/1/51

Fadanelli S, Lavraud B, Califano F, et al (2021) Energy conversions associated with magnetic reconnection. J Geophys Res 126:e2020JA028333

Faganello M, Califano F, Pegoraro F (2008) Numerical Evidence of Undriven, Fast Reconnection in the Solar-Wind Interaction with Earth's Magnetosphere: Formation of Electromagnetic Coherent Structures. Phys Rev Lett 101:105001, DOI 10.1103/PhysRevLett.101.105001

Faganello M, Pegoraro F, Califano F, Marradi L (2010) Collisionless magnetic reconnection in the presence of a sheared velocity field. Phys Plasmas 17:062102, DOI 10.1063/1.3430640

Faganello M, Califano F, Pegoraro F, et al (2012a) Magnetic reconnection and Kelvin-Helmholtz instabilities at the Earth's magnetopause. Plasma Phys Cont Fus 54:124037, DOI 10.1088/0741-3335/54/12/124037

Faganello M, Califano F, Pegoraro F, Andreussi T (2012b) Double mid-latitude dynamical reconnection at the magnetopause: An efficient mechanism allowing solar wind to enter the Earth's magnetosphere. Europhys Lett 100:69001, DOI 10.1209/0295-5075/100/69001

Faganello M, Califano F, Pegoraro F, Retinò A (2014) Kelvin-Helmholtz vortices and double mid-latitude reconnection at the Earth's magnetopause: Comparison between observations and simulations. Europhys Lett 107:19001, DOI 10.1209/0295-5075/107/19001

Faganello M, Sisti M, Califano F, Lavraud B (2022) Kelvin-Helmholtz instability and induced magnetic reconnection at the Earth's magnetopause: a 3D simulation based on satellite data. Plasma Phys Cont Fus 64:044014, DOI 10.1088/1361-6587/ac43f0

Fargette N, Lavraud B, Rouillard AP, et al (2023) Clustering of magnetic reconnection exhausts in the solar wind: An automated detection study. Astron Astrophys 674:A98, DOI 10.1051/0004-6361/202346043

Fermo RL, Drake JF, Swisdak M (2012) Secondary Magnetic Islands Generated by the Kelvin-Helmholtz Instability in a Reconnecting Current Sheet. Phys Rev Lett 108:255005, DOI 10.1103/PhysRevLett.108.255005

Ferrand R, Galtier S, Sahraoui F, et al (2019) On Exact Laws in Incompressible Hall Magnetohydrodynamic Turbulence. Astrophys J 881:50, DOI 10.3847/1538-4357/ab2be9

Franci L, Verdini A, Matteini L, et al (2015) Solar Wind Turbulence From MHD To Sub-Ion Scales: High-Resolution Hybrid Simulations. Astrophys J Lett 804:L39, DOI 10.1088/2041-8205/804/2/L39

Franci L, Cerri SS, Califano F, et al (2017) Magnetic Reconnection as a Driver for a Sub-ion-scale Cascade in Plasma Turbulence. Astrophys J Lett 850:L16

Franci L, Stawarz JE, Papini E, et al (2020) Modeling MMS Observations at the Earth's Magnetopause with Hybrid Simulations of Alfvénic Turbulence. Astrophys J 898:175, DOI 10.3847/1538-4357/ab9a47

Franci L, Papini E, Micera A, et al (2022) Anisotropic electron heating in turbulence-driven magnetic reconnection in the near-sun solar wind. Astrophys J 936:27, DOI 10.3847/1538-4357/ac7da6

Frisch U (1995) Turbulence. The legacy of A.N. Kolmogorov. Cambridge University Press, Cambridge, UK

Fujimoto K (2014) Wave activities in separatrix regions of magnetic reconnection. Geophys Res Lett 41:2721–2728, DOI 10.1002/2014GL059893

Fujimoto K, Sydora RD (2012) Plasmoid-Induced Turbulence in Collisionless Magnetic Reconnection. Phys Rev Lett 109:265004, DOI 10.1103/PhysRevLett.109.265004

Fujimoto K, Sydora RD (2021) Electromagnetic turbulence in the electron current layer to drive magnetic reconnection. Astrophys J Lett 909:L15, DOI 10.3847/2041-8213/abe877

Fujimoto K, Sydora RD (2023) The electron diffusion region dominated by electromagnetic turbulence in the reconnection current layer. Phys Plasmas 30, DOI 10.1063/5.0129591

Fuselier SA, Petrinec SM, Trattner KJ, Lavraud B (2014) Magnetic field topology for northward IMF reconnection: Ion observations. J Geophys Res 119:9051–9071, DOI 10.1002/2014JA020351

Fuselier SA, Petrinec SM, Reiff PH, et al (2024; this collection) Global-Scale Processes and Effects of Magnetic Reconnection on the Geospace Environment. Space Sci Rev 220:34, DOI 10.1007/s11214-024-01067-0

Galtier S (2023) Physics of Wave Turbulence. Cambridge University Press, Cambridge, UK

Galtier S, Nazarenko SV, Newell AC, Pouquet A (2000) A weak turbulence theory for incompressible magnetohydrodynamics. J Plasma Phys 63:447–488, DOI 10.1017/S0022377899008284

Gingell I, Sorriso-Valvo L, Burgess D, et al (2017) Three-dimensional simulations of sheared current sheets: transition to turbulence? J Plasma Phys 83:705830104

Gingell I, Schwartz SJ, Eastwood JP, et al (2019) Observations of magnetic reconnection in the transition region of quasi-parallel shocks. Geophys Res Lett 46:1177–1184, DOI https://doi.org/10.1029/2018GL081804

Gingell I, Schwartz SJ, Eastwood JP, et al (2020) Statistics of reconnecting current sheets in the transition region of earth's bow shock. J Geophys Res 125:e2019JA027119, DOI https://doi.org/10.1029/2019JA027119

Gingell I, Schwartz SJ, Kucharek H, et al (2021) Observing the prevalence of thin current sheets downstream of Earth's bow shock. Phys Plasmas 28:102902, DOI 10.1063/5.0062520

Gingell I, Schwartz SJ, Kucharek H, et al (2023) Hybrid simulations of the decay of reconnected structures downstream of the bow shock. Phys Plasmas 30:012902, DOI 10.1063/5.0129084

Goldman M, Newman DL, Lapenta G, et al (2014) Čerenkov Emission of Quasiparallel Whistlers by Fast Electron Phase-Space Holes during Magnetic Reconnection. Phys Rev Lett 112:145002, DOI 10.1103/PhysRevLett.112.145002

Goldreich P, Sridhar S (1995) Toward a Theory of Interstellar Turbulence. II. Strong Alfvenic Turbulence. Astrophys J 438:763, DOI 10.1086/175121

Gosling JT (2007) Observations of Magnetic Reconnection in the Turbulent High-Speed Solar Wind. Astrophys J Lett 671:L73–L76, DOI 10.1086/524842

Gosling JT, Szabo A (2008) Bifurcated current sheets produced by magnetic reconnection in the solar wind. J Geophys Res 113:A10103, DOI 10.1029/2008JA013473

Gosling JT, Skoug RM, McComas DJ, Smith CW (2005) Direct evidence for magnetic reconnection in the solar wind near 1 AU. J Geophys Res 110:A01107, DOI 10.1029/2004JA010809

Graham DB, Cozzani G, et al (this collection) The role of kinetic instabilities and waves in collisionless magnetic reconnection. Space Sci Rev

Greco A, Matthaeus WH, Servidio S, et al (2009) Statistical Analysis of Discontinuities in Solar Wind ACE Data and Comparison with Intermittent MHD Turbulence. Astrophys J Lett 691:L111–L114, DOI 10.1088/0004-637X/691/2/L111

Grete P, O'Shea BW, Beckwith K, et al (2017) Energy transfer in compressible magnetohydrodynamic turbulence. Phys Plasmas 24:092311, DOI 10.1063/1.4990613

Guo A, Lu Q, Lu S, et al (2023) Properties of Electron-scale Magnetic Reconnection at a Quasi-perpendicular Shock. Astrophys J 955:14, DOI 10.3847/1538-4357/acec48

Hadid LZ, Sahraoui F, Galtier S, Huang SY (2018) Compressible Magnetohydrodynamic Turbulence in the Earth's Magnetosheath: Estimation of the Energy Cascade Rate Using in situ Spacecraft Data. Phys Rev Lett 120(5):055102, DOI 10.1103/PhysRevLett.120.055102

Haggerty CC, Parashar TN, Matthaeus WH, et al (2017) Exploring the statistics of magnetic reconnection X-points in kinetic particle-in-cell turbulence. Phys Plasmas 24:102308, DOI 10.1063/1.5001722

Hansel PJ, Wilder FD, Malaspina DM, et al (2021) Mapping MMS Observations of Solitary Waves in Earth's Magnetic Field. J Geophys Res 126:e29389, DOI 10.1029/2021JA02938910.1002/essoar.10506873.1

Hasegawa H, Fujimoto M, Phan TD, et al (2004) Transport of solar wind into Earth's magnetosphere through rolled-up Kelvin-Helmholtz vortices. Nature 430:755–758, DOI 10.1038/nature02799

Hasegawa H, Retinò A, Vaivads A, et al (2009) Kelvin-Helmholtz waves at the Earth's magnetopause: Multiscale development and associated reconnection. J Geophys Res 114:A12207, DOI 10.1029/2009JA014042

Hasegawa H, Nakamura TKM, Gershman DJ, et al (2020) Generation of Turbulence in Kelvin-Helmholtz Vortices at the Earth's Magnetopause: Magnetospheric Multiscale Observations. J Geophys Res 125:e27595, DOI 10.1029/2019JA02759510.1002/essoar.10501080.2

Haynes CT, Burgess D, Camporeale E (2014) Reconnection and electron temperature anisotropy in sub-proton scale plasma turbulence. Astrophys J 783:38, DOI 10.1088/0004-637X/783/1/38

Hellinger P, Verdini A, Landi S, et al (2018) von Kármán-Howarth Equation for Hall Magnetohydrodynamics: Hybrid Simulations. Astrophys J Lett 857:L19, DOI 10.3847/2041-8213/aabc06

Horbury TS, Wicks RT, Chen CHK (2012) Anisotropy in Space Plasma Turbulence: Solar Wind Observations. Space Sci Rev 172:325–342, DOI 10.1007/s11214-011-9821-9

Hou C, He J, Zhu X, Wang Y (2021) Contribution of Magnetic Reconnection Events to Energy Dissipation in Space Plasma Turbulence. Astrophys J 908:237, DOI 10.3847/1538-4357/abd6f3

Howes GG (2016) The dynamical generation of current sheets in astrophysical plasma turbulence. Astrophys J Lett 827:L28, DOI 10.3847/2041-8205/827/2/L28

Hu A, Sisti M, Finelli F, et al (2020) Identifying magnetic reconnection in 2d hybrid vlasov maxwell simulations with convolutional neural networks. Astrophys J 900:86, DOI 10.3847/1538-4357/aba527

Huang SY, Sahraoui F, Deng XH, et al (2014) Kinetic Turbulence in the Terrestrial Magnetosheath: Cluster Observations. Astrophys J Lett 789:L28, DOI 10.1088/2041-8205/789/2/L28

Huang SY, Hadid LZ, Sahraoui F, et al (2017) On the Existence of the Kolmogorov Inertial Range in the Terrestrial Magnetosheath Turbulence. Astrophys J Lett 836:L10, DOI 10.3847/2041-8213/836/1/L10

Huang YM, Bhattacharjee A (2016) Turbulent Magnetohydrodynamic Reconnection Mediated by the Plasmoid Instability. Astrophys J 818:20, DOI 10.3847/0004-637X/818/1/20

Iroshnikov PS (1964) Turbulence of a Conducting Fluid in a Strong Magnetic Field. Soviet Astron 7:566

Jain N, Muñoz PA, Tabriz MF, et al (2022) Importance of accurate consideration of the electron inertia in hybrid-kinetic simulations of collisionless plasma turbulence: The 2d limit. Phys Plasmas 29:053902, DOI 10.1063/5.0087103

Jara-Almonte J, Daughton W, Ji H (2014) Debye scale turbulence within the electron diffusion layer during magnetic reconnection. Phys Plasmas 21:032114, DOI 10.1063/1.4867868

Jin R, Zhou M, Pang Y, et al (2022) Characteristics of Turbulence Driven by Transient Magnetic Reconnection in the Terrestrial Magnetotail. Astrophys J 925:17, DOI 10.3847/1538-4357/ac390c

Johnson JR, Wing S (2009) Northward interplanetary magnetic field plasma sheet entropies. J Geophys Res 114:A00D08, DOI 10.1029/2008JA014017

Karimabadi H, Roytershteyn V, Wan M, et al (2013) Coherent structures, intermittent turbulence, and dissipation in high-temperature plasmas. Phys Plasmas 20:012303, DOI 10.1063/1.4773205

Karimabadi H, Roytershteyn V, Vu HX, et al (2014) The link between shocks, turbulence, and magnetic reconnection in collisionless plasmas. Phys Plasmas 21:062308, DOI 10.1063/1.4882875

Kiyani KH, Chapman SC, Khotyaintsev YV, et al (2009) Global Scale-Invariant Dissipation in Collisionless Plasma Turbulence. Phys Rev Lett 103:075006, DOI 10.1103/PhysRevLett.103.075006

Klein KG, Spence H, Alexandrova O, et al (2023) HelioSwarm: A Multipoint, Multiscale Mission to Characterize Turbulence. Space Sci Rev 219:74, DOI 10.1007/s11214-023-01019-0

Knoll DA, Chacón L (2002) Magnetic Reconnection in the Two-Dimensional Kelvin-Helmholtz Instability. Phys Rev Lett 88:215003, DOI 10.1103/PhysRevLett.88.215003

Kolmogorov A (1941a) The Local Structure of Turbulence in Incompressible Viscous Fluid for Very Large Reynolds' Numbers. Akademiia Nauk SSSR Doklady 30:301–305, [reprinted in

(1991) Proc. R. Soc. A, 434:9-13, doi:10.1098/rspa.1991.0075]

Kolmogorov AN (1941b) Dissipation of Energy in Locally Isotropic Turbulence. Akademiia Nauk SSSR Doklady 32:16, [reprinted in (1991) Proc. R. Soc. A, 434:15-17, doi:10.1098/rspa.1991.0076]

Kowal G, Lazarian A, Vishniac ET, Otmianowska-Mazur K (2009) Numerical Tests of Fast Reconnection in Weakly Stochastic Magnetic Fields. Astrophys J 700:63–85, DOI 10.1088/0004-637X/700/1/63

Kowal G, de Gouveia Dal Pino EM, Lazarian A (2012) Particle Acceleration in Turbulence and Weakly Stochastic Reconnection. Phys Rev Lett 108:241102, DOI 10.1103/PhysRevLett.108.241102

Kraichnan RH (1965) Inertial-Range Spectrum of Hydromagnetic Turbulence. Phys Fluids 8(7):1385–1387, DOI 10.1063/1.1761412

Lalescu CC, Shi YK, Eyink GL, et al (2015) Inertial-Range Reconnection in Magneto-hydrodynamic Turbulence and in the Solar Wind. Phys Rev lett 115:025001, DOI 10.1103/PhysRevLett.115.025001

Lapenta G, Markidis S, Divin A, et al (2011) Bipolar electric field signatures of reconnection separatrices for a hydrogen plasma at realistic guide fields. Geophys Res Lett 38:L17104, DOI 10.1029/2011GL048572

Lapenta G, Markidis S, Goldman MV, Newman DL (2015) Secondary reconnection sites in reconnection-generated flux ropes and reconnection fronts. Nat Phys 11:690–695, DOI 10.1038/nphys3406

Lapenta G, Berchem J, Alaoui ME, Walker R (2020a) Turbulent energization of electron power law tails during magnetic reconnection. Phys Rev Lett 125:225101, DOI 10.1103/PhysRevLett.125.225101

Lapenta G, Pucci F, Goldman MV, Newman DL (2020b) Local regimes of turbulence in 3d magnetic reconnection. Astrophys J 888:104, DOI 10.3847/1538-4357/ab5a86

Lapenta G, Goldman M, Newman DL, Eriksson S (2022) Formation and reconnection of electron scale current layers in the turbulent outflows of a primary reconnection site. Astrophys J 940:187, DOI 10.3847/1538-4357/ac98bc

Lazarian A, Vishniac ET (1999) Reconnection in a Weakly Stochastic Field. Astrophys J 517:700–718, DOI 10.1086/307233

Lazarian A, Vlahos L, Kowal G, et al (2012) Turbulence, Magnetic Reconnection in Turbulent Fluids and Energetic Particle Acceleration. Space Sci Rev 173:557–622, DOI 10.1007/s11214-012-9936-7

Lazarian A, Eyink G, Vishniac E, Kowal G (2015) Turbulent reconnection and its implications. Phil Trans R Soc A 373:20140144–20140144, DOI 10.1098/rsta.2014.0144

Lazarian A, Eyink GL, Jafari A, et al (2020) 3D turbulent reconnection: Theory, tests, and astrophysical implications. Phys Plasmas 27:012305, DOI 10.1063/1.5110603

Le A, Daughton W, Chen LJ, Egedal J (2017) Enhanced electron mixing and heating in 3-D asymmetric reconnection at the Earth's magnetopause. Geophys Res Lett 44:2096–2104, DOI 10.1002/2017GL072522

Le A, Daughton W, Ohia O, et al (2018) Drift turbulence, particle transport, and anomalous dissipation at the reconnecting magnetopause. Phys Plasmas 25:062103, DOI 10.1063/1.5027086

Leonardis E, Chapman SC, Daughton W, et al (2013) Identification of Intermittent Multi-fractal Turbulence in Fully Kinetic Simulations of Magnetic Reconnection. Phys Rev Lett 110:205002, DOI 10.1103/PhysRevLett.110.205002

Lewis HC, Stawarz JE, Franci L, et al (2023) Magnetospheric Multiscale measurements of turbulent electric fields in earth's magnetosheath: How do plasma conditions influence the balance of terms in generalized Ohm's law? Phys Plasmas 30:082901, DOI 10.1063/5.0158067

Li H, Jiang W, Wang C, et al (2020) Evolution of the Earth's Magnetosheath Turbulence: A Statistical Study Based on MMS Observations. Astrophys J Lett 898:L43, DOI 10.3847/2041-8213/aba531

Li TC, Liu YH, Qi Y, Zhou M (2023) Extended magnetic reconnection in kinetic plasma turbulence. Phys Rev Lett 131:085201

Li W, André M, Khotyaintsev YV, et al (2016) Kinetic evidence of magnetic reconnection due to Kelvin-Helmholtz waves. Geophys Res Lett 43:5635–5643, DOI 10.1002/2016GL069192

Liu TZ, Lu S, Turner DL, et al (2020) Magnetospheric multiscale (mms) observations of magnetic reconnection in foreshock transients. J Geophys Res 125:e2020JA027822, DOI https://doi.org/10.1029/2020JA027822

Liu YH, Daughton W, Karimabadi H, et al (2013) Bifurcated Structure of the Electron Diffusion Region in Three-Dimensional Magnetic Reconnection. Phys Rev Lett 110:265004, DOI 10.1103/PhysRevLett.110.265004

Liu YH, Hessse M, et al (this collection) Ohm's law, the reconnection rate, and energy conversion in collisionless magnetic reconnection. Space Sci Rev

Loureiro NF, Boldyrev S (2017a) Collisionless Reconnection in Magnetohydrodynamic and Kinetic Turbulence. Astrophys J 850:182, DOI 10.3847/1538-4357/aa9754

Loureiro NF, Boldyrev S (2017b) Role of Magnetic Reconnection in Magnetohydrodynamic Turbulence. Phys Rev Lett 118:245101, DOI 10.1103/PhysRevLett.118.245101

Loureiro NF, Boldyrev S (2020) Nonlinear Reconnection in Magnetized Turbulence. Astrophys J 890:55, DOI 10.3847/1538-4357/ab6a95

Loureiro NF, Schekochihin AA, Cowley SC (2007) Instability of current sheets and formation of plasmoid chains. Phys Plasmas 14:100703, DOI 10.1063/1.2783986

Lu Q, Wang H, Wang X, et al (2020) Turbulence-Driven Magnetic Reconnection in the Magnetosheath Downstream of a Quasi-Parallel Shock: A Three-Dimensional Global Hybrid Simulation. Geophys Res Lett 47:e85661, DOI 10.1029/2019GL085661

Lu Q, Yang Z, Wang H, et al (2021) Two-dimensional Particle-in-cell Simulation of Magnetic Reconnection in the Downstream of a Quasi-perpendicular Shock. Astrophys J 919:28, DOI 10.3847/1538-4357/ac18c0

Ma X, Otto A, Delamere PA (2014) Interaction of magnetic reconnection and Kelvin-Helmholtz modes for large magnetic shear: 1. Kelvin-Helmholtz trigger. J Geophys Res 119:781–797, DOI 10.1002/2013JA019224

MacBride BT, Forman MA, Smith CW (2005) Turbulence and Third Moment of Fluctuations: Kolmogorov's 4/5 Law and its MHD Analogues in the Solar Wind. In: Fleck B, Zurbuchen TH, Lacoste H (eds) Solar Wind 11/SOHO 16, Connecting Sun and Heliosphere, ESA Special Publication, vol 592, p 613

MacBride BT, Smith CW, Forman MA (2008) The Turbulent Cascade at 1 AU: Energy Transfer and the Third-Order Scaling for MHD. Astrophys J 679:1644–1660, DOI 10.1086/529575

Mallet A (2020) The onset of electron-only reconnection. Journal of Plasma Physics 86:905860301, DOI 10.1017/S0022377819000941

Mallet A, Schekochihin AA (2017) A statistical model of three-dimensional anisotropy and intermittency in strong Alfvénic turbulence. Mon Not R Astro Soc 466:3918–3927, DOI 10.1093/mnras/stw3251

Mallet A, Schekochihin AA, Chandran BDG (2017) Disruption of sheet-like structures in Alfvénic turbulence by magnetic reconnection. Mon Not R Astro Soc 468:4862–4871, DOI 10.1093/mnras/stx670

Manzini D, Sahraoui F, Califano F, Ferrand R (2022) Local energy transfer and dissipation in incompressible Hall magnetohydrodynamic turbulence: The coarse-graining approach. Phys Rev E 106:035202, DOI 10.1103/PhysRevE.106.035202

Manzini D, Sahraoui F, Califano F (2023) Subion-scale turbulence driven by magnetic reconnection. Phys Rev Lett 130:205201, DOI 10.1103/PhysRevLett.130.205201

Marino R, Sorriso-Valvo L (2023) Scaling laws for the energy transfer in space plasma turbulence. Phys Rep 1006:1–144, DOI 10.1016/j.physrep.2022.12.001

Marino R, Sorriso-Valvo L, Carbone V, et al (2008) Heating the Solar Wind by a Magnetohydrodynamic Turbulent Energy Cascade. Astrophys J Lett 677:L71, DOI 10.1086/587957

Markidis S, Henri P, Lapenta G, et al (2013) Kinetic Simulations of Plasmoid Chain Dynamics. Phys Plasmas 20:082105, DOI 10.1063/1.4817286

Marsch E, Tu CY (1997) Intermittency, non-Gaussian statistics and fractal scaling of MHD fluctuations in the solar wind. Nonlin Proc Geophys 4:101–124, DOI 10.5194/npg-4-101-1997

Matsumoto Y, Amano T, Kato TN, Hoshino M (2015) Stochastic electron acceleration during spontaneous turbulent reconnection in a strong shock wave. Science 347:974–978, DOI 10.1126/science.1260168

Matthaeus WH, Goldstein ML (1982) Measurement of the rugged invariants of magnetohydrodynamic turbulence in the solar wind. J Geophys Res 87:6011–6028, DOI 10.1029/JA087iA08p06011

Matthaeus WH, Lamkin SL (1986) Turbulent magnetic reconnection. Phys Fluids 29:2513, DOI 10.1063/1.866004

Matthaeus WH, Wan M, Servidio S, et al (2015) Intermittency, nonlinear dynamics and dissipation in the solar wind and astrophysical plasmas. Phil Trans R Soc A 373:20140154–

20140154, DOI 10.1098/rsta.2014.0154

Meyrand R, Galtier S (2013) Anomalous $k8/3$ spectrum in electron magnetohydrodynamic turbulence. Phys Rev Lett 111:264501, DOI 10.1103/PhysRevLett.111.264501

Meyrand R, Squire J, Schekochihin AA, Dorland W (2021) On the violation of the zeroth law of turbulence in space plasmas. J Plasma Phys 87:535870301, DOI 10.1017/S0022377821000489

Mininni PD, Pouquet AG, Montgomery DC (2006) Small-Scale Structures in Three-Dimensional Magnetohydrodynamic Turbulence. Phys Rev Lett 97:244503, DOI 10.1103/PhysRevLett.97.244503

Miranda RA, Valdivia JA, Chian ACL, Muñoz PR (2021) Complexity of Magnetic-field Turbulence at Reconnection Exhausts in the Solar Wind at 1 au. Astrophys J 923:132, DOI 10.3847/1538-4357/ac2dfe

Mistry R, Eastwood JP, Hietala H (2015a) Detection of small-scale folds at a solar wind reconnection exhaust. J Geophys Res 120:30–42, DOI 10.1002/2014JA020465

Mistry R, Eastwood JP, Phan TD, Hietala H (2015b) Development of bifurcated current sheets in solar wind reconnection exhausts. Geophys Res Lett 42:10,513–10,520, DOI 10.1002/2015GL066820

Mistry R, Eastwood JP, Phan TD, Hietala H (2017) Statistical properties of solar wind reconnection exhausts. J Geophys Res 122:5895–5909, DOI 10.1002/2017JA024032

Muñoz PA, Jain N, Farzalipour Tabriz M, et al (2023) Electron inertia effects in 3D hybrid-kinetic collisionless plasma turbulence. Phys Plasmas 30:092302, DOI 10.1063/5.0148818

Muñoz PA, Büchner J (2016) Non-Maxwellian electron distribution functions due to self-generated turbulence in collisionless guide-field reconnection. Phys Plasmas 23:102103, DOI 10.1063/1.4963773

Muñoz PA, Büchner J (2018) Kinetic turbulence in fast three-dimensional collisionless guide-field magnetic reconnection. Phys Rev E 98:043205, DOI 10.1103/PhysRevE.98.043205

Muñoz PA, Büchner J, Kilian P (2017) Turbulent transport in 2D collisionless guide field reconnection. Phys Plasmas 24:022104, DOI 10.1063/1.4975086

Nakamura TKM, Daughton W (2014) Turbulent plasma transport across the Earth's low-latitude boundary layer. Geophys Res Lett 41:8704–8712, DOI 10.1002/2014GL061952

Nakamura TKM, Fujimoto M (2005) Magnetic reconnection within rolled-up MHD-scale Kelvin-Helmholtz vortices: Two-fluid simulations including finite electron inertial effects. Geophys Res Lett 32:L21102, DOI 10.1029/2005GL023362

Nakamura TKM, Fujimoto M, Otto A (2006) Magnetic reconnection induced by weak Kelvin-Helmholtz instability and the formation of the low-latitude boundary layer. Geophys Res Lett 33:L14106, DOI 10.1029/2006GL026318

Nakamura TKM, Fujimoto M, Otto A (2008) Structure of an MHD-scale Kelvin-Helmholtz vortex: Two-dimensional two-fluid simulations including finite electron inertial effects. J Geophys Res 113:A09204, DOI 10.1029/2007JA012803

Nakamura TKM, Hasegawa H, Shinohara I, Fujimoto M (2011) Evolution of an MHD-scale Kelvin-Helmholtz vortex accompanied by magnetic reconnection: Two-dimensional particle simulations. J Geophys Res 116:A03227, DOI 10.1029/2010JA016046

Nakamura TKM, Daughton W, Karimabadi H, Eriksson S (2013) Three-dimensional dynamics of vortex-induced reconnection and comparison with THEMIS observations. J Geophys Res 118:5742–5757, DOI 10.1002/jgra.50547

Nakamura TKM, Eriksson S, Hasegawa H, et al (2017a) Mass and Energy Transfer Across the Earth's Magnetopause Caused by Vortex-Induced Reconnection. J Geophys Res 122:11,505–11,522, DOI 10.1002/2017JA024346

Nakamura TKM, Hasegawa H, Daughton W, et al (2017b) Turbulent mass transfer caused by vortex-induced reconnection in collisionless magnetospheric plasmas. Nat Comm 8:1582, DOI 10.1038/s41467-017-01579-0

Nakamura TKM, Plaschke F, Hasegawa H, et al (2020a) Decay of Kelvin-Helmholtz Vortices at the Earth's Magnetopause Under Pure Southward IMF Conditions. Geophys Res Lett 47:e87574, DOI 10.1029/2020GL087574

Nakamura TKM, Stawarz JE, Hasegawa H, et al (2020b) Effects of Fluctuating Magnetic Field on the Growth of the Kelvin-Helmholtz Instability at the Earth's Magnetopause. J Geophys Res 125:e27515, DOI 10.1029/2019JA02751510.1002

Nakamura TKM, Hasegawa H, Genestreti KJ, et al (2021) Fast cross-scale energy transfer during turbulent magnetic reconnection. Geophys Res Lett 48, DOI 10.1029/2021GL093524

Nakamura TKM, Blasl KA, Hasegawa H, et al (2022a) Multi-scale evolution of Kelvin-Helmholtz waves at the Earth's magnetopause during southward IMF periods. Phys Plasmas

29:012901, DOI 10.1063/5.0067391

Nakamura TKM, Blasl KA, Liu YH, Peery SA (2022b) Diffusive plasma transport by the magnetopause Kelvin-Helmholtz instability during southward IMF. Fron Astron Sp Sci 8:247, DOI 10.3389/fspas.2021.809045

Narita Y (2016) Kinetic Extension of Critical Balance to Whistler Turbulence. Astrophys J 831:83, DOI 10.3847/0004-637X/831/1/83

Narita Y, Gary SP (2010) Inertial-range spectrum of whistler turbulence. Ann Geophys 28:597–601, DOI 10.5194/angeo-28-597-2010

Nazarenko S (2011) Wave Turbulence. Springer-Verlag, Berlin

Ng J, Chen LJ, Bessho N, et al (2022) Electron-Scale Reconnection in Three-Dimensional Shock Turbulence. Geophys Res Lett 49:e99544, DOI 10.1029/2022GL099544

Ng J, Bessho N, Dahlin JT, Chen LJ (2024) Reconnection along a Separator in Shock Turbulence. Astrophys J 962:181, DOI 10.3847/1538-4357/ad2204

Nykyri K, Otto A (2001) Plasma transport at the magnetospheric boundary due to reconnection in Kelvin-Helmholtz vortices. Geophys Res Lett 28:3565–3568, DOI 10.1029/2001GL013239

Nykyri K, Ma X, Dimmock A, et al (2017) Influence of velocity fluctuations on the Kelvin-Helmholtz instability and its associated mass transport. J Geophys Res 122:9489–9512, DOI 10.1002/2017JA024374

Oishi JS, Mac Low MM, Collins DC, Tamura M (2015) Self-generated Turbulence in Magnetic Reconnection. Astrophys J Lett 806:L12, DOI 10.1088/2041-8205/806/1/L12

Oka M, Phan T, Øieroset Maea (2022) Electron energization and thermal to non- thermal energy partition during earth's magnetotail reconnection. Phys Plasmas 29:052904, DOI 10.1063/5.0085647

Okamoto N, Yoshimatsu K, Schneider K, et al (2007) Coherent vortices in high resolution direct numerical simulation of homogeneous isotropic turbulence: A wavelet viewpoint. Phys Fluids 19:115109–115109–13, DOI 10.1063/1.2771661

Omidi N, O'Farrell A, Krauss-Varban D (1994) Sources of magnetosheath waves and turbulence. Adv Space Res 14:45–54, DOI 10.1016/0273-1177(94)90047-7

Osman KT, Wan M, Matthaeus WH, et al (2011) Anisotropic Third-Moment Estimates of the Energy Cascade in Solar Wind Turbulence Using Multispacecraft Data. Phys Rev Lett 107:165001, DOI 10.1103/PhysRevLett.107.165001

Osman KT, Matthaeus WH, Wan M, Rappazzo AF (2012) Intermittency and Local Heating in the Solar Wind. Phys Rev Lett 108:261102, DOI 10.1103/PhysRevLett.108.261102

Panov EV, Nakamura R, Baumjohann W, et al (2010) Multiple overshoot and rebound of a bursty bulk flow. Geophys Res Lett 37:L08103, DOI 10.1029/2009GL041971

Papini E, Franci L, Landi S, et al (2019) Can Hall Magnetohydrodynamics Explain Plasma Turbulence at Sub-ion Scales? Astrophys J 870:52, DOI 10.3847/1538-4357/aaf003

Parashar TN, Chasapis A, Bandyopadhyay R, et al (2018) Kinetic range spectral features of cross helicity using the magnetospheric multiscale spacecraft. Phys Rev Lett 121:265101, DOI 10.1103/PhysRevLett.121.265101

Parashar TN, Cuesta M, Matthaeus WH (2019) Reynolds Number and Intermittency in the Expanding Solar Wind: Predictions Based on Voyager Observations. Astrophys J Lett 884:L57, DOI 10.3847/2041-8213/ab4a82

Pecora F, Servidio S, Greco A, Matthaeus WH (2021) Identification of coherent structures in space plasmas: the magnetic helicity-PVI method. Astron Atrophys 650:A20, DOI 10.1051/0004-6361/202039639

Pecora F, Yang Y, Chasapis A, et al (2023) Relaxation of the turbulent magnetosheath. Mon Not R Astro Soc 525:67–72, DOI 10.1093/mnras/stad2232

Phan TD, Gosling JT, Davis MS, et al (2006) A magnetic reconnection X-line extending more than 390 Earth radii in the solar wind. Nature 439:175–178, DOI 10.1038/nature04393

Phan TD, Gosling JT, Davis MS (2009) Prevalence of extended reconnection X-lines in the solar wind at 1 AU. Geophys Res Lett 36:L09108, DOI 10.1029/2009GL037713

Phan, TD, Eastwood JP, Shay MA, et al (2018) Electron magnetic reconnection without ion coupling in earth's turbulent magnetosheath. Nature 557:202–206, DOI https://doi.org/10.1038/s41586-018-0091-5

Phan TD, Bale SD, Eastwood JP, et al (2020) Parker Solar Probe In Situ Observations of Magnetic Reconnection Exhausts during Encounter 1. Astrophys J Supp 246:34, DOI 10.3847/1538-4365/ab55ee

Politano H, Pouquet A (1998a) Dynamical length scales for turbulent magnetized flows. Geophys Res Lett 25:273–276, DOI 10.1029/97GL03642

Politano H, Pouquet A (1998b) von Kármán-Howarth equation for magnetohydrodynamics and its consequences on third-order longitudinal structure and correlation functions. Phys Rev E 57:R21–R24, DOI 10.1103/PhysRevE.57.R21

Politano H, Pouquet A, Sulem PL (1989) Inertial ranges and resistive instabilities in two-dimensional magnetohydrodynamic turbulence. Phys Fluids B 1:2330–2339, DOI 10.1063/1.859051

Pope SB (2000) Turbulent Flows. Cambridge University Press, Cambridge, UK

Pouquet A, Rosenberg D, Stawarz JE, Marino R (2019) Helicity Dynamics, Inverse, and Bidirectional Cascades in Fluid and Magnetohydrodynamic Turbulence: A Brief Review. Earth and Space Science 6:351–369, DOI 10.1029/2018EA000432

Price L, Swisdak M, Drake JF, et al (2016) The effects of turbulence on three-dimensional magnetic reconnection at the magnetopause. Geophys Res Lett 43:6020–6027, DOI 10.1002/2016GL069578

Price L, Swisdak M, Drake JF, et al (2017) Turbulence in Three-Dimensional Simulations of Magnetopause Reconnection. J Geophys Res 122:11,086–11,099, DOI 10.1002/2017JA024227

Price L, Swisdak M, Drake JF, Graham DB (2020) Turbulence and transport during guide field reconnection at the magnetopause. J Geophys Res 125:e2019JA027498, DOI 10.1029/2019JA027498

Pritchett PL (2005) Onset and saturation of guide-field magnetic reconnection. Phys Plasmas 12:062301, DOI 10.1063/1.1914309

Pritchett PL, Coroniti FV (2010) A kinetic ballooning/interchange instability in the magnetotail. J Geophys Res 115:A06301, DOI 10.1029/2009JA014752

Pritchett PL, Mozer FS, Wilber M (2012) Intense perpendicular electric fields associated with three-dimensional magnetic reconnection at the subsolar magnetopause. J Geophys Res 117:A06212, DOI 10.1029/2012JA017533

Pu ZY, Yei M, Liu ZX (1990) Generation of vortex-induced tearing mode instability at the magnetopause. J Geophys Res 95:10559–10566, DOI 10.1029/JA095iA07p10559

Pucci F, Servidio S, Sorriso-Valvo L, et al (2017) Properties of Turbulence in the Reconnection Exhaust: Numerical Simulations Compared with Observations. Astrophys J 841:60, DOI 10.3847/1538-4357/aa704f

Qi Y, Ergun R, Pathak N, et al (2024) Investigation of a Magnetic Reconnection Event with Extraordinarily High Particle Energization in Magnetotail Turbulence. Astrophys J Lett 962:L39, DOI 10.3847/2041-8213/ad24eb

Quijia P, Fraternale F, Stawarz JE, et al (2021) Comparing turbulence in a Kelvin-Helmholtz instability region across the terrestrial magnetopause. Mon Not R Astron Soc 503:4815–4827, DOI 10.1093/mnras/stab319

Retinò A, Sundkvist D, Vaivads A, Mozer F (2007) In situ evidence of magnetic reconnection in turbulent plasma. Nat Physics 3:235–238, DOI doi:10.1038/nphys574

Retinò A, Khotyaintsev Y, Le Contel O, et al (2022) Particle energization in space plasmas: towards a multi-point, multi-scale plasma observatory. Exp Astron 54:427–471, DOI 10.1007/s10686-021-09797-7

Richard L, Sorriso-Valvo L, Yordanova E, et al (2024) Turbulence in Magnetic Reconnection Jets from Injection to Sub-Ion Scales. Phys Rev Lett 132:105201, DOI 10.1103/PhysRevLett.132.105201

Roytershteyn V, Daughton W, Karimabadi H, Mozer FS (2012) Influence of the Lower-Hybrid Drift Instability on Magnetic Reconnection in Asymmetric Configurations. Phys Rev Lett 108:185001, DOI 10.1103/PhysRevLett.108.185001

Sahraoui F, Belmont G, Rezeau L, et al (2006) Anisotropic Turbulent Spectra in the Terrestrial Magnetosheath as Seen by the Cluster Spacecraft. Phys Rev Lett 96:075002, DOI 10.1103/PhysRevLett.96.075002

Schwartz SJ, Kucharek H, Farrugia CJ, et al (2021) Energy Conversion Within Current Sheets in the Earth's Quasi Parallel Magnetosheath. Geophys Res Lett 48:e91859, DOI 10.1029/2020GL09185910.1002/essoar.10505071.1

Servidio S, Matthaeus WH, Dmitruk P (2008) Depression of Nonlinearity in Decaying Isotropic MHD Turbulence. Phys Rev Lett 100(9):095005, DOI 10.1103/PhysRevLett.100.095005

Servidio S, Matthaeus WH, Shay MA, et al (2009) Magnetic reconnection in two-dimensional magnetohydrodynamic turbulence. Phys Rev Lett 102:115003, DOI 10.1103/PhysRevLett.

102.115003

Servidio S, Matthaeus WH, Shay MA, et al (2010) Statistics of magnetic reconnection in two-dimensional magnetohydrodynamic turbulence. Phys Plasmas 17:032315, DOI 10.1063/1.3368798

Servidio S, Greco A, Matthaeus WH, et al (2011) Statistical association of discontinuities and reconnection in magnetohydrodynamic turbulence. J Geophys Res 116:A09102, DOI 10.1029/2011JA016569

Sharma Pyakurel P, Shay MA, Phan TD, et al (2019) Transition from ion-coupled to electron-only reconnection: Basic physics and implications for plasma turbulence. Phys Plasmas 26:082307, DOI 10.1063/1.5090403

Shay MA, et al (this collection) Simulation models for exploring magnetic reconnection. Space Sci Rev

Shay MA, Haggerty CC, Matthaeus WH, et al (2018) Turbulent heating due to magnetic reconnection. Phys Plasmas 25:012304, DOI 10.1063/1.4993423

Shibata K, Tanuma S (2001) Plasmoid-induced-reconnection and fractal reconnection. Earth, Planets and Space 53:473–482, DOI 10.1186/BF03353258

Sisti M, Faganello M, Califano F, Lavraud B (2019) Satellite Data-Based 3-D Simulation of Kelvin-Helmholtz Instability and Induced Magnetic Reconnection at the Earth's Magnetopause. Geophys Res Lett 46:11,597–11,605, DOI 10.1029/2019GL083282

Sisti M, Fadanelli S, Cerri SS, et al (2021) Characterizing current structures in 3d hybrid-kinetic simulations of plasma turbulence. Astronomy and Astrophysics 655:A107, DOI 10.1051/0004-6361/202141902

Sorriso-Valvo L, Carbone V, Veltri P, et al (1999) Intermittency in the solar wind turbulence through probability distribution functions of fluctuations. Geophys Res Lett 26:1801–1804, DOI 10.1029/1999GL900270

Sorriso-Valvo L, Carbone F, Perri S, et al (2018) On the Statistical Properties of Turbulent Energy Transfer Rate in the Inner Heliosphere. Sol Phys 293:10, DOI 10.1007/s11207-017-1229-6

Sorriso-Valvo L, Catapano F, Retinò A, et al (2019) Turbulence-Driven Ion Beams in the Magnetospheric Kelvin-Helmholtz Instability. Phys Rev Lett 122:035102, DOI 10.1103/PhysRevLett.122.035102

Squire J, Meyrand R, Kunz MW, et al (2022) High-frequency heating of the solar wind triggered by low-frequency turbulence. Nat Astron 6:715–723, DOI 10.1038/s41550-022-01624-z

Stanier A, Daughton W, Le A, et al (2019) Influence of 3D plasmoid dynamics on the transition from collisional to kinetic reconnection. Phys Plasmas 26:072121, DOI 10.1063/1.5100737

Stawarz JE, Smith CW, Vasquez BJ, et al (2009) The Turbulent Cascade and Proton Heating in the Solar Wind at 1 AU. Astrophys J 697(2):1119–1127, DOI 10.1088/0004-637X/697/2/1119

Stawarz JE, Vasquez BJ, Smith CW, et al (2011) Third Moments and the Role of Anisotropy from Velocity Shear in the Solar Wind. Astrophys J 736:44, DOI 10.1088/0004-637X/736/1/44

Stawarz JE, Ergun RE, Goodrich KA (2015) Generation of high-frequency electric field activity by turbulence in the Earth's magnetotail. J Geophys Res 120:1845–1866, DOI 10.1002/2014JA020166

Stawarz JE, Eriksson S, Wilder FD, et al (2016) Observations of turbulence in a Kelvin-Helmholtz event on 8 September 2015 by the Magnetospheric Multiscale mission. J Geophys Res 121:11,021–11,034, DOI 10.1002/2016JA023458

Stawarz JE, Eastwood JP, Phan TD, et al (2019) Properties of the turbulence associated with electron-only magnetic reconnection in earth's magnetosheath. Astrophys J Lett 877:L37, DOI 10.3847/2041-8213/ab21c8

Stawarz JE, Matteini L, Parashar TN, et al (2021) Comparative Analysis of the Various Generalized Ohm's Law Terms in Magnetosheath Turbulence as Observed by Magnetospheric Multiscale. J Geophys Res 126:e8447, DOI 10.1029/2020JA02844710.1002/essoar.10503618.1

Stawarz JE, Eastwood JP, Phan TD, et al (2022) Turbulence-driven magnetic reconnection and the magnetic correlation length: Observations from magnetospheric multiscale in earth's magnetosheath. Phys Plasmas 29:012302, DOI 10.1063/5.0071106

Steinvall K, Gingell I (2024) The Influence of Rotational Discontinuities on the Formation of Reconnected Structures at Collisionless Shocks—Hybrid Simulations. J Geophys Res 129:e2023JA032101, DOI 10.1029/2023JA032101

Sturner AP, Eriksson S, Nakamura T, et al (2018) On Multiple Hall-Like Electron Currents and Tripolar Guide Magnetic Field Perturbations During Kelvin-Helmholtz Waves. J Geophys Res 123:1305–1324, DOI 10.1002/2017JA024155

Sundkvist D, Retinò A, Vaivads A, Bale SD (2007) Dissipation in Turbulent Plasma due to Reconnection in Thin Current Sheets. Phys Rev Lett 99:025004, DOI 10.1103/PhysRevLett.99.025004

Swisdak M (2016) Quantifying gyrotropy in magnetic reconnection. Geophys Res Lett 43:43–49, DOI doi:10.1002/2015GL066980

Takagi K, Hashimoto C, Hasegawa H, et al (2006) Kelvin-Helmholtz instability in a magnetotail flank-like geometry: Three-dimensional MHD simulations. J Geophys Res 111:A08202, DOI 10.1029/2006JA011631

Taylor GI (1938) The spectrum of turbulence. Proc R Soc A 164:476–490, DOI 10.1098/rspa.1938.0032

TenBarge JM, Howes GG (2013) Current Sheets and Collisionless Damping in Kinetic Plasma Turbulence. Astrophys J Lett 771:L27, DOI 10.1088/2041-8205/771/2/L27

TenBarge JM, Howes GG, Dorland W (2013) Collisionless Damping At Electron Scales in Solar Wind Turbulence. Astrophys J 774:139, DOI 10.1088/0004-637X/774/2/139

Trotta D, Pezzi O, Burgess D, et al (2023) Three-dimensional modelling of the shock-turbulence interaction. Mon Not R Astro Soc 525:1856–1866, DOI 10.1093/mnras/stad2384

Uritsky VM, Pouquet A, Rosenberg D, et al (2010) Structures in magnetohydrodynamic turbulence: Detection and scaling. Phys Rev E 82:056326, DOI 10.1103/PhysRevE.82.056326

Usanova ME, Ergun RE (2022) Electron Energization by High-Amplitude Turbulent Electric Fields: A Possible Source of the Outer Radiation Belt. J Geophys Res 127:e30336, DOI 10.1029/2022JA030336

Usanova ME, Ergun RE, Stawarz JE (2023) Ion Energization by Turbulent Electric Fields in Fast Earthward Flows and Its Implications for the Dynamics of the Inner Magnetosphere. J Geophys Res 128:e2023JA031704, DOI 10.1029/2023JA031704

Vapirev A, Lapenta G, Divin A, et al (2013) Formation of a transient front structure near reconnection point in 3-D PIC simulations. J Geophys Res 118:1435–1449, DOI 10.1002/jgra.50136

Vega C, Roytershteyn V, Delzanno GL, Boldyrev S (2020) Electron-only reconnection in kinetic-alfven turbulence. Astrophys J Lett 893:L10, DOI 10.3847/2041-8213/ab7eba

Vega C, Roytershteyn V, Delzanno GL, Boldyrev S (2023) Electron-scale current sheets and energy dissipation in 3D kinetic-scale plasma turbulence with low electron beta. Mon Not R Astron Soc 524:1343–1351, DOI 10.1093/mnras/stad1931

Vernisse Y, Lavraud B, Eriksson S, et al (2016) Signatures of complex magnetic topologies from multiple reconnection sites induced by Kelvin-Helmholtz instability. J Geophys Res 121:9926–9939, DOI 10.1002/2016JA023051

Verscharen D, Wicks RT, Alexandrova O, et al (2022) A Case for Electron-Astrophysics. Exp Astron 54:473–519, DOI 10.1007/s10686-021-09761-5

Vishniac ET, Pillsworth S, Eyink G, et al (2012) Reconnection current sheet structure in a turbulent medium. Nonlin Proc Geophys 19:605–610, DOI 10.5194/npg-19-605-2012

Volwerk M, Glassmeier KH, Nakamura R, et al (2007) Flow burst-induced Kelvin-Helmholtz waves in the terrestrial magnetotail. Geophys Res Lett 34:L10102, DOI 10.1029/2007GL029459

Vörös Z, Baumjohann W, Nakamura R, et al (2004) Magnetic turbulence in the plasma sheet. J Geophys Res 109:A11215, DOI 10.1029/2004JA010404

Vörös Z, Baumjohann W, Nakamura R, et al (2006) Bursty Bulk Flow Driven Turbulence in the Earth's Plasma Sheet. Space Sci Rev 122:301–311, DOI 10.1007/s11214-006-6987-7

Vörös Z, Yordanova E, Varsani A, et al (2016) Mms observation of magnetic reconnection in the turbulent magnetosheath. J Geophys Res 122:11,442–11,467, DOI 10.1002/2017JA024535

Vörös Z, Yordanova E, Graham DB, et al (2019) Mms observations of whistler and lower hybrid drift waves associated with magnetic reconnection in the turbulent magnetosheath. J Geophys Res 124:8551–8563, DOI 10.1029/2019JA027028

Wan M, Servidio S, Oughton S, Matthaeus WH (2009) The third-order law for increments in magnetohydrodynamic turbulence with constant shear. Phys Plasmas 16:090703, DOI 10.1063/1.3240333

Wan M, Matthaeus WH, Karimabadi H, et al (2012) Intermittent Dissipation at Kinetic Scales in Collisionless Plasma Turbulence. Phys Rev Lett 109:195001, DOI 10.1103/PhysRevLett.109.195001

Wan M, Matthaeus WH, Roytershteyn V, et al (2015) Intermittent Dissipation and Heating in 3D Kinetic Plasma Turbulence. Phys Rev Lett 114:175002, DOI 10.1103/PhysRevLett.114.175002

Wan M, Matthaeus WH, Roytershteyn V, et al (2016) Intermittency, coherent structures and dissipation in plasma turbulence. Phys Plasmas 23:042307, DOI 10.1063/1.4945631

Wang R, Wang S, Lu Q, et al (2023) Direct observation of turbulent magnetic reconnection in the solar wind. Nat Astron 7:18–28, DOI 10.1038/s41550-022-01818-5

Wang S, Chen L, Bessho N, et al (2019) Observational evidence of magnetic reconnection in the terrestrial bow shock transition region. Geophys Res Lett 46:562–570, DOI 10.1029/2018GL080944

Wang S, Chen L, Bessho N, et al (2020) Ion-scale current structures in short large-amplitude magnetic structures. Astrophys Journal 898:121, DOI 10.3847/1538-4357/ab9b8b

Wang Y, Cheng X, Guo Y, et al (2024) A method for determining the locations and configurations of magnetic reconnection within three-dimensional turbulent plasmas. Astron Astrophys 683:A224, DOI 10.1051/0004-6361/202347564

Weygand JM, Kivelson MG, Khurana KK, et al (2005) Plasma sheet turbulence observed by Cluster II. J Geophys Res 110:A01205, DOI 10.1029/2004JA010581

Wilder FD, Ergun RE, Schwartz SJ, et al (2016) Observations of large-amplitude, parallel, electrostatic waves associated with the Kelvin-Helmholtz instability by the magnetospheric multiscale mission. Geophys Res Lett 43:8859–8866, DOI 10.1002/2016GL070404

Wilder FD, Ergun RE, Burch JL, et al (2018) The role of the parallel electric field in electron-scale dissipation at reconnecting currents in the magnetosheath. J Geophys Res 123:6533–6547, DOI 10.1029/2018JA025529

Wilder FD, Conley M, Ergun RE, et al (2022) Magnetospheric multiscale observations of waves and parallel electric fields in reconnecting current sheets in the turbulent magnetosheath. J Geophys Res 127:e2022JA030511, DOI 10.1029/2022JA030511

Wu P, Perri S, Osman K, et al (2013) Intermittent Heating in Solar Wind and Kinetic Simulations. Astrophys J Lett 763:L30, DOI 10.1088/2041-8205/763/2/L30

Yang Y, Matthaeus WH, Parashar TN, et al (2017) Energy transfer, pressure tensor, and heating of kinetic plasma. Phys Plasmas 24:072306, DOI 10.1063/1.4990421

Yokoyama N, Takaoka M (2021) Energy-flux vector in anisotropic turbulence: application to rotating turbulence. J Fluid Mech 908:A17, DOI 10.1017/jfm.2020.860

Yordanova E, Vaivads A, André M, et al (2008) Magnetosheath Plasma Turbulence and Its Spatiotemporal Evolution as Observed by the Cluster Spacecraft. Phys Rev Lett 100:205003, DOI 10.1103/PhysRevLett.100.205003

Yordanova E, Vörös Z, Varsani A, et al (2016) Electron scale structures and magnetic reconnection signatures in the turbulent magnetosheath. Geophys Res Lett 43:5969–5978, DOI doi:10.1002/2016GL069191

Zharkova V, Xia Q (2021) Plasma turbulence generated in 3D current sheets with single and multiple X-nullpoints. Fron Astron Space Sci 8:178, DOI 10.3389/fspas.2021.665998

Zhdankin V, Uzdensky DA, Perez JC, Boldyrev S (2013) Statistical Analysis of Current Sheets in Three-Dimensional Magnetohydrodynamic Turbulence. Astrophys J 771:124, DOI 10.1088/0004-637X/771/2/124

Zhdankin V, Boldyrev S, Perez JC, Tobias SM (2014) Energy dissipation in magnetohydrodynamic turbulence: Coherent structures or "nanoflares"? Astrophys J 795:127, DOI 10.1088/0004-637X/795/2/127

Zhdankin V, Boldyrev S, Uzdensky DA (2016) Scalings of intermittent structures in magnetohydrodynamic turbulence. Phys Plasmas 23:055705, DOI 10.1063/1.4944820